Goldstone Solar System Radar (GSSR) Learning Manual

Planetary Radar and Radio Sciences Group (332K)
Jet Propulsion Laboratory, California Institute of Technology
Nereida Rodriguez-Alvarez
Contributions: Martin A. Slade, Joseph Jao, Clement Lee, Kamal Oudrhiri, Joseph Lazio

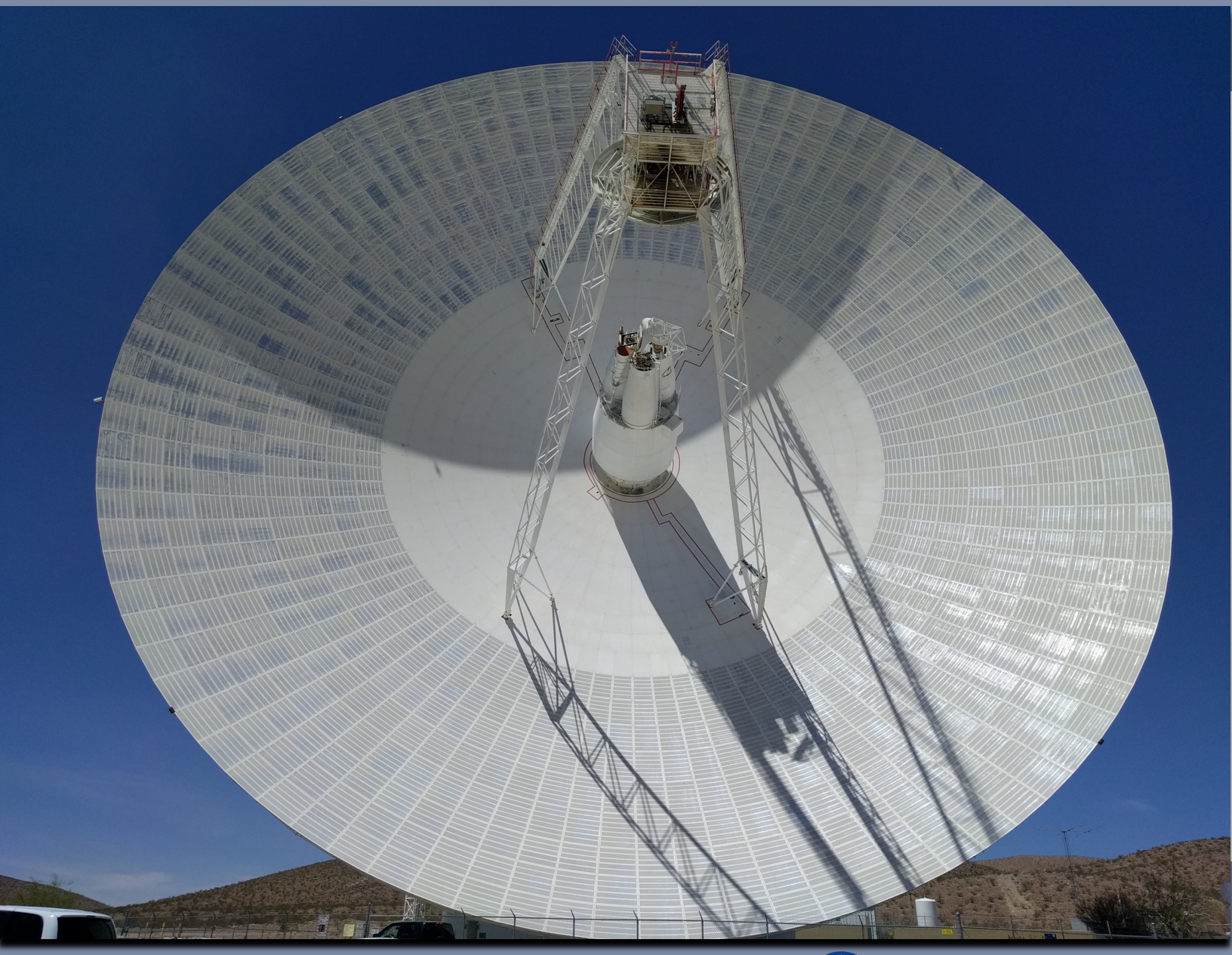

October 2019

Jet Propulsion Laboratory
California Institute of Technology

Abstract

This manual is written in order to train staff that requires a global end-to-end knowledge of the Goldstone Solar System Radar (GSSR). The new user needs to be able to understand the basics of the GSSR as well as the received radar signal and the different modes of operation. In addition, the user needs to be able to process the received signal and analyze the different parameters to be able to relate the measurements with the information that these measurements contain.

New GSSR users will seek answers to very basic questions as:

- What is it, where is it, how it became important?
- What is it made off? Components?
- What is the received signal? Understand the equation.
- What does the signal measure? To what is it sensitive?
- How it operates? What are the possible configurations?

While basic questions are answered and concepts are assimilated, the GSSR user will seek exemplification. This manual provides specific examples of the different configurations and different applications made in the past from the literature.

The last step in the learning process is to be able to process data and analyze the results. This manual provides a full chapter of practical case examples, where the users are guided through the post-processing of near-earth objects measurements, by providing them the tools for handling the data and using the processing codes. The main idea of this chapter is to allow new GRSS users to *learn by doing*.

The summary presented in this document gathers, therefore, the answers to the questions exposed above. Those answers have been extracted from various sources, all of them listed in the reference section. The only original part in this document is chapter 7, where a number of practices on the post-processing of near-earth objects have been prepared to allow new GRSS users to learn in a guided way.

Table of Contents

ABSTRACT **3**

TABLE OF CONTENTS **5**

REFERENCES **8**

CHAPTER 1. THE GOLDSTONE SOLAR SYSTEM RADAR (GSSR) **12**

CHAPTER 2. THE GSSR COMPONENTS **17**

THE TRANSMITTER SUBSYSTEM **17**
THE ANTENNA SUBSYSTEM **20**
ANTENNA MOUNT AND ROTATION 21
ANTENNA HISTORY AND PERFORMANCE SPECIFICATIONS 21
ANTENNA PARTS DESCRIPTION 21
THE RECEIVER SUBSYSTEM **23**
RECEIVER SUBSYSTEM 23
MICROWAVE SUBSYSTEM 25
FRONT-END MODULES 25
INTERMEDIATE FREQUENCY STAGES 27
EPHEMERIDES TUNING AND LOCAL OSCILLATORS 28
DATA ACQUISITION SUBSYSTEM **29**

CHAPTER 3. THE GSSR MEASUREMENTS **30**

PARAMETERS OF THE RADAR ECHO **30**
AMPLITUDE 31
DOPPLER FREQUENCY SHIFT 32
TIME DELAY (RANGE) 37
DELAY-DOPPLER MAPPING 39
POLARIZATION 41
RADAR CROSS SECTION σ **43**
DIRECTIVITY (g) 44
BACKSCATTER FUNCTION (σ) 46
REFLECTIVITY AND DIELECTRIC CONSTANT (ρ, ε) 46

CHAPTER 4. APPLICATIONS **48**

EPHEMERIDES **48**

EPHEMERIDES - CASE EXAMPLE 53
SURFACE CHARACTERISTICS, TOPOGRAPHY AND RADAR MAPS 55
BULK DENSITY AND POROSITY 57
SPIN VECTORS 59
MULTIPARTICLE SYSTEMS 63

CHAPTER 5. MODES OF OPERATION 65

DIFFERENT MODES REGARDING THE SELECTED WAVEFORM 65
CONTINUOUS WAVE (CW) 65
BINARY PHASE CODED (BPC) 69
LINEAR FREQUENCY MODULATION (LFM OR CHIRP) 72
RESOLUTION AND RANGE COVERAGE 75
DIFFERENT MODES REGARDING THE DIFFERENT TRANSMITTER/RECEIVER CONFIGURATIONS 76
MONOSTATIC 76
BISTATIC AND MULTISTATIC 76
NEW CAPABILITY ADDED TO GSSR TO PERFORM RANGING MEASUREMENTS: THE LONG CODE 78
ORIGIN OF THE LONG-CODE PROCESSING 78
MOTIVATION TO DEVELOP THE LONG CODE 79
LIMITATIONS OF THE STANDARD "SHORT-CODE" 79
LONG-CODE PROCESSING 80
LONG-CODE MODIFICATION REQUIREMENTS 80

CHAPTER 6. SUMMARY OF RADAR SCIENCE SERVICES SUPPORT TYPES 81

SUMMARY 81
CURRENT AND PAST OBSERVATIONS OF PLANETS AND PLANETARY OBJECTS 83
RESOURCES 87

CHAPTER 7. POST-PROCESSING OF NEAR-EARTH OBJECTS 88

PRACTICE 1: SETTING UP THE ENVIRONMENT 89
PRACTICE 2: POST-PROCESSING OF CW DATA 92
PART 1: LOOPBACK FILE 92
PART 2: CW RUNS 94
PRACTICE 3: POST-PROCESSING OF BPC DATA 99
PART 1. BPC AT 10 US 99
PART 2. BPC AT 11 US 103
PART 3. BPC AT 1 US 106
PART 4. BPC AT 0.25 US 108
PART 5. BPC AT 0.125 US 111
PRACTICE 4: POST-PROCESSING OF CHIRP DATA 114
PRACTICE 5: POST-PROCESSING OF CW AND CHIRP DATA ON BISTATIC CONFIGURATION 117
PART A. CW DATA IN BISTATIC MODE. 118

PART B. CHIRP DATA IN BISTATIC MODE. 120
PRACTICE 6: UNDERSTANDING THE CONFIGURATION FILE. 124
CW DATA 128
Part 1. Loopback file 129
Part 2. CW data 130
BPC DATA 132
PART 1. Loopback file 132
Part 2. BPC data 134

APPENDIX 139

A. EVOLUTION OF THE GSSR TRANSMITTER 139
S-BAND TRANSMISSIONS AT A 2388 MHZ 139
X-BAND TRANSMISSIONS AT 8495 MHZ 140
X-BAND TRANSMISSIONS AT 8560 MHZ 141
EVOLUTION OF GSSR KLYSTRONS 141
B. DESCRIPTION OF A PUNCH FILE 145

References

[1] M. A. Slade, L. A. Benner and A. Silva, "Goldstone Solar System Radar Observatory: Earth-Based Planetary Mission Support and Unique Science Results," *Invited paper on Proceedings of the IEEE,* vol. 99, no. 5, May 2011.

[2] J. D. Dvorsky, N. A. Renzetti and D. E. Fulton, The Goldstone Solar System Radar: A Science Instrument for Planetary Research, JPL Publication 92-29, 1992.

[3] H. Kauffman, "A DX record: To the moon and back," *QST,* vol. 30, pp. 65-68, May 1946.

[4] R. M. Goldstein and R. L. Carpenter, "Rotation of Venus—Period estimated from radar measurements," *Science,* vol. 139, no. 3558, pp. 910-911, March 1963.

[5] W. K. Victor and R. Stevens, "Exploration of Venus by radar—Precision range and velocity data can be obtained with a supersensitive radar receiving system," *Science,* vol. 134, no. 3471, pp. 46-48, July 1961.

[6] G. H. Pettengill, Radar Studies of the Planets, in Radar Astronomy, New York: McGraw-Hill (T. Hagfors and J. V. Evans, Eds.), 1968.

[7] I. I. Shapiro, M. A. Slade, S. H. Zisk, A. E. E. Rogers and T. W. Thompson, "Lunar topography—Global determination by radar," *Science,* vol. 178, no. 4064, p. 939–948, December 1972.

[8] G. S. Downs, T. W. Thompson, P. J. Mouginis-Mark and S. H. Zisk, "New radar-derived topography for the Northern Hemisphere of Mars," *Journal of Geophysical Research ,* vol. 87, no. NB12, pp. 9747-9754, November 1982.

[9] J. M. Goldspiel, S. W. Squyres, M. A. Slade, R. F. Jurgens and S. H. Zisk, "Radar-derived topography of low southern latitudes of Mars," *Icarus,,* vol. 106, no. 2, p. 346–364, December 1993.

[10] G. H. Pettengill, C. C. Counselman, L. P. Rainville and I. I. Shapiro, "Radar Measurements of Martian Topography," *The Astronomical Journal,* vol. 74, no. 3, pp. 461- 482, 1969.

[11] K. W. Larsen, R. F. Jurgens, A. F. C. Haldemann, M. A. Slade and H. C. J. Rumsey, "Terrestrial Quadstatic Interferometric Radar Observations of Mars," *IEEE Transactions on Geoscience and Remote Sensing,* vol. 48, no. 6, pp. 2670-2684, June 2010.

[12] M. A. Slade, B. J. Butler and D. 0. Muhleman, "Mercury Radar Imaging: Evidence for Polar Ice," *Science,* 1992.

[13] D. O. Muhleman, A. W. Grossman and B. B. J., "Radar Investigation of Mars, Mercury, and Titan," *Annual Review of Earth and Planetary Sciences,* vol. 23, pp. 337-374, 1995.

[14] A. F. C. Haldemann, R. F. Jurgens, K. W. Larsen, R. E. Arvidson and M. A. Slade, "Mars Radar Observations with the Goldstone Solar System Radar," *Solar System Remote Sensing Symposium,* 2002.

[15] D. O. Muhleman, B. J. Butler, A. W. Grossman and M. A. Slade, "Radar Images of Mars," *Science,* vol. 253, pp. 1508-1513, 1991.

[16] D. O. Muhleman, A. W. Grossman, B. J. Butler and M. A. Slade, "Radar Reflectivity of Titan," *Science,* vol. 248, pp. 975-980, 1990.

[17] D. O. Muhleman, A. W. Grossman, M. A. Slade and B. J. Butler, "The Surface of Titan and Titan's Rotation: What is Radar Telling Us," *Bulletin of the American Astronomical Society,* vol. 24, pp. 954-955, 1992.

[18] D. O. Muhleman, A. W. Grossman, M. A. Slade and B. J. Butler, "Titan's Radar Reflectivity and Rotation," *Bulletin of the American Astronomical Society,* vol. 25, p. 1099, 1993.

[19] J.-L. Margot, S. J. Peale, R. F. Jurgens, M. A. Slade and I. V. Holin, "Large longitude libration of Mercury reveals a molten core," *Science,* vol. 316, pp. 710-714, 2007.

[20] National Research Council, Defending Planet Earth: Near-Earth-Object Surveys and Hazard Mitigation Strategies, Washington, DC: The National Academies Press, 2010.

[21] DAMIEN-IWG, "Nation Near-Earth Object Preparedness Strategy and Action Plan," *Interagency Working Group for Detecting and Mitigating the Impacts of Earth-Bound Near-Earth Objects - National Science and Technology Council,* June 2018.

[22] L. Teitelbaum, R. Liou, Y. Vodonos, J. Velazco, K. Andrews and D. Kelley, "The Klystron Engineering Model Development (KEMD) Task — A New Design for the Goldstone Solar System Radar (GSSR)," *IPN Progress Report,* 2017.

[23] C. T. Stelzried, A. J. Freiley and M. S. Reid, System Noise Concepts with DSN Applications, Vols. Volume 10: Low-Noise Systems in the Deep Space Network, DESCANSO Book Series, Deep Space Communications and Navigation Series, 2008, pp. Chapter 2, 14-93.

[24] S. P. Naidu, L. A. Benner, J.-L. Margot, M. Busch and P. Taylor, "Capabilities of Earth-based Radar Facilities for Near-Earth Asteroid Observations," *The Astronomical Journal,* vol. 152, no. 4, p. 99, 2016.

[25] S. H. Zisk and P. J. Mouginis-Mark, "nomalous Region on Mars: Implications for Near-Surface Liquid Water," *Nature,* vol. 288, no. 18, pp. 735-738, 25 December 1980.

[26] S. J. Ostro, "Planetary Radar," in *The Encyclopedia of the Solar System*, New York, Academic Press, 1992.

[27] S. Hensley, E. Gurrola, L. Harcke, M. Slade, K. Quirk, M. Srinivasan, C. Lee, S. Yun, J. Jao, B. Wilson, E. De Jong, N. Marechal, L. Weintraub, R. Dickinson, R. Bloom, G. Karamyan and L. A., "Lunar topographic mapping using a new high resolution mode for the GSSR radar," in *IEEE National Radar Conference*, Washington DC, May 10-14, 2010.

[28] D. O. Muhleman, "Radar Scattering from Venus and the Moon," *The Astronomical Journal,* vol. 69, no. 1, pp. 34-41, 1964.

[29] R. F. Jurgens, M. A. Slade and S. H. Zisk, "Normal Incidence Radar Observations of the 'Stealth' South Tharsis Region," in *Lunar and Planetary Science XXU*, Houston, Lunar and Planetary Science Institute, 1991, pp. 673-674.

[30] P. G. Kamoun, D. B. Campbell, S. J. Ostro, G. H. Pettengill and I. I. Shapiro, "Comet Encke: Radar Detection of Nucleus," *Science,* vol. 2, no. 16, p. 293, 1982.

[31] S. J. Ostro, K. D. Rosema and R. F. Jurgens, "The Shape of Eros," *Icanrs,* vol. 84, pp. 334-351, 1990.

[32] J.-L. Margot, S. J. Peale, S. C. Solomon, S. A. Hauck II, F. D. Ghigo, R. F. Jurgens, M. Yseboodt, J. D. Giorgini, S. Padovan and D. B. Campbell, "Mercury's moment of inertia from spin and gravity data," *Journal of Geophysical Research,* vol. 117, no. E00L09, 2012.

[33] G. H. Pettengill, R. B. Dyce and I. I. Shapiro, "A Radar Determination of the Rotation of the Planet Mercury," *Nature,* vol. 206, no. 4990, p. 1240, 19 June 1965.

[34] M. A. Slade, S. Zohar and R. F. Jurgens, "Venus: Improved Spin Vector from Goldstone Radar Observations," *Astronomical Journal,* vol. 100, no. 4, pp. 1369-1374, 1990.

[35] M. Yseboodt, J.-L. Margot and S. J. Peale, "Analytical model of the long-period forced longitude librations of Mercury," *Icarus,* vol. 207, pp. 536-544, 2010.

[36] S. J. Ostro, G. Pettengill, D. B. Campbell and R. M. Goldstein, "Delay-Doppler radar observations of Saturn's rings," *Icarus,* vol. 49, no. 3, pp. 367-381, 1982.

[37] S. J. Ostro, Encyclopedia of the Solar System (Second Edition) - Chapter 2.4 Radar waveforms, Academic Press, 2007.

[38] J. K. Harmon, "Planetary delay-Doppler radar and the long-code method," *IEEE Transactions as Geoscience Remote Sensing,* vol. 40, no. 9, pp. 1904-1916, September 2002.

[39] C. E. Cook and M. Bernfeld, Radar Signals, New York: Academic, 1967.

[40] C. Elachi, Introduction to the Physics and Techniques of Remote Sensing, New York: Wiley, 1987.

[41] J.-L. Margot, "Planetary, Radar Astronomy With Linear FM (Chirp) Waveforms," Internal Arecibo Memo, June 2000.

[42] K. Quirk and M. Srinivasan, "GSSR Waveforms for Lunar Observations," Internal JPL Study, March 2008.

[43] T. Hagfors and D. B. Campbell, "Mapping of Planetary Surfaces by Radar," *Proceedings of the IEEE,* vol. 61, no. 9, pp. 1219-1225, September 1973.

[44] J. McMichael and e. al., "Development of Long-Code Capability at Goldstone and Initial Results for NEA (357439) 2004 BL86, Venus, and Galilean Satellites," in *The Future of Planetary Radio Astronomy with Single-Dish Telescopes Workshop*, 2015.

[45] J. K. Harmon, M. P. Sulzer, P. J. Perillat and J. F. Chandler, "Mars radar mapping: Strong backscatter from the Elysium basin and outflow channel," *Icarus,* vol. 95, pp. 153-156, 1992.

[46] L. Harcke, "Radar Imaging of Solar System Ices.," *Ph.D. Dissertation, Stanford University,* 2005.

[47] L. Teitelbaum, R. Liou, Y. Vodonos, J. Velazco, K. Andrews and D. Kelley, "The Klystron Engineering Model Development (KEMD) Task — A New Design for the Goldstone Solar System Radar (GSSR)," *IPN Progress Report,* Vols. 42-210, August 15, 2017.

[48] A. J. Butrica, To See The Unseen: A History of Planetary Radar Astronomy, Vols. NASA SP-4218, The NASA History Series, 1996.

[49] R. M. Goldstein and G. Morris, "Radar observations of the rings of Saturn," *Icarus,* vol. 20, pp. 260-262, 1973.

[50] R. Hartop and D. A. Bathker, "The High-Power X-Band Planetary Radar at Goldstone: Design, Development, and Early Results," *IEEE Transactions on Microwave Theory and Techniques,* Vols. MTT-24, no. 12, pp. 958-963, December, 1976.

[51] A. G. Smith and T. D. Carr, Radio Exploration of the Planetary System, Commission on College Physics, 1964.

[52] D. J. Mudgeway, "Uplink–Downlink: A History of the Deep Space Network 1957–1997," *The NASA History Series, NASA Office of External Relations,* Vols. SP-2001-4227, 2001.

[53] R. Cormier and A. Mizuhara, "250-kW CW Klystron Amplifier for Planetary Radar," *The Telecommunications and Data Acquisition Progress Report,* vol. 42, no. 108, pp. 1-13, February 15,1992.

[54] A. Mizuhara, "Bandwidth and Group Delay Extension for an X-band 250 kW CW Klystron for JPL/NASA Deep Space Radar," *Proceedings of the IEEE 5th Conference on Vacuum Electronics,* pp. 77-78, April 2004.

[55] S. J. Ostro, "Asteroid Radar Astronomy," in *Asteroids III*, University of Arizona Press, 2002, p. 152.

[56] A. Balkcum, A. Mizuhara, B. Stockwell, R. Begum and L. e. a. Cox, "Design and Operation of a 100 kW CW X-band Klystron for Spacecraft Communications," *IEEE IVEC 2012 Conference Proceedings,* pp. 315-316, April 2012.

[57] D. B. Campbell, G. J. Black, L. M. Carter and S. J. Ostro, "Radar evidence for liquid surfaces on Titan," *Science,* vol. 302, no. 5644, pp. 431-434, October 2003.

Chapter 1. The Goldstone Solar System Radar (GSSR)

This information has been extracted mainly from [1] and [2].

The Goldstone Solar System Radar (GSSR) facility is the only fully steerable radar in the world for high-resolution ranging and imaging of planetary and small-body targets. The resulting data are used not just for scientific studies of these targets, but also for enabling support of the National Aeronautics and Space Administration (NASA) flight projects, including many solar system exploration missions over the last three decades.

Figure 1. (Left) Photo Lara Hartley. 26-meter diameter and three 34-meter antennas, (right) 70-meter diameter antenna.

There are two powerful ground-based radars in the world capable of investigating solar system objects: the NASA Goldstone Solar System Radar (GSSR) and Arecibo Observatory (supported by the University of Central Florida, partnered with Yang Enterprises and UMET), which is located in Puerto Rico. NASA derives both scientific and programmatic benefits from their use, including investigations of the Moon, planets, and other solar system bodies, including near-Earth objects (NEOs). These studies provide images and topography, and information on surface characteristics, shapes, composition, orbits, rotations, and distribution of liquids or ices on or below their surfaces. The capabilities of these two instruments are different and often provide complementary data, so the combination of results from both radars has often proven to be much more valuable to NASA than each individually, sometimes yielding valuable information that neither could obtain alone.

GSSR is located in Barstow, California, at one of the three Deep Space Network (DSN) sites. The other DSN sites are the Australian complex, which is located 40 kilometers (25 miles) southwest of Canberra near the Tidbinbilla Nature Reserve., and the Spanish complex, which is located 60 kilometers (37 miles) west of Madrid at Robledo de Chavela. The Goldstone complex is located on the U.S. Army's Fort Irwin Military Reservation, approximately 72 kilometers (45 miles) northeast

of the desert city of Barstow, California. Once a spacecraft reaches a distance of 30,000 km from Earth, it falls in the field of view of one of the three DSN stations, fig. 2.

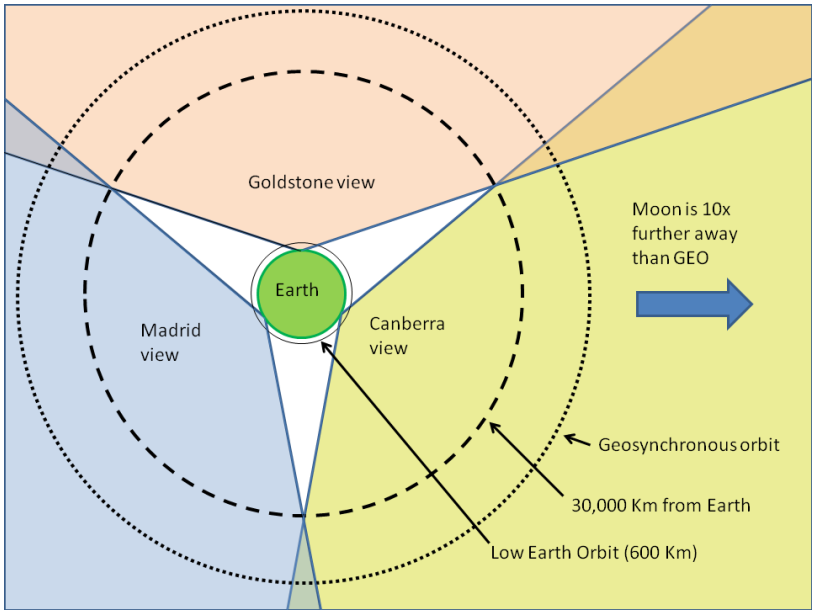

Figure 2. View from the Earth's north pole, showing the field of view of the main DSN antenna locations. Once a mission gets more than 30,000 km from earth, it is always in view of at least one of the stations.

Each complex is situated in semi-mountainous, bowl-shaped terrains to shield against external radio frequency interference. Each of the three DSN sites has multiple large antennas and is designed to enable continuous radio communication between several spacecraft and Earth. All three complexes consist of at least four antenna stations, each equipped with large, parabolic dish antennas and ultra-sensitive receiving systems capable of detecting incredibly faint radio signals from distant spacecraft.

The NASA/JPL DSN supports the GSSR. The GSSR consists of a 500-kW transmitter with center frequency at X-band (8560 MHz or 3.5-cm wavelength) on the 70-m antenna at the Goldstone DSN site (near Barstow, CA). Chapter 3 describes the evolution of the GSSR transmitter and the current capabilities.

The GSSR originated in 1958 with initiation of the space program under NASA. In particular, NASA funded a technology development program recognizing that planetary research would require a state-of-the-art two-way communications capability on Earth. This technology development by JPL, universities, and industry made use of natural solar system objects to advance such elements of communication technology as low-noise amplifiers, high-power transmitters, and signal processing equipment. In carrying out field experiments at Goldstone, technology development

had the benefit of the antennas required by the DSN for such efforts as Project Echo[1] (1960-1964), which required a high-power transmitter to perform its experiment. The NASA Office of Tracking and Data Acquisition, now known as the Office of Space Communications and Navigation (SCaN), provided the funding for this technology development making possible for the DSN stations to achieve the state of the art of telecommunications. Over the next few years subsequent to these experiments, it became obvious to the NASA science community that this instrument could provide some of the information needed to design spacecraft missions to the planets, their satellites, and comets. As sensitivity of the instrument grew, asteroids were added to the list of targets. NASA began to fund scientific investigators who, in turn, brought continuing requirements for new capabilities.

The first detection of a radar echo from an exterior body occurred on 1946, when the radar signal reflected from the Moon was measured [3]. From that moment many observations have occurred making possible the advancement of the accuracy, resolution and different techniques using ground radar. One of the natural targets for this development was the Planet Venus. Many radar installations around the world competed to be the first to detect an echo from Venus; however, it was the Goldstone radar that achieved this first. The detection of a radar echo from Venus provided an absolute measure for the astronomical unit, which up to that moment was uncertain and would have made interplanetary navigation difficult. These early experiments advanced our knowledge on the rotational state of Venus [4], [5] and the topography of the Apollo landing sites [6], [7] Those measurements also made possible many findings on Mars, as [8], [9], [10], which advances our knowledge on Mars topography and [11], which advances the knowledge on the roughness of various sites within Mars using the known topography as an a-priori known variable. The capabilities of radar measurements have improved over the years making possible observations of targets as Mercury, [12] and [13], and Mars, [14], [15] and [13], and very distant targets as Titan, [16], [17], [18], and [13], where the Goldstone 70 m antenna was used to transmit and the 26 antennas of the Very Large Array were used for receiving providing evidence for the presence of polar ice, or [19], were observations of radar speckle patterns linked to the rotation of Mercury allowed to prove that Mercury has a molten core. Voyager 1 Titan flyby predicted a global ocean, radar measurements from Goldstone/VLA proved that the ocean was confined to large lakes, [16]. Over the years the detection of NEO has become of highly importance. The United States annual expense in the search for NEO is close to $4 million [20].The main goal is to keep track of those NEO that suppose a hazard since they may potentially impact the Earth. Thanks to the annual budget, several observatories are funded to search for NEO. Some of the funding is also dedicated to mitigation, which studies how Earth can be protected in case of potential impacts from NEOs, and some to characterization of their orbits and physical properties.

According to [20], Congress dictated two mandates for the search of NEOs:

[1] Project Echo was the first passive communications satellite experiment. Each of the two American spacecraft, launched in 1960 and 1964, was a metalized balloon satellite acting as a passive reflector of microwave signals. Communication signals were bounced off them from one point on Earth to another.

- The Spaceguard Survey (1998). Required to "discover 90 % of NEOs with a diameter of 1 kilometer or greater within 10 years", [20]. This size corresponds to the minimum size that could cause global devastation in case of impact. This mandate has been well implemented by NASA, and it should be accomplished in the next years.
- The George E. Brown, Jr. Near-Earth Object Survey Act (2005). Required to "detect 90 percent of NEOs 140 meters in diameter or greater by 2020", [20].

Characterization of NEOs is defined as the determination of their orbit and physical properties. Characterization is key to plan in case Earth defense is needed. According to [20], "such defense would be carried out through a suitable attack on any object predicted with near certainty to otherwise collide with Earth and cause significant damage". The best possible option is a spacecraft reconnaissance mission, but such a mission would not be possible without enough time to plan. For this reason, characterization of NEOs from ground observations becomes important:

- Optical observations: to obtain information on NEOs, such as their reflectivity, which is related to their surface properties and composition, and their rotation periods.
- Radar measurements (Arecibo Observatory and GSSR): to help obtaining advanced information as making 3D images of the NEOs and determining if those bodies have smaller satellites orbiting around them. Arecibo has a higher sensitivity than GSSR more restricted sky coverage. GSSR also offers a more accurate orbit determination.

Mitigation of NEOs, is defined as the ways of defending Earth from the damage that a NEO impact would cause. According to NASA report on Near-Earth Object Survey and Deflection Analysis of Alternatives (available at https://www.nasa.gov/pdf/171331main_NEO_report_march07.pdf) there are different mitigation strategies. As stated in [21], there are three organizations in charge of developing strategies and action plan for preparedness in case a possible NEO Earth impact. Those agencies are: the National Science and Technology Council (NSTC), the Office of Science and Technology Policy (OSTP) and the Detecting and Mitigating the Impact of Earth-bound Near-Earth Objects (DAMIEN) Interagency Working Group (IWG). For more information on those agencies, please refer to [21]. The main objective of the *National Near-Earth Object Preparedness Strategy and Action Plan* developed by those agencies, is to help on preparedness by "organizing and coordinating NEO-related efforts within Federal Departments and Agencies, with a particular focus on efforts that are already existing and resourced". There are a number of goals, with their objectives and actions, to help on preparedness, among them "Enhance NEO Detection, Tracking, and Characterization Capabilities".

Currently, the NASA's Planetary Defense Coordination Office (PDCO) is managed in the Planetary Science Division of the Science Mission Directorate at NASA Headquarters in Washington, D.C. The PDCO is responsible for:

- Ensuring the early detection of potentially hazardous objects (PHOs) – asteroids and comets whose orbits are predicted to bring them within 0.05 Astronomical Units of Earth;

and of a size large enough to reach Earth's surface – that is, greater than approximately 30 to 50 meters;
- Tracking and characterizing PHOs and issuing warnings about potential impacts;
- Providing timely and accurate communications about PHOs; and
- Leading the coordination of U.S. Government planning for response to an actual impact threat.

The PDCO relies on data from projects supported by NASA's Near-Earth Object (NEO) Observations Program. The PDCO also coordinates NEO observation efforts conducted at ground-based observatories sponsored by the National Science Foundation and space situational awareness facilities of the United States Air Force. In addition to finding, tracking, and characterizing PHOs, NASA's planetary defense goals include developing techniques for deflecting or redirecting PHOs, if possible, that are determined to be on an impact course with Earth. In the event that deflection or redirection is not possible, the PDCO is responsible for providing expert input to the Federal Emergency Management Agency for emergency response operations should a PHO be on an impact course or actually impact the Earth. Radar is recognized as one of the key ways to track and characterize NEOs, therefore the GSSR plays an important role in addressing this goal.

As it has been depicted, many applications and discovering have arisen from the use of ground radars as the GSSR. The importance of this instrument goes beyond what many people thought at its first stages, and probably further of what we can think today. Next chapters focus on the GSSR components, the evolution of its transmitter, the types of measurements that can be done, the different applications and the modes of operation. In addition, a summary of radar science services support types is also provided. The last chapter is dedicated to the post-processing of NEO observations, showing practical and guided examples to apply different techniques in obtaining the radar echoes.

Chapter 2. The GSSR components

This information has been extracted mainly from [1] and [2].

The GSSR capability is built around an X-band (8.6 GHz) high-power transmission capability, and can be broken down into the transmitter, the antenna, the receiver, and the data-acquisition subsystems. A conceptual diagram is shown in the following figure:

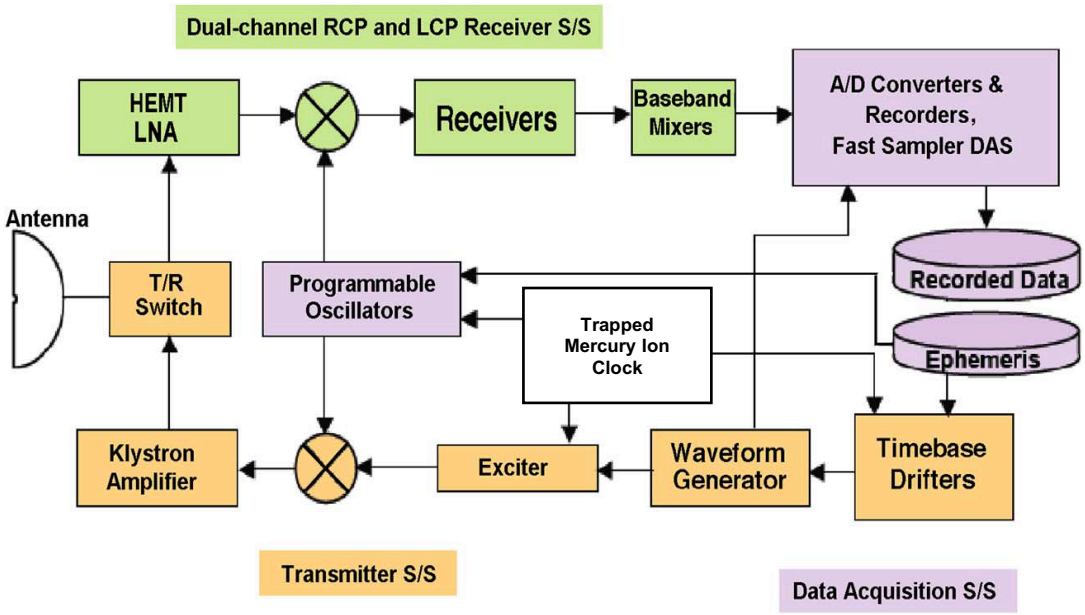

Figure 3. Diagram of GSSR subsystem (S/S) interfaces. The colors in the figure are linked to the transmitter (orange), receiver (green) and purple (data acquisition system) main components. This figure has been obtained from [1].

The transmitter subsystem

The exciter uses the ultrastable Mercury trapped ion time reference (see Figure 3) along with modulation information from the virtual address extension (VAX) computer, a discontinued computer architecture developed by Digital Equipment Corporation (DEC) in the mid-1970s, to generate the radar waveform to be transmitted. The exciter is common to the transmitted 3.5-cm (X-band) wavelength signals. Depending on the mode of operation the exciter will generate the waveform differently:

⇒ in the binary phased-coded (ranging) mode, pseudo-noise (PN) codes are used for modulation

⇒ in the continuous wave, a constant radio frequency signal with no time modulation is transmitted.

⇒ in the chirping mode, linear frequency modulation is used.

This signal is then sent to the transmitter where it is amplified to a very high power, using the Klystron amplifier[2], [22]. The high-power radar signal is transmitted out its horn, and a "quasi-optical" transmit–receive (T/R) switch, which is a GSSR component especially developed for NEO applications, allows for receiving with low latency. The transmitter subsystem (including exciter) interfaces to the Data Acquisition Subsystem (DAS) for monitor and control. The transmitter performance specifications are shown in the following table.

Table 1. Transmitter performance

Parameter	Value
Transmitter power, kW	465[3]
Frequency, MHz	8560
Antenna gain, dB	73.23 ± 0.2 dBi
Antenna beamwidth, deg	0.038 ± 0.004 deg
Polarization	RC, LC
Frequency accuracy	+/- 3 x 10^{-13}
Modulation	Biphase
Cross polarization, dB	<-25
Frequency hopping	10 kHz (2 hops), 20 kHz (4 hops)
Max Doppler shift, MHz	1.2

Very high transmitter power levels are used to overcome the large signal losses caused by the extreme distances to solar system targets, see eqn.2. The signal is amplified using klystrons, as mentioned above. The following items give specifics on how klystrons work.

- The 3.5-cm-wavelength final amplifiers are water-cooled klystrons. Two klystrons are connected in parallel, and their power output is added.
- They are located in the 3.5-cm X-band transmit/receive (XTR) feedcone to place them as close as possible to the radar-dedicated transmit feedhorn (see fig.5).

[2] Klystrons are specialized linear-beam vacuum tubes invented in 1937 by American electrical engineers Russell and Sigurd Varian, which are used as amplifier for high radio frequencies, from UHF up into the microwave range. In a klystron, an electron beam interacts with radio waves as it passes through resonant cavities, metal boxes along the length of a tube. The electron beam first passes through a cavity to which the input signal is applied. The energy of the electron beam amplifies the signal, and the amplified signal is taken from a cavity at the other end of the tube. The output signal can be coupled back into the input cavity to make an electronic oscillator to generate radio waves.

[3] The maximum transmitted power for monostatic observations is currently 100 kW. Klystrons can operate above 150 kW for bistatic observations. To be updated as new klystrons become operative.

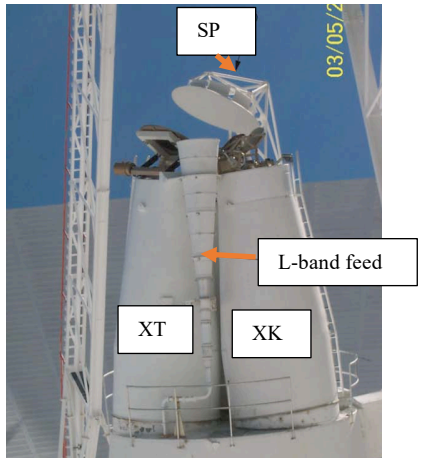

Figure 4. (Left) Goldstone 70-m antenna tricones S-band polarization diversity (SPD) feedcone located behind the X-band/K-band radar (XKR) and X-band transmit/receive (XTR) feedcone. Figure extracted from [23].

- This location minimizes energy loss in the thick-walled waveguide, a loss that can be as much as 1 kW/ft. The klystrons amplify the signal from the exciter for a combined output power at the feedhorn of 465 kW (currently 100 kW).
- Klystrons can amplify carriers with either binary phase-coded or continuous wave modulation, with or without frequency hopping.
- In these tubes, electromagnets focus electrons falling through a potential drop of some 51 kV.
- The electron beam's velocity is modulated by the excitation signal, and this in turn modulates the electron density and energy flux at radio frequencies.
- Internal resonant cavities enhance this modulation and about one-half of the nearly 1 MW of input direct-current power is converted to radio frequency power, which is sent out through a waveguide to the antenna feedhorn and radiated toward the target.
- The other half of the input power is waste heat, which, in addition to heat from waveguide losses, is transported away from the klystrons and feedlines by cooling water to the Heat Exchanger Assembly (HEA).
- Radio frequency power measurement, an important quantity in radar experiments, is via temperature sensing of this cooling water flow; water loads are used during test and adjustment.
- One selected polarization is transmitted, either right circular or left circular.

The antenna subsystem

The primary GSSR antenna subsystem consists of the 70-m-diameter main reflector, the sub-reflector and its supporting quadripod, the pointing system, and the concrete pedestal building. Figure 6 show more detail on the antenna subsystem elements.

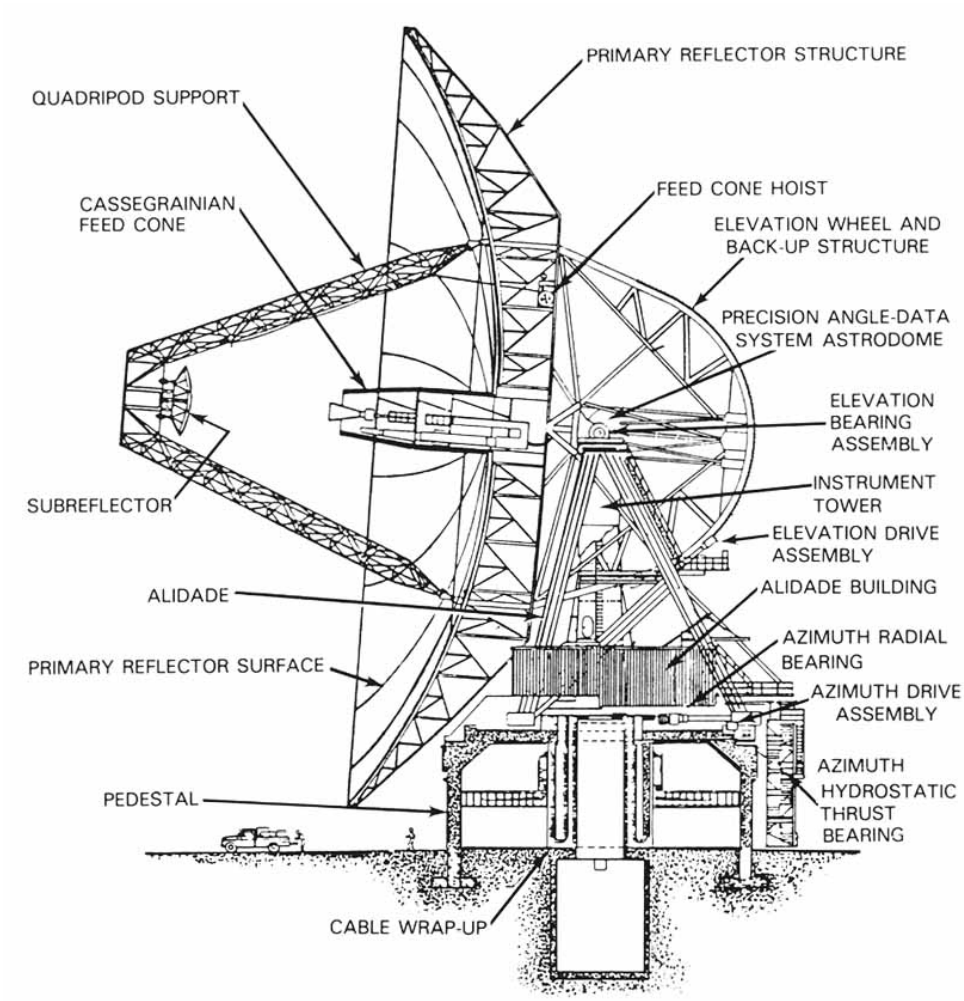

Figure 5. Image showing the antenna in Cassegrain configuration and all its parts, from nasa.gov. Figure obtained from [2].

Some specifics of this elements:

- The pedestal is partitioned into the offices of the Radio Astronomy and Radar Group (RARG), equipment rooms, and the radar control room.
- The total weight of the antenna including the pedestal is about 7258 metric tons.
- Its overall height is 71 m (234 ft), making it the largest Goldstone antenna.
- The weight of the rotating structure is about 2700 metric tons.
- The pedestal is over 10 m high and contains 4400 metric tons of reinforced concrete

Antenna mount and rotation

For an antenna of this size, an azimuth-elevation mount is more economical than an equatorial or X-Y mount. The giant dish and its azimuth-elevation mount atop the pedestal rotate in azimuth on three flat bearing surfaces that float on a thin film of oil over a flat circular runner or track several feet wide. The counterweighted dish assembly is supported in elevation by two horizontal stub shafts, each of which rests on two roller-bearing assemblies.

Antenna history and performance specifications

Construction as a 64-m antenna was completed in 1966. The antenna began operation as part of the DSN in 1966 by communicating with the 1964 Mariner Mars spacecraft, which was then 328 million km or about 2 astronomical units away. The upgrade to the present 70-m diameter was completed, about 30 years ago, in June 1988. Performance specifications for the present antenna are listed in following table.

Table 2. Antenna performance at 3.5 cm.

Parameter	Value
Azimuth coverage, deg.	0 to 360 (full)
Elevation coverage, deg.	10 to 89.5
Slew rate, each axis, deg/s	0.25
Pointing accuracy, each axis, single track rms, deg.	< 0.002
Effective collecting area, m^2	2.5×10^3
Transmit-to-receive switch time, s	5
Effective elevation limit, deg	20

Antenna parts description

The main reflector and sub-reflector are shown in fig. 6, along with some other relevant parts.

1. The main reflector:
   The 70-m Goldstone antenna is a fully steerable beam-shaped reflector with horn feeds. Its configuration is Cassegrain[4]. The wavelength of operation 3.5-cm, X-band Greater sensitivity is achieved with the shorter wavelength. The benefit of a very large aperture on the received signal power comes from its variation as the square of the antenna gain. Also, the Cassegrain design positions the feed so the loss in gain associated with waveguide

[4] The Cassegrain reflector is a combination of a primary concave mirror and a secondary convex mirror, often used in optical telescopes and radio antennas. This design puts the focal point at a convenient location behind the primary mirror and the convex secondary adds a telephoto effect creating a much longer focal length in a mechanically short system.

length is minimized. Note that waveguide losses also become more significant as the frequency is increased. The large size of the main reflector makes it possible to mount the feedhorns, low-noise maser[5] amplifiers, and high-power final amplifiers right within the antenna dish.

The main reflector, fig. 6b, surface accuracy is now described:

- The main reflector surface consists of about 1200 precision-shaped aluminum trapezoidal panels individually adjusted for optimum performance by means of screws. Optical techniques and radio frequency holography are used for alignment. While the panels near the center of the dish are solid, the panels near the rim are perforated to reduce weight and the effects of wind.
- Regardless of where the antenna is pointed in azimuth or elevation, the reflecting surface must remain accurate to a fraction of the signal wavelength, meaning that the measured surface across the 3850 m^2 surface has to be within 1 cm of the calculated surface.
- Usually, the accuracy required is 1/16 of a wavelength for near-perfect performance.
- There is some small distortion of the antenna shape as a function of elevation pointing angle, that result in a small loss in gain, due to:
    - the varying stresses from gravity on the structure;
    - wind loading and thermal stress as well can cause the structure to deviate slightly from the preferred theoretical shape.
- The effect of mechanical surface deviations on antenna gain is greatest at smaller wavelengths and is roughly 0.5 dB at 8560 MHz (X-band).

2. The subreflector subsystem

   The subreflector is mounted on a quadripod support structure inside the main antenna dish, and its shape is nearly hyperbolic (fig. 6a). During radar operation at 3.5-cm, the subreflector physically moves to switch the radar system from transmit to receive: the focal point of the subreflector is moved from the transmit to the receive feedhorn. At the origins this motion required about 30 s, the target of a 3.5-cm observation must be at least 4,500,000 km from Earth. This has been improved using a quasi-optical switch that can cycle from transmit to receive in 5 seconds. The same technique is used to switch from 3.5-cm- to 12.9-cm-wavelength operation because the single 12.9-cm receive horn is in a separate feedcone.

[5]Maser stands for microwave amplification by stimulated emission of radiation. A maser is a device that produces coherent electromagnetic waves through amplification by stimulated emission. Modern masers can be designed to generate electromagnetic waves at not only microwave frequencies but also radio and infrared frequencies.

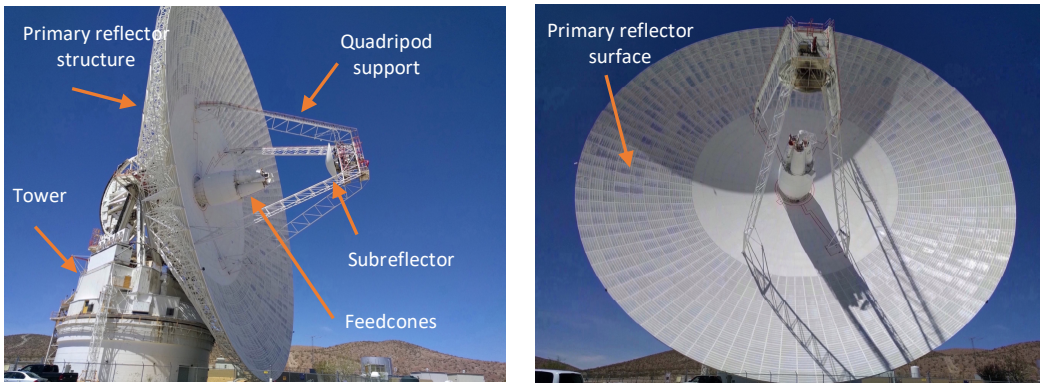

Figure 6. Goldstone 70-m antenna, showing: (a) subreflector, feedcones, quadripod support, primary reflector structure, tower, and (b) primary reflector surface. Images from Goldstone trip on May 4, 2018.

3. The pointing system

   The pointing coordinates are given in right ascension and declination form. The antenna pointing system ensures:

   - a stable, vibration-free platform: installed in the rotatable instrument tower that rises through the center of the pedestal but is completely separate from it,
   - high pointing accuracies: avoiding losses in signal power and permitting the use of signal integration techniques,
   - remote pointing control of the antenna: done from the signal processing center-housed in an adjacent building,
   - access to the entire sky north of declination -50 deg,
   - track a target at declinations near 35 deg for nearly 11 hours, and
   - pointing accuracy maintained during windy conditions: deflections on the order of millidegrees occur with winds of 45 mph.

   The primary high-accuracy pointing method is the master equatorial pointing. The necessary hardware is contained in the instrument tower. The methodology is:

   i. the tower first rotates in response to a pointing command sent from the computer in the signal processing center,
   ii. a light source mounted on the rotating antenna structure aims a beam at a mirror mounted on the rotating tower,
   iii. after several reflections, the beam is ultimately detected by a precise autocollimation light sensor also mounted on the movable antenna structure, and
   iv. this feedback signal controls hydraulic motors that continue moving the antenna until the commanded coordinates are reached.

The receiver subsystem

Receiver subsystem

The receiver amplifies the extremely weak echoes received by the antenna. The receiver must perform this function while adding little noise of its own to the signal. To achieve this:

- special ultralow noise liquid-helium-cooled maser front-end amplifiers is used, and
- the crucial first receiver stages within the antenna are located at a minimum distance from the feedhorns.

The amplified signals from the liquid-helium-cooled masers are then sent to the remainder of the receiving equipment at the base of the antenna. The receiver outputs the amplified signal to the DAS, where analog and digital signal processing is performed.

Stages in the receiver chain:

- Frequencies and polarizations: The nominal frequency at which the receiver can operate is 8560 MHz (3.5-cm wavelength, X-band). The Goldstone receivers can process two orthogonal circular polarizations (left and right circular), while a single circularly polarized signal is transmitted. For signals of either wavelength, there are in effect two identical receiver channels, one for each polarization. By operating two channels, investigators can observe the two polarizations simultaneously.
- Downconversion: The receiver is superheterodyne. This design converts, in steps, the maser-amplified microwave radio signal to lower frequencies called intermediate frequencies (IF). Then downconverts this radar echo to a final IF of 7.5 MHz. This is achieved by a process of mixing, or heterodyning, the echoes with frequency stable, pure sine waves called local oscillators. The advantages of this design are small transmission line losses and high-gain electronic amplification, which is more readily optimized at IF rather than higher microwave frequencies.
- Next stages: In the radar control room, the 3.5-cm (X-band) wavelength signals are selected for further processing; this is achieved through the receiver select module. The selected signal is then passed to the receive-transmit switch module, which prevents the transmitted signal from leaking into the receiver. This module is followed by several IF modules that provide signal gain, mixing, and filtering. The performance parameters of the receiver are listed in following table.

Table 3. Receiver Performance

Parameter	Value
Frequency range, MHz.	8560
Antenna gain, dB	74.55 ± 0.1 dBi
Antenna beamwidth, deg.	0.032 ± 0.003 deg.
Aperture efficiency, %	64
Sensitivity, K/Jansky	0.90
Feed polarization	RC, LC
Pointing loss, dB, 3 σ	0.020
Low-noise amplifier	High-Electron Mobility Transistor (HEMT) Low-Noise Amplifier (LNA)
System temperature, K	18
Intermediate Frequency, MHz	325, 75, 50, 7.5

Microwave subsystem

The microwave subsystem hardware for reception is located in both the 3.5-cm and 12.9-cm feedcones within the antenna. Two separate feedhorns are used at 8560 MHz - one for receive and one for transmit. The 3.5-cm receive horn collects energy from the sub-reflector and passes it to the orthomode[6] transducer, which resolves the signal into right- and left-circular polarization components. From this stage forward to the output of the receiver, there are two identical channels. Next items describe some of the specifics of the microwave subsystem:

- the 3.5-cm orthomode transducer and the masers are cryogenically cooled to a temperature of 4 K to reduce the amount of thermal noise added to the signal - a liquid helium closed-cycle refrigeration system is used,
- the 3.5-cm dual maser is a traveling wave maser with superconducting magnets and klystron (amplifier tube) pumps. The pump frequencies are 19 GHz and 24 GHz,
- the maser is followed by a post-amplifier stage that uses field-effect transistors as the active elements, and
- this output is fed to the 3.5-cm Front-End Module (also in the feedcone) for mixing, amplification, and filtering.

Front-end modules

The received radar signals, even though greatly amplified by the maser low-noise amplifiers of the microwave subsystem, are still extremely weak. Much more amplification is required to increase the signal strength to useful levels. The front-end modules, located in the feedcones, provide the additional needed signal gain. Next items describe some of the specifics of the front-end modules and figure 7 supports graphically the signal path.

- The 3.5-cm front-end module accomplishes this task by using mixers to convert the signal to lower frequencies, amplifiers to boost signal strength, and filters to reject unwanted (spurious) signals. These functions are applied to both polarizations.
- The signal from the microwave subsystem is first applied to a front-end mixer that downconverts the 3.5-cm radio signal to an IF of 325 MHz.
- The local oscillator required by the mixer to do this is located in the pedestal and referenced to the stable DSN Mercury trapped ion frequency standard.
- Typically, an IF amplifier requires a fixed frequency of operation to facilitate the extensive filtering and amplification of the signal. However, the frequency of the echo will vary from the frequency of the transmitted carrier because of the Doppler effect.
- Since the mixer outputs the difference in frequency between the echo and the local oscillator, one mixer input (the local oscillator) must be adjustable if the other mixer input (echo) varies and the output (IF) must remain fixed.

[6] An orthomode transducer (OMT) is a waveguide component. It is commonly referred to as a polarization duplexer. Orthomode transducers serve either to combine or to separate two orthogonally polarized microwave signal paths.

- This "ephemerides tuning" requirement is implemented by a computer-controlled Programmable Local Oscillator (PLO).

Next items describe some more specifics for each wavelength.

- The local oscillator signal used with 3.5-cm signals begins with a frequency of about 25.5 MHz at the pedestal. The signal is sent over coaxial cable to the front-end module in the feedcone, where it is multiplied by an amount necessary to produce 325 MHz when mixed with the 8560-MHz echo. The downconverted signal is now amplified and filtered. The 325-MHz signal is then mixed with a fixed-frequency 400-MHz signal sent from the pedestal over coax; the 400-MHz signal is derived from the frequency and time subsystem 100-MHz reference (the Mercury trapped ion frequency standard). The resulting frequency difference of 75 MHz is filtered and amplified, then output to the pedestal for further processing.

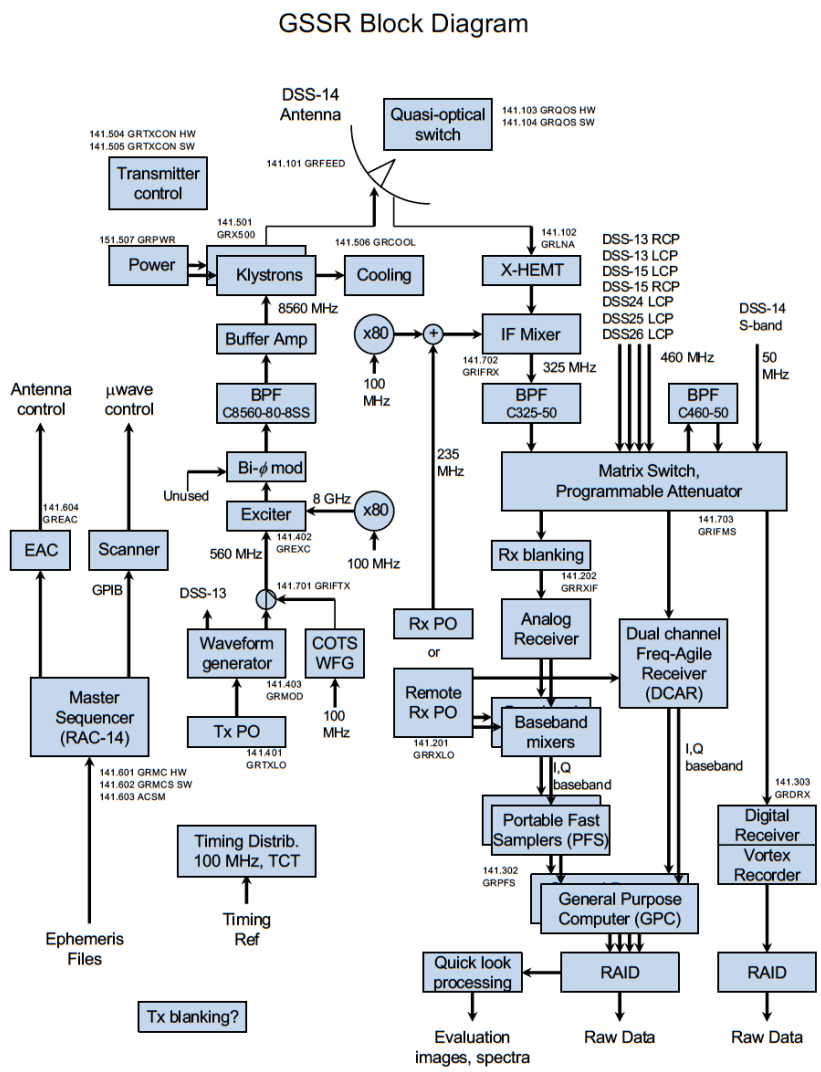

Figure 7. A block diagram of the GSSR hardware – signal path in the DSS-14. HEMT stands for High Electron Mobility Transistor Amplifiers, WFG stands for Waveform Generator.

Intermediate Frequency stages

The IF stages (75 MHz for the 3.5-cm wavelength) in the pedestal provide additional signal gain and filtering to the downconverted radar return signal. Because there is only one pair of IF amplifier stages (one for each of the two polarizations), provision is made for selection of 3.5-cm wavelength signal. Finally, test signals are injected and monitored with test instrumentation to verify subsystem performance and perform troubleshooting. Next items describe the intermediate frequency stages (shown in figure 7):

- The receive signal path begins with the receiver select module in the pedestal room at the base of the antenna. When a switch selects:
  - the IF used by 3.5-cm signals, a 50-MHz difference frequency output is produced by mixing the 75-MHz IF with a 125-MHz local oscillator signal,
- After the receiver select module, signal processing in the pedestal is the same for either wavelength signal.
- The signal is carried to the receive-transmit switch module, which contains attenuators and switches that prevent the transmitted signal from leaking into the receive path and connection points to allow test inputs such as noise to be injected into the receive signal path.
- The next stage, the first IF module, is a 50-MHz intermediate frequency amplifier that provides filtering to approximately a 10-MHz bandwidth and a large signal gain.
- The amplified 50-MHz signal is next split into three paths within this module:
  - one path is output to the final IF amplifier,
  - the second is connected to a filter with a 10-MHz bandwidth. This filter's output can be monitored with a spectrum analyzer, noise measurement instrument, or other test instrumentation. The third 50-MHz signal is applied to a mixer to produce a 10-MHz output that is split into three paths. Two of these paths produce outputs of 10-MHz and are filtered to about 2-MHz bandwidth, and
  - the third 10-MHz path is output to the 10-MHz IF Module. Bandwidth is important because it controls the amount of noise power in the final receiver stage:

$$P_n = kTB \tag{1}$$

where:

k = Boltzmann's constant, 1.38×10^{-23} W*s/K
T = absolute temperature, K
B = bandwidth, Hz
P = maximum power in the load, W

It can be seen from this thermal noise equation that noise power varies directly with receiver bandwidth. The bandwidth must be wide enough to pass the signal, but not so wide as to allow excessive noise to degrade the signal.

- Continuing with signal flow through the receiver, one of the 10-MHz outputs with 2-MHz bandwidth from the first intermediate frequency amplifier is connected to the 10-MHz IF Module. This module splits the 10-MHz input signal into two branches, each of which is filtered. One branch becomes an output of 10 MHz with a reduced bandwidth of 150 kHz, and the other branch is divided into two other 10-MHz outputs, each of which has a narrow 10.8-kHz bandwidth.
- The last stage of the receiver is the Final IF Amplifier, which contains a mixer that downconverts the 50-MHz input to 7.5 MHz. It also provides signal gain and filtering. The 7.5-MHz echo signal output from this last receiver module has been amplified many times since entering the feedhorn; it is now sent to the DAS for analog-to-digital conversion and digital signal processing.

Ephemerides Tuning and Local Oscillators

The DSN frequency and time subsystem maintains an extremely stable Mercury trapped ion time and frequency standard. These reference frequencies are used by the radar system for fixed and variable local oscillators and for the DAS. The fixed and variable frequencies required by the mixers in the receivers are generated from the reference frequencies by the local oscillators in the radar control room. A PLO is used at 3.5-cm wavelengths as the local oscillator input to the first mixer.

In planetary radar, the Doppler shift of the echo is typically not negligible, and in fact, provides important information about the target. If a radar echo changes in frequency because of Doppler shift, the local oscillator must be adjusted in real time to compensate for this change; alternatively, the transmitter's exciter frequency must be adjusted. Goldstone applies most of the correction to the exciter, and a smaller amount of correction to the receiver.

The design goal is to keep the received radar signal centered within the narrow IF passband of the receiver even as the input signal varies in frequency. This generally requires advance knowledge of the object's motion. The orbit of the Earth and its rotational motion are well known. For planets and some other solar system objects, knowledge of the orbital motions (perhaps from optical or previous radar observations) is sufficient to provide a good prediction of the required Doppler compensation. If an object's ephemerides are not well refined, there is uncertainty in the required Doppler compensation. If the magnitude of the uncertainty is small compared with the bandwidth of the receiver, the Doppler shift can be used to refine the ephemerides.

In part, Doppler shift is affected by the motional characteristics of the planet, asteroid, or comet. Rotation, for instance, may be complex; one observed asteroid appears as an irregular shape

rotating about several axes. Mars has a relatively rapid rotation rate on the order of one Earth day and a characteristically large frequency bandwidth. Venus, on the other hand, has a slow rotation of several hundred days per one revolution. Most of the information of interest from Venus is contained in a frequency band only 30 to 80 Hz wide. Therefore, one would choose a narrow-bandwidth receiver to process the signal; but if the Doppler correction is not accurately known, the signal will not appear in the later stages of the receiver although it is present at the front end, where the bandwidth is wider. Thus, a process of refinement of Doppler correction and receiver bandwidth may be required over several target tracks. The procedure uses a wider than optimum receiver bandwidth for first observations and accepts greater than optimum receiver noise power. (Some marginal objects may not even be detectable because of this noise degradation.) The actual Doppler shift of the signal can then be measured; from this measurement, future, more accurate ephemerides are calculated. During the next track, the refined local oscillator (or exciter) settings are used along with a narrower receiver bandwidth. Corrections occur throughout a radar track. Recording the actual measured PLO frequency at the start of a radar track is standard operating procedure to verify proper Doppler compensation. The result of this process is a better signal because of the reduced noise power from a narrower receiver bandwidth and a more accurate knowledge of the ephemerides of the object. Only extremely stable transmitter and receiver local oscillator frequencies allow the Doppler shift to be measured precisely enough to improve knowledge of the rotation rate or the ephemerides or both. The PLO, located in the Goldstone radar control room, is a commercial instrument under digital control via a data bus (IEEE interface) linking the VAX to a MAC-16 dedicated computer. The computer performs Doppler calculations based on ephemerides (from JPL) that have been downloaded to it from the VAX 11/780 general-purpose computer.

Data acquisition subsystem

The data acquisition subsystem (DAS) is critical for conversion of the analog signals from the receiver to digital data (A/D converters) that is recorded to disks for offline data analysis. The receiver performs appropriate signal processing of the LNA's output, depending on the goals of the particular observation. We include the software that is used to command and control the radar in the DAS. Parts of that software use ephemerides information to drive the programmable oscillators (POs) that are an important part of the GSSR system. The POs take input from the DSN's stable master frequency reference.

Chapter 3. The GSSR measurements

This information has been extracted mainly from [1] and [2].

The GSSR measurements are explained through the basic radar equation and a description of its main parameters is provided. Also, the bistatic radar cross section is defined in more detail.

Parameters of the radar echo

A pure sinusoid waveform is transmitted at radio frequencies. At the receiver, the signal is spectrally analyzed, range gated and separated by polarization. Those analysis have successfully provided knowledge of our solar system.

The general equation for the radar echo [24] is:

$$P_{rx} = \frac{P_{tx} G_{tx} G_{rx} \lambda^2}{(4\pi)^3 R_{rx}^2 R_{tx}^2} \sigma \tag{2}$$

where:

- P_{rx} = the echo received power, W
- P_{tx} = the transmitted power, W
- G_{tx} = the antenna gain of the transmitter antenna
- G_{rx} = the antenna gain of the receiver antenna
- λ = the wavelength of radar signal, m
- R_{tx} = the distance from the transmitter to the target, m
- R_{rx} = the distance from the receiver to the target, m
- σ = the radar cross section, m

R_{tx} and R_{rx} are usually assumed to be the same (R), since the difference is minimal. In case of a monostatic measurements, the receiving antenna and the transmitter antenna are the same so eqn. (2) takes the expression:

$$P_{rx} = \frac{P_{tx} G^2 \lambda^2}{(4\pi)^3 R^4} \sigma \tag{3}$$

The received signal carries information on a number of quantities, the amplitude, the time delay, the Doppler shift and the polarization, which are now discussed.

Amplitude

The physical information extracted from the amplitude is shown in next figure.

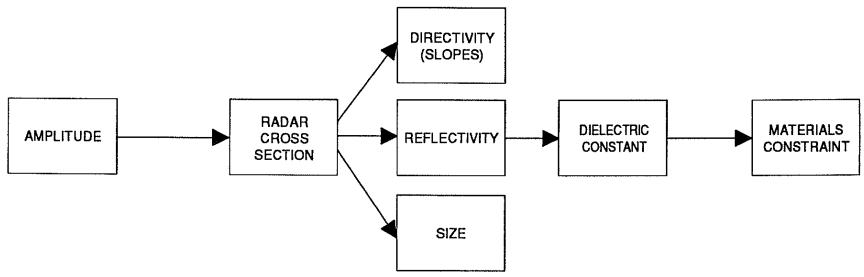

Figure 8. Amplitude of the radar echo related physical information.

The amplitude (strength) of the signal returning from a solar system target has been diminished by the signal's round trip of interplanetary distances. As it was shown in eqn. (3) it decays as R^4. When targets are really far away, echoes cannot even be discerned individually without extensive computer processing. Depending on their bandwidth, many echoes can be added together (integrated) for hours before they can be recognized. As can be seen from eqn. (3), the amplitude of the received signal depends on distance, R, but also on the transmitter power, P_{tx}, antenna gain, G, and how much of the incident energy the target reflects back to the Earth station, σ. As mentioned above, the received signal strength varies inversely as the fourth power of distance and is the primary reason that solar system radar requires the highest power transmitters, largest antenna apertures, and most sensitive receivers. A 3:1 signal-to-noise ratio is usually the minimum required for reliable detectability.

The amplitude, then, determines whether the target can be seen at all, and the echo strength influences the quality of the conclusions and the resolution. In terms of the target, detectability is a function of distance, cross-sectional area, reflectivity (albedo[7]) and the direction and magnitude of the target's spin vector. The strength of the return signal depends on the characteristics of the surface and subsurface material, and the topographic relief or shape of the surface features.

Given that the distance to targets is approximately known and the size can be estimated from optical observations, the strength of the return signal can be predicted quite accurately. Usually, the subradar point has the strongest amplitude because the general orientation of the surface is perpendicular to the line of sight, so the radar wave is reflected directly to the Earth station.

When analyzing radar data looking at the amplitude magnitude there are light and dark areas:

[7] The albedo of a radar target is the fraction of radar energy striking the target that has been scattered back to the observer. The product of the albedo and the size of the target gives the target's net radar reflectivity

- radar dark: rough surfaces, smooth surfaces sloped so that the incident wave reflects into space away from Earth, or surfaces very absorptive of radio waves at the wavelength used.
- radar bright: smooth and highly reflective surfaces, rough surfaces with the right slope to reflect the wave back to Earth.

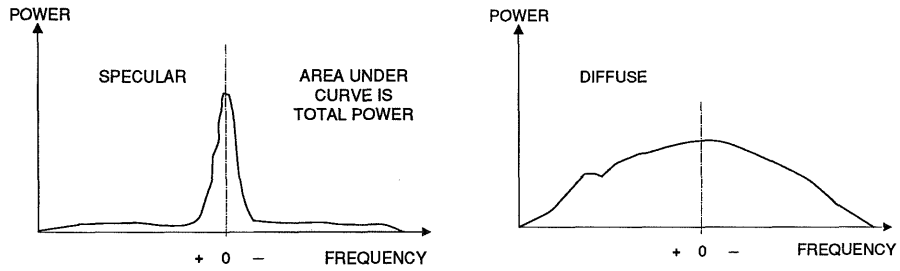

Figure 9. Different types of echoes, (left) smooth specular echoes, and (right) rough diffuse echoes.

In general, smooth areas give echoes that look like a sharp spike, and rough areas produce diffuse echoes. The state of the same material may change with temperature, influencing the radar signature. Water and water ice reflect differently, for example.

Examples of findings:

- On Mars, the reflectivity of the Solis Lacus region was measured at several seasons during the Martian year, and characteristic changes in the radar signature indicate the possible presence of near-surface liquid water [25].
- Jupiter's Galilean satellites Europa, Ganymede, and Callisto have very strong radar echoes and have extraordinary polarization. They have unexpectedly high geometric albedo relative to most other solar system objects, with Europa reflecting nearly as much energy (in one polarization) as that of a metal sphere [26].

Doppler Frequency Shift

The physical information extracted from the Doppler shift is shown in next figure.

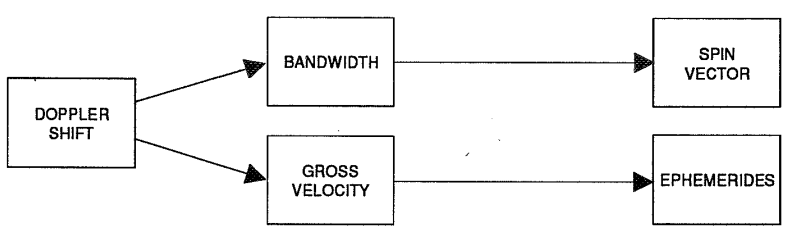

Figure 10. Doppler frequency of the radar echo related physical information

The Doppler frequency shift is the change in frequency from the transmitted to the received signal. Spectrally pure, single-frequency waves are transmitted to the target, but when the radar signal is reflected from an object in relative motion to the Earth-based radar station, its frequency changes and its frequency spectrum broadens. The amount of change depends on the relative velocity along the line of sight, which includes:

- the Earth rotation,
- the difference in orbital velocities (gross motion) between Earth and the planet, and
- the rotational motion of the object.

The echo spectral shape alone provides information about the target. Doppler shift is usually analyzed by forming its frequency spectrum, which resolves the dispersion[8] into frequency cells or bins. Assuming a spherical target, the spectrum often appears to have a central peak and left and right "skirts", see figure:

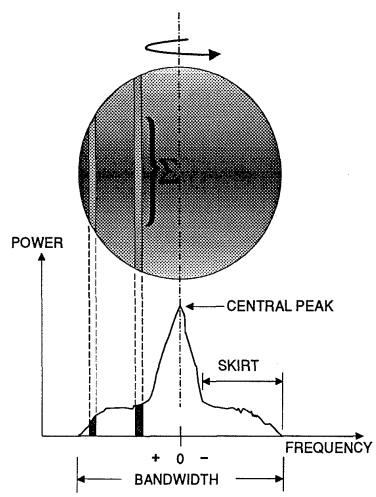

Figure 11 Constant Doppler regions.

- On one hand, the center frequency gives the Doppler frequency shift of the subradar point and so the line-of sight velocity or gross motion.

- On the other hand, the frequency spread is caused by target rotation. Spectrum bandwidth is measured from skirt edge to skirt edge: large, fast-rotating objects have a large radial velocity component and therefore a wide band width, while slower rotators have a narrow frequency spread.

Doppler measurements enable investigators to make extremely accurate orbital velocity measurements; on the order of 1 or 2 cm/s accuracy. The ephemerides of the objects can be refined from this data.

[8] Dispersion here refers to the difference between the highest and lowest frequencies.

The Doppler equation (eqn. (4)) predicts the amount of overall frequency shift in the echo, and eqn. (5) describes the bandwidth of the signal.

$$\Delta f = \frac{2\vec{v} \cdot \vec{r}}{\lambda} \tag{4}$$

$$B = \frac{4\pi D}{\lambda P} \sin(\alpha) \tag{5}$$

where:

- Δf = Doppler shift, Hz
- $\vec{v}$ = relative velocity along the line of sight to the radar, m/s
- $\vec{r}$ = unit vector along the line of sight to the radar
- λ = wavelength, m
- B = bandwidth of Doppler spread, Hz
- D = the width, measured normal to the line of sight, of the object's polar silhouette, m
- α = the aspect angle, between the line of sight and the apparent spin vector, rad
- P = target rotation period, s

The spectrum width depends on object size, apparent spin period, wavelength, and the angle of the pole with respect to the line of sight from the target to the radar:

- when viewed parallel with the pole or spin axis (polar silhouette), Doppler broadening would be zero;
- when viewed perpendicular to the apparent spin axis, Doppler broadening would be maximum.

When looking at dispersions, the limb-to-limb bandwidth is only the projection of the radial velocity, not the actual velocity. To obtain actual velocity, the viewing geometry is important. Figure shows the extreme aspect angles of 0 deg (polar aspect) and 90 deg (equatorial aspect):

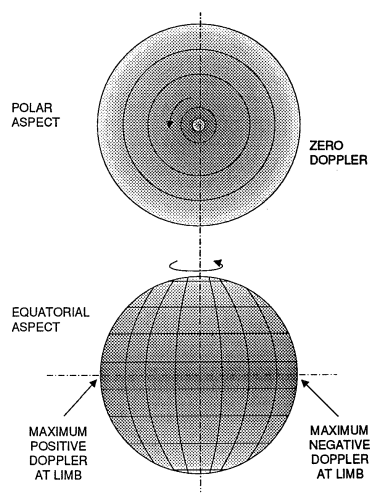

Figure 12. Polar and equatorial aspects

The line of sight must be perpendicular to the equator (90 deg) to get the peak bandwidth. A further complication is that the orbital motion causes an apparent spin that algebraically adds to the actual rotation. This effect can be quantified and removed.

A region of constant Doppler (fig. 11) is a strip parallel to the apparent spin axis; the part of the sphere approaching has a positive Doppler shift (increasing frequency), while the receding part has a negative frequency shift.

Some information is given by examining the whole frequency spectrum:

- If the target were a smooth sphere and highly reflective, a very bright return would be expected at the subradar bounce point, with very little energy returned from the limbs. This type of target produces a spectrum with a sharp central peak.
- If the target were rough, half power points are wide apart and the skirts are thick. The reason is that a rough surface does not have as strong a dependence on the angle of incidence at regions near the limbs.

When a series of time-contiguous frames is examined features can be observed moving through Doppler frequency spectra. Although a given point on a frequency spectrum represents the sum of all energy reflected from a vertical strip, the latitude of major surface features can be resolved by noting the passage of the features as they traverse the frequency spectrum with planet rotation.

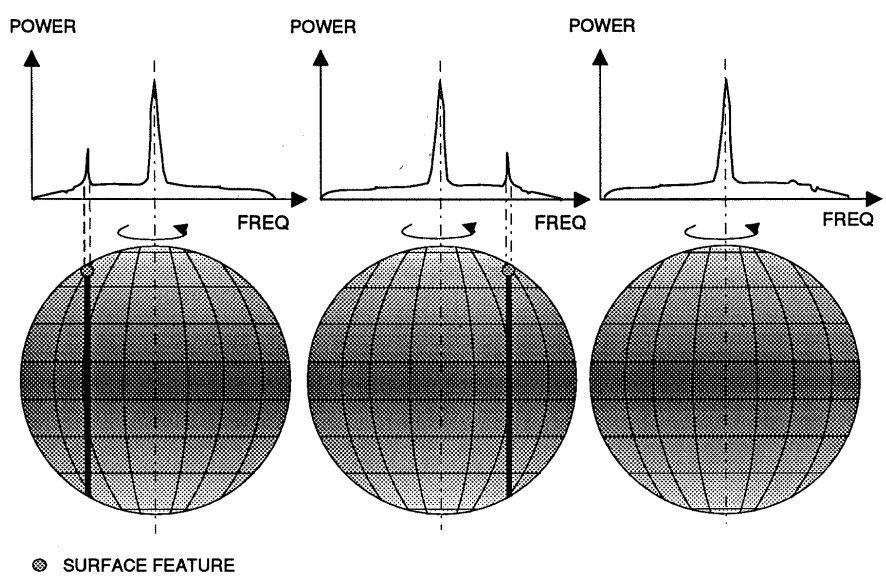

Figure 13. Tracking a surface feature.

The span of the left-to-right movement in the spectrum depends on the latitude of the anomalous reflection. Features present in the equatorial regions will be observed traversing the complete limb-to-limb span, but polar features will move only near the center of the spectrum.

Since an "ephemerides-tuned" receiver is used, the echo's central peak position, left to right, indicates the error in ephemerides.

Examples of findings:

- In the 1960s, Dr. Richard Goldstein of JPL conducted planetary radar experiments at 12.5 cm using the Goldstone facility. The ephemerides-tuned receivers then in use kept the frequency within 1/4 Hz. The frequency resolution of the receivers' local oscillators was as fine as 1/32 Hz.
- Given the narrow bandwidth of some targets, it can be seen that extraordinarily stable frequency references are needed to avoid blurring the frequency data. Venus has a bandwidth of only about 30 Hz at 12.9-cm wavelength, depending on when it is measured, and if this dispersion is divided into 100 frequency bins 0.3 Hz wide, a frequency stability of about several parts in 10" is needed to avoid smearing the data. Stable tuning is also required to keep the signal within the very narrow range of frequencies that the receiver will pass. Doppler shift and antenna pointing ephemerides are major unknowns at first observation, especially for newly discovered objects. The rotation of a planet during one observation time (one round-trip light time) is significant if the angular velocity is high. In this case, the subradar point shifts slightly during one transmit-receive cycle. High spin rates can produce blurred spectral images like those of camera snapshots of fast motion taken with too long an exposure. The choice of measurement time for a specific target is influenced by this phenomenon.
- The round-trip light time for Mars, for example, is about 11 minutes, which is also significant in choosing the echo integration time. Mars can be a problem target, since it rotates relatively fast at 0.25 deg of longitude per minute; Venus and Mercury, however, rotate more slowly. On Venus, the longitude of the subradar point changes by only 0.85 deg per day. This means that the echoes from the subradar strip can be integrated for minutes or longer without blurring. Thus a trade-off exists: on one hand, there are long integration times and better signal-to-noise ratios and, on the other, there is high resolution along the frequency axis.
- Mars is a difficult target also because the echo power is spread out over a large bandwidth, resulting in weak spectral densities. For purposes of comparison, there is a 200: 1 ratio in Venus-to-Mars bandwidth. Even if the total power of the Mars echo were the same as that of one from Venus, an echo from Mars would have a worse signal-to-noise ratio (weaker power spectral density). The Mars limb-to-limb bandwidth is about 8,000 Hz at 12.5-cm wavelength and 30,000 Hz at 3.5-cm wavelength.

Time delay (range)

The physical information extracted from the time delay is shown in next figure.

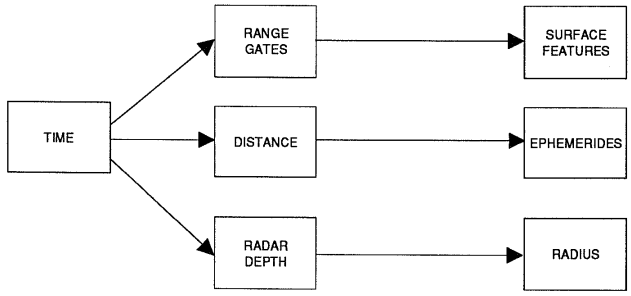

Figure 14. Time delay of the radar echo related physical information.

Typically, a radar experiment is done by transmitting to the target for the round-trip light time, and then listening for the echo with the receiver for a similar time. Because an individual signal is weak, many such cycles are usually repeated, and the echoes are added together to increase their strength. This overall process is one observation. Radar ranging measures the round-trip light time to the target, and from this measurement the distance R can be calculated using the speed of light c, and time t:

$$R = \frac{ct}{2} \tag{6}$$

The measurement is made from the time the signal leaves the transmitter to the time it arrives at the receiver.

The overall time of flight can be predicted in advance, given an accurate ephemerides. For example:

- the Moon: is the closest target in the solar system and the round-trip light time is 2.5 seconds.
- the rings of Saturn: are the furthest detectable target and the time is at least 2.5 hours.

The distance of various points on the planet's surface can be determined by measuring the corresponding echo time. Each radar installation has a reference point for precise time measurements. The antennas for planetary radar are so large and the time so accurately measured that an arbitrary specific point, such as the top of an antenna feedcone, is designated the reference point.

On a spherical target, an area of constant range is a ring or annulus concentric with the subradar point. Figure 15, shows the rings of constant delays. As the time resolution increases to the order of several microseconds, the region of constant range no longer is a set of exact concentric circles. Instead, it is defined by the topography.

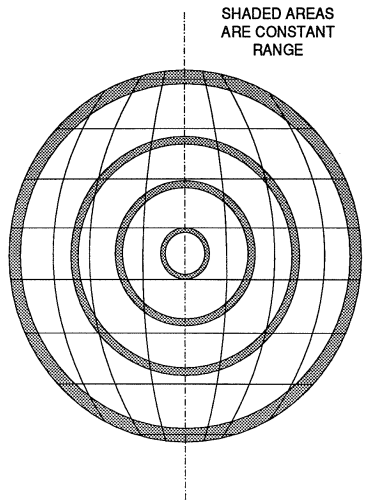

Figure 15. Constant range rings.

Signals with various delays are organized into range gates. A range gate is a device that accepts or passes signals from one range or time delay and rejects all others. For spherical targets such as the planets, the signal in one range gate is the summation of all energy reflected from a constant range ring.

- The overall distance to the surface is measured by the earliest range gate, the one corresponding to the subradar bounce point.
- Later range gates measure reflections from constant range rings successively farther back from this point.

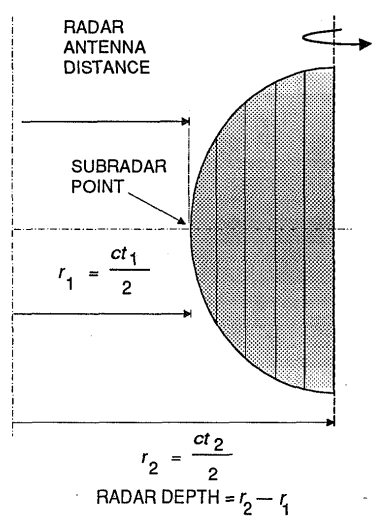

Figure 16. Ranging

Near the subradar region, the range-Doppler cells give poor resolution in latitude and longitude, but good resolution in altitude.

- In early experiments, the transmitter was keyed off-and on so that the radio quiet background noise level could be measured. It was against this extremely low-level of cosmic background noise that a change in noise level was noted, indicating target detection.
- Current practice is to apply time modulation to the transmit waveform to perform ranging. If a 1-μs pulse were transmitted, the resolution would be 150 m. But the energy in only one transmitted pulse may not be sufficient for detection. Usually, the echoes are added together or integrated; both coherent and incoherent integrations are used. The signal-to-noise ratio improves because the signals add coherently, but the noise does not. Radar astronomers modulate the transmitted signals with binary phase-coded continuous waveforms that change only in phase, and often the transmitter remains switched on for nearly the round-trip light time so maximum energy can be collected. At the end of the round-trip light time, the antenna is switched to the receiver to listen for the echo, and the signal is demodulated by looking for a replica of the transmitted waveform at the receiver. When the echo matches, the signal has peaked and this is considered the instant when the signal has been received. The time delay of the radar signal is measured precisely, using Goldstone's ultrastable Mercury trapped ion time reference. The speed at which the radar wave travels through vacuum is well known. The result is the distance to the point of reflection measured with great accuracy.

The subradar point has the shortest time delay. The difference between the shortest and longest delays is the range dispersion, radar depth, and the corresponding distance should match well with the radius of the planet. In practice, the strength of the signal at the subradar range gate is usually much greater than the signals from gates corresponding to points further away. Generally, this is explained by backscattering. Near the limbs, the average angle of the surface is such that the radar wave is predominantly reflected into space away from Earth, except for reflections from rough areas.

Delay-Doppler Mapping

The beam width of the antenna, a function of the antenna pattern, usually illuminates the entire visible hemisphere of the planet, and many of these areas return echoes. The echoes from each surface patch have an amplitude, direction, polarization, delay, and phase that depend on the orientation, composition, and location of the surface patch. Performing a Fourier transform on range gates produces a frequency spectrum from this, delay-Doppler maps are created.

Forming delay-Doppler maps is a way to resolve the composite return signal in terms of the latitude and longitude of the target. For near-spherical targets, it is seen that concentric rings are regions of constant delay. Echoes from one of these rings fall into one range gate, that is, energy

from all points on the ring is combined into one composite quantity. Generally, it is not possible to resolve points along the ring, if only time is considered. Using both time delay and frequency provides two dimensions and resolves the ring of constant delay and the constant Doppler strip.

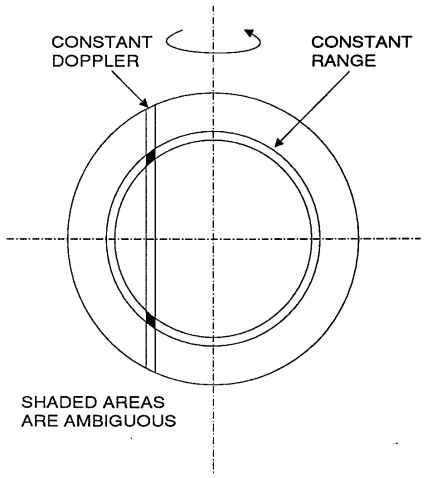

Figure 17. North-South Ambiguity

A delay-Doppler cell is the intersection of a concentric ring with a strip parallel to the spin axis and many of these cells combine to form a delay-Doppler map. Since both positive and negative Doppler shift can be uniquely identified, a surface patch is resolved except for a north-south hemispherical ambiguity points in the northern hemisphere have conjugate points in the southern hemisphere. The reflections from both of these surface points fall in the same delay-Doppler cell. It is not possible to resolve the source of the echo with only one monostatic observation, but the areas can be resolved if the viewing geometry changes.

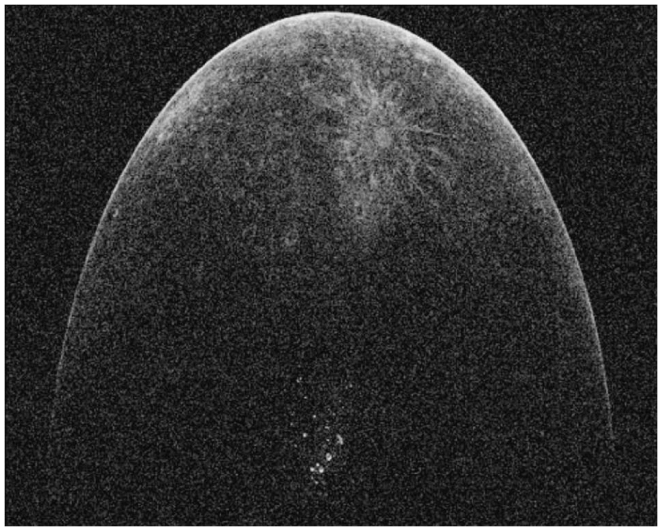

Figure 18. Example of a Delay-Doppler map of Mercury obtained on June 16, 2000, at Arecibo, [27], [12]. The leading edge of the radar echo is the parabolic locus that is brightest at the top. The North Pole craters that are filled with radar-bright material (putatively water ice) are at the bottom. The delay resolution is 3 km.

A trade-off usually exists between the delay resolution and the Doppler resolution. Multistatic observations are also a way to resolve this problem.

Examples of findings:

- Present interplanetary time-delay measurements have been used to test Einstein's theory of relativity. Measurements of the orbit of Mercury tend to verify the theory that echoes from radar waves passing near the Sun have extra delay caused by the Sun's gravitational distortion of space.
- In the 1960s, the first JPL radar studies of the time delay to Venus were important in establishing the value of the astronomical unit (the mean radius of the Earth's orbit), some 150 million km. The precision of the measurement was on the order of microseconds, giving an accuracy of better than 1 km. This was an order of magnitude improvement over the optical-based data then available; subsequent radar data refined the measurement by an additional factor of one hundred.
- Measurement of the astronomical unit to such great accuracy allowed refinement of planetary ephemerides, which are essential for interplanetary spacecraft navigation.
- One simplifying assumption useful in early experiments was that the planets were spherical. However, real planets are not exactly spherical, but slightly oblate, and they have varied topography. In accurate ranging experiments, the topography of a planet is accounted for, if possible.

Polarization

The physical information extracted from the polarization is shown in next figure.

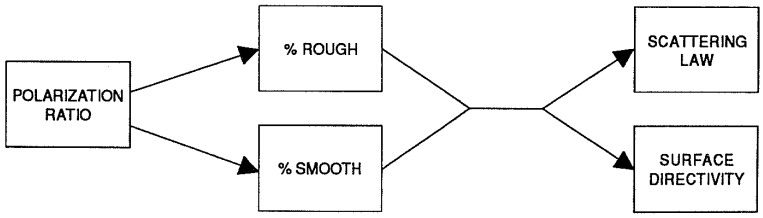

Figure 19. Polarization of the radar echo related physical information.

Analysis of the polarization of planetary radar signatures can add insights into the nature of the surface and near surface. Usually, Goldstone transmits a radio wave that is completely right-circularly polarized. Circularly polarized waves reverse their sense upon reflection from a smooth surface. If right-circular polarization is transmitted, left-circular will be received after reflection. These polarizations are conventionally described as same sense (SC) for the same sense as that transmitted, and opposite sense (OC), for the opposite sense to that transmitted.

- A relatively smooth reflecting surface, designated a quasi-specular reflector, will reflect almost all the energy in the opposite sense.
- A rough reflector will reflect considerable energy in the same sense

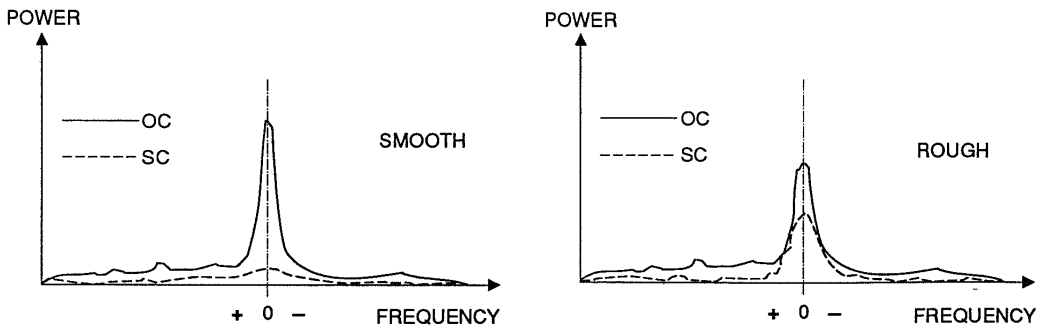

Figure 20. Echoes in two polarizations.

If both the same and opposite polarization sense components of the echo are measured simultaneously, the amount of near-surface roughness on the order of a radar wavelength can be estimated. This quantity is called the polarization ratio μ_c and is formed from the radar cross sections of same sense (σ_{SC}) and radar cross section of opposite sense (σ_{OC}) polarizations:

$$\mu_c = \frac{\sigma_{SC}}{\sigma_{OC}} \tag{7}$$

- Low μ_c (near zero) means reflections from smooth-surface elements are the dominant source of the echo.
- A ratio near one or larger means a very rough surface on the order of a radar wavelength.
- In between are the quasi-specular reflectors.

From experience, most echoes have both a specular and a diffuse component. The polarization ratio can be calculated at each point in the frequency spectrum, adding further value to the range-Doppler matrix. It may be possible, for example, to localize the smooth and rough areas from their position in the frequency spectrum, because the center or zero Doppler is at the subradar point, and the edges of the spectrum are near the limbs.

Examples of findings:

- ❖ Certain features on Mercury have the ability to depolarize waves, becoming randomly polarized, more than adjacent areas; these are the rougher areas. Using the Goldstone Solar System Radar, JPL scientists have found that on Mercury, rough features are more frequent at middle latitudes than near the polar regions.
- ❖ On Venus, the bright region Alpha and Beta were found to be depolarized regions; that is, they are rough regions and good reflectors.

Degree of Polarization

The resolution of two circularly polarized channels to provide a gross estimate of surface roughness is achieved through a four-parameter Stokes vector of circular polarization. The circular polarization is obtained from two simultaneous antenna outputs, one left-circularly polarized and the other right. Both outputs must be in complex form (I and Q components). The four parameters necessary for the vector are:

- the sum of the left and right received polarized power,
- the excess of left over right, and
- two quantities that result from a cross correlation of the left and right outputs.

These four Stokes parameters enable resolution of the two circularly polarized channels into polarized and depolarized components, which in turn provide the degree of polarization, which is the ratio of received polarized power to received total power. From the degree of polarization, the estimate of surface roughness of a hard target can be made.

Example of findings:

- The typical circular polarization ratio for solid solar system objects is about 0.1.
- Recent Goldstone/VLA imaging of Mercury has shown the circular polarization ratio, μ_c, of the north polar region to be about 1.0 to 1.4 [12], a value similar to that for icy regions observed elsewhere in the solar system. The radar observations are interpreted as water ice.

Farday Rotation Effect

When a radio wave leaves or returns to Earth and passes through the ionosphere and terrestrial magnetic field, it experiences Faraday rotation of its polarization. This effect is dependent on the square of frequency and is small at the 3.5-cm wavelength. The Faraday rotation effect on linearly polarized waves changes their polarization. With circular polarization, the effect of Faraday rotation is avoided.

Radar Cross Section σ

The radar cross section σ is a measure of how well a target reflects radio waves. A target that is a good "mirror" to radio waves will have a high radar cross section (RCS). More exactly, the radar cross section is the total power scattered in the direction of the receiver divided by the total incident power. The RCS depends only on the target: it is a disk-integrated quantity that depends on the summation of all echoes from all points on the surface.

The transmitter power, antenna gain, wavelength, and usually the distance are known, eqn. (2) can be used to determine the experimental RCS by solving for s. In other words, measurement of the actual RCS demands accurate determination of the radar system characteristics because the

absolute echo power is used to calculate RCS. The strength of the echo, after the other parameters have been accounted for, depends only on how well the target reflects the radar wave. The RCS can vary with the wavelength and polarization of the transmitted radar signal. Generally, the RCS can be further resolved into several components, all of which are functions of target geometry and composition:

$$\sigma = \pi a^2 g \rho \tag{8}$$

where

- σ = radar cross section, m2
- a = radius of target, m
- g = the directivity or gain of the surface (slope)
- ρ = reflectivity (dependent on target materials)

Examples of findings:

- In 1961 it had been determined by JPL investigators that the RCS ratio of Venus is about 11%. This means Venus reflects back to the radar station 11 % of the 12.5-cm radar energy that impinges upon it.
- In another early study, JPL radar astronomers using the Goldstone facilities determined the reflectance of Mars to be 3.2%. To a first approximation, the energy not received was: absorbed by the target as a wave transmitted into the medium of the near surface, absorbed by the target atmosphere, or reflected into space in a direction away from the receiving antenna.

The RCS is further dependent on:

- the basic size of the object, a large target will return more energy than a small one,
- the surface slope and roughness, and
- the type of surface and near-surface material.

Usually, the data acquired are the product of several factors rather than that of an isolated factor. Other constraints are needed to resolve the RCS into its individual components. Sometimes, existing knowledge of an object (perhaps from optical light curves or previous radar experiments) can be applied to the new radar data to constrain each component of RCS.

The different variables in eqn. (6) are now explained.

Directivity (g)

The directivity of a target surface is a measure of the complex geometry of the planetary surface and possibly the subsurface: it is the ratio of signal power scattered in a particular direction (per

unit solid angle) to the power scattered in all directions (per unit solid angle). The directivity mainly depends on three aspects:

- Orientation. The directivity of a surface area depends on its angle of orientation relative to the line of sight to the radar; the radar wave reflects from the surface in the way that the angle of incidence equals the angle of reflection. When the surface is perpendicular to the line of sight, maximum energy is returned. This principle of orientation rises in complexity with the complexity of the surface: from the simplest smooth plain through one strewn with boulders, solidified lava flows, or craters.

- Shape. Net directivity varies with the overall shape of the target. To a first approximation, planets are spherical; this is not a bad assumption for Venus, since it is only slightly oblate. The directivity for a sphere or a near sphere with gentle slopes (about 3 deg or less) is 1. For a uniformly rough (Lambert) sphere, directivity is 8/3. The directivity is larger for the rough sphere, because more energy is returned from the area near the limbs, where the rough areas scatter energy about in many directions.

    - Rough areas are radar bright at larger angles of incidence since these areas scatter energy in many directions, including the direction back to the radar antenna.
    - Near the subradar point or at small angles of incidence, rough areas are radar dark.
    - Smooth surface patches reflect energy mostly in one direction and so look dark unless they are oriented to the radar's line of sight.
    - The frequency spectrum of a smooth, spherical targets have most of the energy returned from the subradar point. The radar signature from a rough target shows more power away from the central peak; that is, the skirts are thicker.

- Local surface features. Directivity is also influenced by local surface features. An approximate relative brightness at a point on the surface could be predicted, given the basic shape of the target. Large departures from this prediction might mean a rougher or smoother surface than expected, or that the shape deviates from the expected shape. Asteroids vary greatly in their surface smoothness, and many asteroids have been found to be extremely rough.

Examples of findings:

❖ A model using a Gaussian scattering law has predicted at least a 20-deg surface slope for the asteroid Pallas, [26].

Describing a planetary surface, even if it were as well known to us as that of Earth, is obviously a complicated geometric problem; directivity can be different at every point. Polarization ratios, which quantify the relative proportion of rough and smooth areas, can help constrain the determination of surface slopes.

Different kinds of surfaces can be quantified, on an average, through use of a mean surface slope. Mathematical models have been developed to describe the mean slope of a planet's entire visible hemisphere. These models make assumptions about the overall statistics of surface slopes, such as whether the distributions are exponential or Gaussian. The models are checked against the radar data for best fit. An area with large mean or rms surface slope is rough on the average, possibly with jagged mountains, craters, boulders, or strewn with rocks, while an area with small mean surface slope is smoother.

Examples of findings:

- A type of analytical technique using mean surface slopes, the angle of incidence, and the backscatter function has been applied to radar data sets from Venus [28].

Backscatter function (σ)

The backscatter function describes the average power reflected from the surface as a function of the angle of incidence. An equation as (9) describes large-scale geometry and gross shape:

$$\sigma(\phi) \propto \frac{\rho_0 C}{2}[cos^2\phi + Csin^2\phi] - 3/2 \tag{9}$$

where:

- σ = radar cross section, m2
- ϕ = angle of incidence, radians
- ρ_0 = reflectivity
- C = Hagfors' parameter for slopes

The simplest model of a planet usually used is that of a uniformly rough sphere, the Lambert scatterer. The Lambert scattering law for a such a sphere is a cosine-squared function. The Hagfors model gives a good fit to measured data for angles of incidence of 50 deg and is most accurate for the region near the subradar point.

Reflectivity and dielectric constant (ρ, ε)

The nature of the surface material, metals, gases, ices, water, rock, and soils in various stages of compaction, each have different radar reflectivity. Reflectivity is the efficiency of reflection, that

is, energy output divided by energy input, regardless of the reflection angle. Metallic concentrations make good reflectors and appear radar bright. Reflectivity of solar system objects varies over a wide range

Example of findings:

- On Mars, there is an area called Stealth because it returns no echo, [15]. Stealth has very low reflectivity and has been studied at normal incidence angles [29].
- Jupiter and Saturn are examples where the sizes are large enough that a good echo should be received, but this is not the case, because their atmospheric absorption of the radar signal makes them targets with low reflectivity.
- Even though signatures from the moons of Jupiter are obtainable (Callisto, Europa, and Ganymede have high reflectivity), Jupiter itself has not returned unmistakable echoes.

When a radar wave passes from one medium to another, it is reflected in a predictable way. This occurs, for example, when a wave passes from the vacuum of space or the atmosphere of a planet to the planet's solid surface. The reflection occurs at the interface between the two materials and depends on the dielectric constants of the two media.

The dielectric constant is an important mathematical link between radar reflectivity (from radar cross section measurements) and near-surface material properties, because it can constrain the bulk density. The following equation applies:

$$\varepsilon = \left|\frac{1+\sqrt{\rho}}{1-\sqrt{\rho}}\right|^2 \tag{10}$$

If the reflectivity of a surface type is known, the average dielectric constant can be estimated. Although this is a constraint on the material, it may not be possible to uniquely determine the material from the dielectric constant.

- Materials of the same chemical composition may have different dielectric constants because they have different physical states: solid, liquid, or various degrees of pulverization.
- Different substances may have the same dielectric constant.

It is possible to constrain the material, however, if accessory information is available: the polarization ratio can sometimes be used to constrain the average dielectric constant, for example.

Example of findings:

- Dry or sandy soil on Earth is known to have a dielectric constant of 3.75.
- Using the Goldstone Solar System Radar during the 1960s, JPL experimenters determined the average dielectric constant of an observed area on Venus to be 3.75.

Chapter 4. Applications

This information has been extracted mainly from [1] and [2].

There are a number of relevant applications for the measured data:

- ephemerides,
- surface characteristics, topography and radar maps,
- bulk density and porosity,
- spin vectors, and
- multiparticle systems.

Those applications are defined now.

Ephemerides

Because the orbits of planets and asteroids essentially follow mathematical laws (first discovered by Kepler), future apparitions of the object can be predicted. To predict orbits, the velocity of the planet and its distance from Earth must be determined from three viewing locations; planetary radar does this very well. The predictions, called ephemerides, are needed for the navigation of interplanetary space probes and for such scientific experiments as tests of the theory of general relativity. The predictability of the orbits is affected by some factors that impact its precision.

Example of findings:

- The mass of asteroids in the main asteroid belt, for example, may be sufficient to perturb the orbit of Mars.
- Mercury is affected by solar oblateness and relativity effects.
- Earth is part of a complicated Earth-Moon system and exhibits polar drift.

Orbits are described by a set of numbers called Keplerian elements. Once the Keplerian element set of any planet has degraded to the point that accurate ephemerides cannot be generated from it, a new set of orbital elements must be obtained. Doppler spectroscopy and radar ranging provide the needed data; the new orbital elements are computed, and the ephemerides are once again precise.

The refinement of planetary ephemerides can be performed by measurements of orbiting spacecraft; however, these spacecrafts are not always available. At such times, it is essential to perform Earth-based radar ranging to the terrestrial planets Mercury, Venus, and Mars. Continued radar ranging of these three planets is necessary to maintain the integrity of their orbital predictions.

The first task in determining the ephemerides of a newly discovered asteroid is an initial estimation of its orbit in the hope that recurrent close apparitions can be predicted; a correct prediction is called the recovery of an asteroid. When tracking a new target with radar, antenna pointing may

not be perfect because of limited angular position information, and this may cause some loss in signal strength, according to the pattern of the antenna. Assuming the coordinates are good enough to at least track the object, radar experiments will initially be performed using dual-polarization Doppler spectroscopy (continuous-wave measurements), which determines the gross velocity to an accuracy of about 1 part in 105. These data are fed back to the tracking system and used to refine the receiver tuning. Next, ranging measurements will be made. Depending on signal strength and the amount of data, the spin vector, shape, and surface properties may be determined at this point. Also, note that asteroids are very difficult objects to observe optically because of their small size and because the illumination is not under the control of the observer.

Time-delay (distance) and Doppler-shift (velocity) data from the Goldstone planetary radar station provide orbit information complementary to that of optical measurements, which are typically celestial angular coordinates. Radar coordinates are orthogonal to the optical coordinates; both are normally needed. Typical uncertainties for recent time-delay measurements are on the order of a microsecond, corresponding to position uncertainties of only a few hundred meters. The additional use of data gathered with only a few radar observations greatly improves future orbital predictions, especially for objects with a small number of optical measurements. The best data are gained from radar during the object's closest approach to Earth, because then the echoes are strong and clear.

Example of findings:

- Astrometric radar data were first used to refine the orbit of an asteroid in 1968 when Icarus was probed by the ground-based radar facilities of JPL at Goldstone and MIT at Haystack.
- At least 138 main belt asteroids (MBAs, in orbit in the asteroid belt between Earth and Mars), 754 near-Earth asteroids (NEAs, orbits that cross the orbit of Earth), and 20 comets have been observed by radar. Current totals are updated regularly at: http://echo.jpl.nasa.gov/asteroids/index.html. The following figure shows how these detections are exponentially growing.

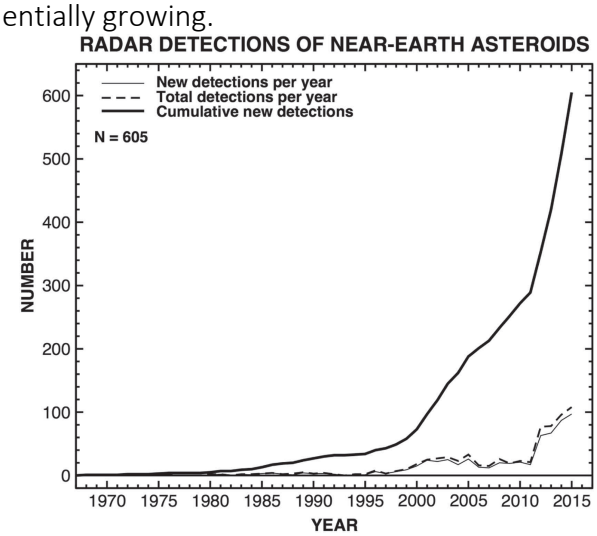

Figure 21. Total number of near-Earth asteroids detected by ground-based radar facilities each year until 2015. The cumulative number of radar detections as a function of time is shown using a solid bold line.

- For NEA Icarus, the orbital path as observed by radar could not be explained by gravitational forces alone. One plausible explanation is a rocket-like thrust that acts on and originates from the comet's nucleus as a result of ice vaporization (sublimation). Thus an "asteroid may actually be an older, but not yet extinct, comet.
- The first comet observed with Earth based radar was Encke, [30].

A large population of NEAs are on Earth approach and may even intersect the orbit of Earth. There is a critical need to accurately monitor possible "megaton impactors." Precise extrapolations of asteroid motions can be accomplished most readily by using radar data obtained during close approaches.

Following there is an example of ephemerides file for asteroid 2013 US3. Last observation of the asteroid happened on April 24, 2018. It is classified as potentially hazardous. The absolute magnitude is about 200 meters. Given the narrow bandwidth observed, the asteroid is likely to be a slow rotator (rotation period is high) or it was seen from pole (aspect angle α tends to zero if viewed parallel to the pole or spin axis). Example of ephemerides file obtained from https://ssd.jpl.nasa.gov/horizons.cgi#top

```
*******************************************************************************
JPL/HORIZONS                    (2013 US3)              2018-Apr-24 19:28:52
Rec #:  738069 (+COV) Soln.date: 2018-Apr-23_07:30:22    # obs: 154 (2013-2018)

IAU76/J2000 helio. ecliptic osc. elements (au, days, deg., period=Julian yrs):

  EPOCH=  2457027.5 ! 2015-Jan-05.00 (TDB)        Residual RMS= .32064
   EC= .184538897679618    QR= .9787110538317922   TP= 2457236.0170146925
   OM= 39.64538793353396   W=  133.6133462437278   IN= 12.31376050937569
   A= 1.20019342559306     MA= 203.6964984604631   ADIST= 1.421675797354328
   PER= 1.31488            N= .74959589            ANGMOM= .018521807
   DAN= 1.32842            DDN= 1.02841            L= 173.9250301
   B= 8.8823632            MOID= .0201756          TP= 2015-Aug-01.5170146925

Asteroid physical parameters (km, seconds, rotational period in hours):
   GM= n.a.                RAD= n.a.               ROTPER= n.a.
   H= 21.1                 G= .150                 B-V= n.a.
                      ALBEDO= n.a.            STYP= n.a.

ASTEROID comments:
1: soln ref.= JPL#41, PHA  OCC=0
2: source=ORB
*******************************************************************************

*******************************************************************************
Ephemerides / WWW_USER Tue Apr 24 19:28:52 2018 Pasadena, USA      / Horizons
*******************************************************************************
Target body name: (2013 US3)                    {source: JPL#41}
Center body name: Earth (399)                   {source: DE431}
Center-site name: GEOCENTRIC
*******************************************************************************
Start time      : A.D. 2018-Apr-24 00:00:00.0000 UT
Stop  time      : A.D. 2018-May-24 00:00:00.0000 UT
Step-size       : 1440 minutes
*******************************************************************************
Target pole/equ : No model available
```

```
Target radii    : (unavailable)
Center geodetic : 0.00000000,0.00000000,0.0000000 {E-lon(deg),Lat(deg),Alt(km)}
Center cylindric: 0.00000000,0.00000000,0.0000000  {E-lon(deg),Dxy(km),Dz(km)}
Center pole/equ : High-precision EOP model         {East-longitude positive}
Center radii    : 6378.1 x 6378.1 x 6356.8 km      {Equator, meridian, pole}
Target primary  : Sun
Vis. interferer : MOON (R_eq= 1737.400) km         {source: DE431}
Rel. light bend : Sun, EARTH                       {source: DE431}
Rel. lght bnd GM: 1.3271E+11, 3.9860E+05 km^3/s^2
Small-body perts: Yes                              {source: SB431-N16}
Atmos refraction: NO (AIRLESS)
RA format       : HMS
Time format     : CAL
EOP file        : eop.180423.p180715
EOP coverage    : DATA-BASED 1962-JAN-20 TO 2018-APR-23. PREDICTS-> 2018-JUL-14
Units conversion: 1 au= 149597870.700 km, c= 299792.458 km/s, 1 day= 86400.0 s
Table cut-offs 1: Elevation (-90.0deg=NO ),Airmass (>38.000=NO), Daylight (NO )
Table cut-offs 2: Solar elongation (  0.0,180.0=NO ),Local Hour Angle( 0.0=NO )
Table cut-offs 3: RA/DEC angular rate (     0.0=NO )
*******************************************************************************
Initial IAU76/J2000 heliocentric ecliptic osculating elements (au, days, deg.):
  EPOCH=  2457027.5 ! 2015-Jan-05.00 (TDB)        Residual RMS= .32064
   EC= .184538897679618    QR= .9787110538317922   TP= 2457236.0170146925
   OM= 39.64538793353396   W=  133.6133462437278   IN= 12.31376050937569
  Equivalent ICRF heliocentric equatorial cartesian coordinates (au, au/d):
   X= 1.376757047284033E+00  Y= 2.940205705589408E-01  Z=-3.462253150434266E-02
  VX=-2.936233908420939E-03 VY= 1.055327797345001E-02 VZ= 7.329038426384408E-03
Asteroid physical parameters (km, seconds, rotational period in hours):
   GM= n.a.              RAD= n.a.             ROTPER= n.a.
   H= 21.1               G= .150               B-V= n.a.
                      ALBEDO= n.a.           STYP= n.a.
*******************************************************************************************************
 Date_(UT)_HR:MN    R.A.(ICRF/J2000.0)DEC    APmag          delta                  deldot    S-O-T     /r     S-T-O
*******************************************************************************************************
$$SOE
 2018-Apr-24 00:00    11 51 15.28 +60 09 57.0  16.51 0.03531389339368  -5.1618091 102.3755 /T  75.6734
 2018-Apr-25 00:00    11 52 45.09 +54 27 37.9  16.20 0.03248861132692  -4.5961706 106.6191 /T  71.6232
 2018-Apr-26 00:00    11 54 06.74 +47 44 12.5  15.88 0.03003644080257  -3.8647157 111.5673 /T  66.8585
 2018-Apr-27 00:00    11 55 22.03 +39 55 56.0  15.57 0.02806095612794  -2.9429185 117.1733 /T  61.4225
 2018-Apr-28 00:00    11 56 32.33 +31 07 15.7  15.29 0.02667372918414  -1.8309787 123.2175 /T  55.5297
 2018-Apr-29 00:00    11 57 38.78 +21 34 47.1  15.07 0.02597435063533  -0.5726685 129.2453 /T  49.6277
 2018-Apr-30 00:00    11 58 42.29 +11 46 57.4  14.93 0.02602307931989   0.7414272 134.6068 /T  44.3574
 2018-May-01 00:00    11 59 43.65 +02 17 05.0  14.89 0.02682005538286   2.0004158 138.6629 /T  40.3490
 2018-May-02 00:00    12 00 43.54 -06 27 00.3  14.95 0.02830581280709   3.1153187 141.0754 /T  37.9349
 2018-May-03 00:00    12 01 42.58 -14 09 33.7  15.08 0.03038262004563   4.0441667 141.9487 /T  37.0117
 2018-May-04 00:00    12 02 41.31 -20 46 48.9  15.26 0.03294157305417   4.7876430 141.6916 /T  37.1773
 2018-May-05 00:00    12 03 40.20 -26 22 53.5  15.48 0.03588198064765   5.3701803 140.7633 /T  37.9824
 2018-May-06 00:00    12 04 39.70 -31 05 31.9  15.70 0.03911992412191   5.8232571 139.5169 /T  39.0827
 2018-May-07 00:00    12 05 40.21 -35 03 14.3  15.92 0.04258934272567   6.1762947 138.1729 /T  40.2645
 2018-May-08 00:00    12 06 42.08 -38 23 52.1  16.14 0.04623970517353   6.4534316 136.8518 /T  41.4122
 2018-May-09 00:00    12 07 45.64 -41 14 07.9  16.34 0.05003280148092   6.6732855 135.6117 /T  42.4712
 2018-May-10 00:00    12 08 51.19 -43 39 31.9  16.54 0.05393977622390   6.8498063 134.4756 /T  43.4209
 2018-May-11 00:00    12 09 59.01 -45 44 30.6  16.72 0.05793873787254   6.9933281 133.4482 /T  44.2580
 2018-May-12 00:00    12 11 09.35 -47 32 37.0  16.90 0.06201294572718   7.1114907 132.5255 /T  44.9880
 2018-May-13 00:00    12 12 22.44 -49 06 41.9  17.06 0.06614947112266   7.2099582 131.6991 /T  45.6198
 2018-May-14 00:00    12 13 38.49 -50 29 01.9  17.21 0.07033821796893   7.2929511 130.9597 /T  46.1635
 2018-May-15 00:00    12 14 57.67 -51 41 27.5  17.36 0.07457120656659   7.3636327 130.2978 /T  46.6290
 2018-May-16 00:00    12 16 20.15 -52 45 28.5  17.49 0.07884204891096   7.4243921 129.7043 /T  47.0257
 2018-May-17 00:00    12 17 46.02 -53 42 18.3  17.62 0.08314556461585   7.4770525 129.1713 /T  47.3619
 2018-May-18 00:00    12 19 15.37 -54 32 57.1  17.75 0.08747750167532   7.5230282 128.6913 /T  47.6452
 2018-May-19 00:00    12 20 48.23 -55 18 15.0  17.87 0.09183433569095   7.5634413 128.2579 /T  47.8820
 2018-May-20 00:00    12 22 24.59 -55 58 53.6  17.98 0.09621312660278   7.5992050 127.8655 /T  48.0783
 2018-May-21 00:00    12 24 04.43 -56 35 27.7  18.08 0.10061141568924   7.6310807 127.5089 /T  48.2392
```

```
 2018-May-22 00:00    12 25 47.67 -57 08 26.4  18.19 0.10502714932175   7.6597148 127.1839 /T  48.3690
 2018-May-23 00:00    12 27 34.25 -57 38 14.4  18.28 0.10945861996646   7.6856627 126.8866 /T  48.4717
 2018-May-24 00:00    12 29 24.10 -58 05 12.6  18.38 0.11390441855239   7.7094050 126.6135 /T  48.5507
$$EOE
**********************************************************************************************************
```

Column meaning:

TIME

Prior to 1962, times are UT1. Dates thereafter are UTC. Any 'b' symbol in the 1st-column denotes a B.C. date. First-column blank (" ") denotes an A.D. date. Calendar dates prior to 1582-Oct-15 are in the Julian calendar system. Later calendar dates are in the Gregorian system.

Time tags refer to the same instant throughout the solar system, regardless of where the observer is located. For example, if an observation from the surface of another body has an output time-tag of 12:31:00 UTC, an Earth-based time-scale, it refers to the instant on that body simultaneous to 12:31:00 UTC on Earth.

The Barycentric Dynamical Time scale (TDB) is used internally as defined by the planetary equations of motion. Conversion between TDB and the selected non-uniform UT output time-scale has not been determined for UTC times after the next July or January 1st. The last known leap-second is used as a constant over future intervals.

NOTE: "n.a." in output means quantity "not available" at the print-time.

R.A._(ICRF/J2000.0)_DEC = J2000.0 astrometric right ascension and declination of target center. Adjusted for light-time. Units: HMS (HH MM SS.ff) and DMS (DD MM SS.f)

APmag = Asteroid's approximate apparent visual magnitude from the standard IAU H-G magnitude relationship:
APmag = H + 5*log10(delta) + 5*log10(r) - 2.5*log10((1-G)*phi1 + G*phi2).
For solar phase angles > 90 deg, the error could exceed 1 magnitude. For phase angles > 120 degrees, output values are rounded to the nearest integer to indicate error could be large and unknown.
Units: MAGNITUDE

delta deldot = Range ("delta") and range-rate ("delta-dot") of target center with respect to the observer at the instant light seen by the observer at print-time would have left the target center (print-time minus down-leg light-time); the distance traveled by a light ray emanating from the center of the target and recorded by the observer at print-time. "deldot" is a projection of the velocity vector along this ray, the light-time-corrected line-of-sight from the coordinate center, and indicates relative motion. A positive "deldot" means the target center is moving away from the observer (coordinate center). A negative "deldot" means the target center is moving toward the observer.
Units: AU and KM/S

S-O-T /r = Sun-Observer-Target angle; target's apparent SOLAR ELONGATION seen from the observer location at print-time.
Angular units: DEGREES

The '/r' column indicates the target's apparent position relative to the Sun in the observer's sky, as described below.

For an observing location on the surface of a rotating body (considering its rotational sense):
/T indicates target TRAILS Sun (evening sky; rises and sets AFTER Sun)
/L indicates target LEADS Sun (morning sky; rises and sets BEFORE Sun)

For an observing point NOT on a rotating body (such as a spacecraft), the "leading" and "trailing" condition is defined by the observer's heliocentric orbital motion: if continuing in the observer's current direction of heliocentric motion would encounter the target's apparent longitude first, followed by the Sun's, the target LEADS the Sun as seen by the observer. If the Sun's apparent longitude would be encountered first, followed by the target's, the target TRAILS the Sun.

NOTE: The S-O-T solar elongation angle is numerically the minimum separation angle of the Sun and target in the sky in any direction. It does NOT indicate the amount of separation in the leading or trailing directions, which are defined in the equator of a spherical coordinate system.

S-T-O = "S-T-O" is the Sun->Target->Observer angle; the interior vertex angle at target center formed by a vector to the apparent center of the Sun at reflection time on the target and the apparent vector to the observer at print-time. Slightly different from true PHASE ANGLE (requestable separately) at the few arcsecond level in that it includes stellar aberration on the
down-leg from target to observer.
Units: DEGREES

Computations by ...
Solar System Dynamics Group, Horizons On-Line Ephemerides System

4800 Oak Grove Drive, Jet Propulsion Laboratory
Pasadena, CA 91109 USA
Information: http://ssd.jpl.nasa.gov/
Connect : telnet://ssd.jpl.nasa.gov:6775 (via browser)
telnet ssd.jpl.nasa.gov 6775 (via command-line)
Author : Jon.D.Giorgini@jpl.nasa.gov

****

Ephemerides - case example

Next is an example of the procedure followed in NEO observations to determine detectable objects based on ephemerides information. In [24], the authors give a detailed explanation of the steps they followed in order to evaluated the planetary radar capabilities at Arecibo, the Goldstone 70 m DSS-14 and 34 m DSS-13 antennas, the 70 m DSS-43 antenna at Canberra, the Green Bank Telescope (GBT), and the Parkes Radio Telescope in terms of their relative sensitivities and the number of known near-Earth asteroids (NEAs) detectable per year in monostatic and bistatic configurations. The following are the main highlights of their procedure, [24].

- Perform an automated search of all NEAs listed on the minor planet center (MPC) website (http://www.minorplanetcenter.net/iau/mpc.html) during a year.
- Download trajectories of the NEAs from the Jet Propulsion Laboratory' s Horizons Ephemerides Service (http://ssd.jpl.nasa.gov/?horizons_doc)
- Estimate radar SNRs for transmission/reception at the station or stations: Arecibo, DSS-13, DSS-14, DSS-43, Parkes, and the GBT.
- For each telescope, create a short list of objects that came within 1 astronomical unit (au) of Earth and passed through the declination window of the telescope (Table 6).
    - Compute the positions of the objects at 1 hour - intervals throughout the year.
    - Compute detailed observing windows or radar track durations by finding the time intervals in which the asteroids were above the minimum viewable elevation of the telescope.
    - Compute the minimum range to the target and estimate the SNR of its radar echo, for each observing window, as $P_{rx}/\Delta P_{noise}$, where P_{rx} is the power of the received echo as defined in eqn (2), with $G^2 = G_{tx}G_{rx}$, and ΔP_{noise} is the standard deviation of the receiver noise. Note that G_{tx} and G_{rx} are the gain of the transmitted and received antennas, respectively, and those are not the same when in bistatic configuration.

$$\Delta P_{noise} = \frac{kT_{sys}\Delta f}{(\Delta t \Delta f)^{\frac{1}{2}}} \tag{11}$$

where k is the Boltzman's constant, T_{sys} is the receiver temperature, Δf is the frequency resolution and Δt is the total integration time of the received signal. Note that:

- ✓ SNR is maximized if $\Delta f = B$.
- ✓ Because receiver noise is stochastic in nature, the standard deviation of noise power falls off as the square root of the integration time.

The radar cross-section and echo bandwidth depend on the physical properties of the target and are often unknown.

- ✓ The radar cross section is given by $\sigma = \hat{\sigma}A$, where $\hat{\sigma}$ is the radar albedo and A is the projected area of the target.
- ✓ For a spherical object, the echo's bandwidth is given by $B = 4\pi D cos\delta/\lambda P$, where D is the diameter, δ is the sub-radar latitude of the object, λ is the radar wavelength, and P is the spin period of the object.
- ✓ The telescope parameters used for the calculations are provided in Table 6.

Table 4. Telescope parameters assumption

	DSS-13	DSS-14	DSS-43	Arecibo	GBT	Parkes
Declination range	−35° to +90°	−35° to +90°	−90° to +34°.5	−1° to +38°	−46° to +90°	−90° to +26°.5
Min. elevation (degrees)	20	20	20	70	5	30.5
Accessible sky fraction (%)	79	79	78	32	86	72
Diameter (m)	34	70	70	305	100	64
Aperture efficiency	0.71	0.64	0.64	0.38 0.17 (X-band)	0.71	0.45
Transmitter frequency (MHz)	7190	8560	2290	2380	NA	NA
Transmitter power (kW)	80	450	100	900	NA	NA
System temperature (K)	20	18	NA	23	25	28
Transmit-receive switch time (s)	NA	5	NA	5	NA	NA

- The relative sensitivities per round-trip light time (RTT), the time for the transmitted signal to reach, reflect off of, and return from the target, are given in Table 7 for various combinations of transmitters and receivers.
- Obtain estimates of D and P, from European Asteroid Research Node (earn.dlr.de). When a diameter estimate is not available, compute a value for D from the absolute magnitude of the object by assuming a typical S-class optical albedo of 0.18. For objects with unknown rotation periods, assume a P of 2.1 h if the object was larger than 140 m in diameter and 0.5 h for smaller objects.
- Set the integration time several seconds less than 50% of the observing window (account for the monostatic case).
- Set SNR cutoff of ≥ 30/track (rate of successful detection is close to 100% above this threshold). Asteroids with SNRs <30/track are infrequently scheduled at Goldstone because the telescope is heavily subscribed with spacecraft communications and only asteroids with high probabilities of success are scheduled.
- Radar beam sizes, approximately given by λ/D_{ant}, where D_{ant} is the antenna diameter, are on the order of 1 arcmin, so pointing uncertainties should ideally be

significantly smaller than that prior to a radar observation. In practice, 3σ pointing uncertainties < 20 arcsec are preferred.

Table 5. Relative Sensitivities of Various Transmitter–Receiver Combination. The first column indicates transmitting telescope, the second column indicates receiving telescope, and the third column indicates S/N/RTT values normalized to those at DSS-14. Transmitter and receiver parameters are provided in Table 6.

Transmitter	Receiver	Relative sensitivity
DSS-14	DSS-14	1
	Arecibo	5.1
	GBT	2.3
	DSS-13	0.3
Arecibo	Arecibo	15
	GBT	5
	DSS-13	0.6
	DSS-14	2.2
DSS-43	Parkes	0.007
DSS-43 (400 kW)	Parkes	0.03
DSS-13	Arecibo	0.2
	GBT	0.08

The conclusions for the study were that in the 2015 calendar year:

- Monostatic observations with Arecibo and DSS- 14 were capable of detecting 253 and 131 NEAs respectively, with signal-to-noise ratios (SNRs) greater than 30/ track.
- Combined, Arecibo and DSS-14 were capable of detecting 276 NEAs. Of these, Arecibo detected 77 and Goldstone detected 32, or 30% and 24% of the numbers that were possible. The two observatories detected an additional 18 and 7 NEAs respectively, with SNRs of less than 30/track.
- The bistatic configuration with DSS-14 transmitting and the GBT receiving was capable of detecting about 195 NEAs, or ~50% more than with monostatic observations at DSS-14. Most of the detectable asteroids were targets of opportunity that were discovered less than 15 days before the end of their observing windows. About 50% of the detectable asteroids have absolute magnitudes >25, which corresponds to diameters <~30 m.

Surface characteristics, topography and radar maps

Topographic data are obtained from delay-Doppler maps and interferometry. A radar derived map of a planet is similar to a terrestrial topographic relief map in that it shows mountains, craters,

plains, hills, ice caps, crevices, and generally smooth or rough areas. Surface features can be positively identified when the radar observations are performed over time and from different viewing geometries, and then compared with observations from other data types. Other useful data sets are generated from spacecraft photographic reconnaissance, Earth-based optical and infrared studies, and radio emission studies. The best altitude resolution is obtained where the area surveyed is in the subradar region; there the achievable accuracy is about 1 or 2 μs.

In measurements for studies in celestial mechanics, including astronomical unit determination, or for scientific experiments such as relativity tests, topography must be considered, and the distance to the center of mass (the position of the planet in space) is a required measurement. Local height variations from the modelled mean radius must be accounted for. In the collection of altimetry data, the target affects the observation strategy.

Example of findings:

- On Mars, a 15-km peak-to-peak topography variation has been measured by mapping the longitude of interest as it transits the subradar point.
- In the case of Venus, radar imaging has to be performed over a period of many days or longer, because the rotation rate is only 0.85 deg of longitude per day.
- Asteroid and comet shapes have been determined by analysis of their radar signatures, as asteroid Eros, [31].

Monostatic observations experience a north-south ambiguity: two areas on the surface at nearly the same longitude but in opposite hemispheres produce echoes that fall in the same delay/Doppler cell. Methods to solve the ambiguity:

- Interferometer measurements, which use several receiving antennas.
- As the planet rotates, the newly imaged points are independent of the previously imaged points; a series of such maps provides data for a large set of simultaneous equations. This is a difficult method because of the large number of equations that must be solved.
- Follow a surface feature over a period of time, say several months. Each point on the surface will trace a unique delay-Doppler signature.
- Average the reflectivity from many different directions.

Following there is an example of the lunar topographic mapping obtained with the GSSR.

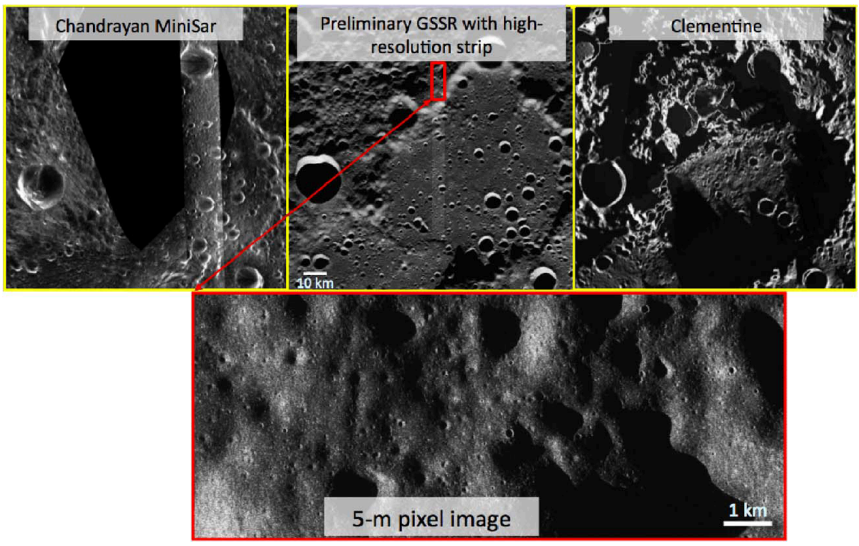

Figure 22. Example of 2009 capability of Goldstone radar at the lunar North Pole compared with two images of the same region from lunar orbiters. The pixel resolution is 5 m by 5 m in the bottom image [27].

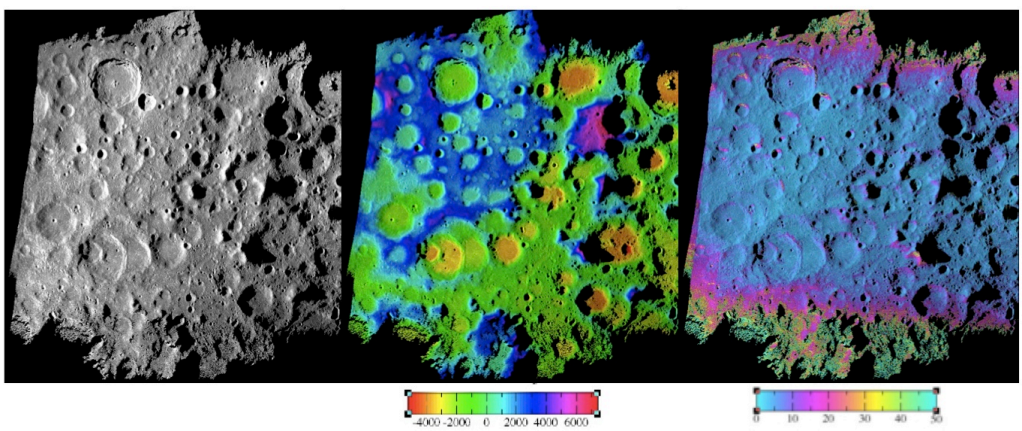

Figure 23. The left most image is the GSSR radar magnitude image, the middle image is the elevation map obtained by Earth-based radar interferometry. Both spatial and elevation resolutions are ~4 m. The right most image is the elevation error map, [27].

Bulk density and porosity

Radar can be used to investigate the composition of the surface and subsurface of a solar system object. Bulk density is a useful measure of surface material composition and porosity in units of g/cm3. The combined percent and specific gravity of each constituent in the surface material specifies the bulk density of the material as a whole. Porosity affects bulk density and porosity depends on grain shape, size distributions, and grain arrangement. Rock, water ice, soils with various packing factors, or metals-each has a characteristic bulk density: bulk densities range from 0.5 g/cm3 for ash or dust, to 3.6 g/cm3 for the material of an ordinary meteorite, to 4.9 gm/cm3 for dense, stony iron. Although it may not be possible to determine bulk density directly from radar, it can be constrained either by the dielectric constant from ground-based radar data sets,

or by the combination of radar data with other types of data. The measure of microwave emissivity of the area also provides an additional constraint on the dielectric constant.

Measure of the dielectric constants of many materials with many different packing factors made evident the problem that different packing factors can cause a different dielectric constant in the same material.

From studies of the dielectric constant and density of typical basaltic soil, it was learned that reflectivity and hence radar brightness of ice is depressed significantly with the addition of even small concentrations of this soil.

Example of findings:

- Thermal inertia maps of Mars made from infrared measurements taken with the Viking Orbiter and other missions showed that regions with high thermal inertia generally are denser than those with low thermal inertia: ash, fluff, dust, and other unconsolidated material have low thermal inertia.
- Caltech and JPL investigators using the Goldstone Radar/Very Large Array as an interferometer have analyzed reflections from the Martian south pole, [15]. It is known from optical observations that the region exhibits whitening that waxes and wanes with the Martian seasons but never vanishes; a residual ice cap remains in the Martian summer. The radar data showed that the south polar region is a nearly perfect reflector and it is theorized that the polar cap is carbon dioxide ice or water ice free from soils, that is, "clean ice."
- Mars Goldstone radar data sets were searched for both high Hagfors' C factor (smooth surface) and a high dielectric constant (characteristic of liquid water) at the same region. A further constraint was to search for a change in reflectivity with a change in season. The combination of these factors in the same area might mean the presence of surface or subsurface water; such a region was found on Mars at Solis Lacus [25].
- Mars Goldstone Radar/Very Large Array interferometer data led to the conclusion that the Stealth region near the Tharsis volcano system has a surface bulk density of less than 0.5 gm/cm3. This under dense material may be dust or ash transported and distributed by winds.

Following there is an example of the results presented by [25], where the authors analyzed the anomaly detected in the seasonal reflectivity change for Solis Lacus region in Mars.

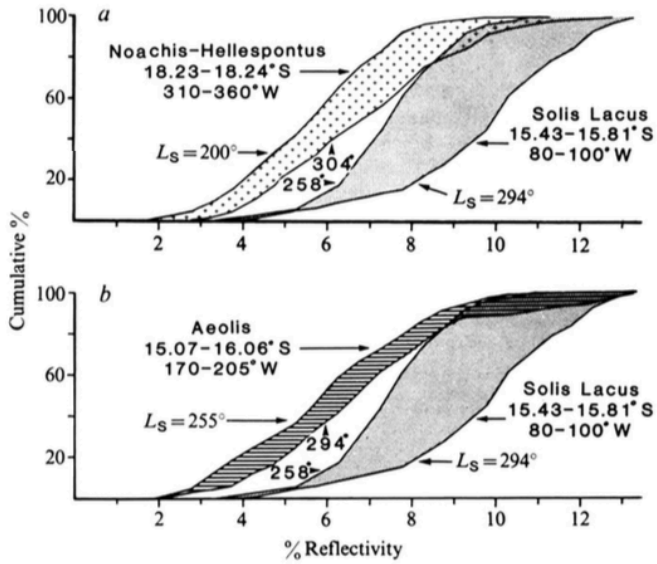

Figure 24. The seasonal variations in radar reflectivity are compared for three regions of Mars. The horizontal axis is reflectivity and the vertical axis is the percentage of data points having less than the indicated reflectivity. (a) Compares the strongly anomalous Solis Lacus area with the weakly anomalous Noachis-Hellespontus region. (b) Compares Solis Lacus with an area in Aeolis, which is taken to be representative of Mars as a whole and shows no anomaly. Note that all three areas display an increase in percentage reflectivity with increasing martian season, but that Solis Lacus has a much more pronounced seasonal change, in addition to its higher absolute radar reflectivity. Figure and text extracted from [25].

Spin vectors

The magnitude of the spin vector is the period of planet rotation (angular velocity), while the direction of the spin axis (tilt) is given in right ascension and declination. Also, the magnitude can be positive or negative, indicating retrograde or direct rotation:

- Direct (or prograde) means that rotation is in the same direction as the planet's orbit about the Sun. This is the same direction of the Earth's rotation, which is counterclockwise as seen looking down at the North Pole.
- Retrograde means rotation is opposite to the direction of the orbit.

Typically, the spin vector of a planet is, to first approximation, the rotation of a near sphere about an axis; the direction of this axis is roughly aligned with the orbital axis of the planet. The spin vector of some asteroids is considerably more complex because their shapes are typically irregular.

Several methods have been used to determine the spin characteristics of a solar system object from the radar signature, and this depends on the nature of the data.

- When evaluating the spectra of echoes from consecutive continuous-wave runs, a prominence or feature can be identified as it moves along the frequency axis. This kind of signature corresponds to a surface feature moving as the planet rotates. The spin period can be determined by measuring the time it takes the feature to completely traverse the target frequency spectrum.

- Comparing spectra from different viewing geometries and notes the limb-to-limb bandwidth observed during one particular experiment. The technique plots the bandwidth from data gathered from many experiments performed over a long period of time; the resultant plot looks like a sinusoidal curve. From this curve, the spin period can be determined. Measuring bandwidth exactly can be difficult because echo strength from the limbs is minimal, although there is a greater return for rough surfaces than for smooth. In other words, the edge may not be well defined because the signal is buried in the noise at the limbs. Limb-to-limb bandwidth is maximum when the line of sight to the radar is aligned with the equatorial plane of the planet; this is because the radial velocity is greatest at that plane.
- If it were possible for the radar to look directly along a pole, there would be no component of velocity toward or away from the observer, and therefore no Doppler shift. The Doppler bandwidth of the spin vector for a given wavelength depends on the angle of observation, aspect angle a. It is noted that the total angular motion is the sum of angular motions of the target plus the apparent angular motion due to the orbit. Using these facts, the direction of the spin vector can be determined.
- Measurements of delay-Doppler features.
- Interferometry can be used to track features over time and thus determine the spin period and direction.
- Radar Speckle Displacements (RSD). [32] This is a technique based on the fact that radar echoes from solid planets or objects can display a high degree of correlation when observed by two receiving stations with appropriate positions in four-dimensional space-time. Each station observes a specific time history of fluctuations in the echo power (corrugations or speckles), and the signal recorded at different antennas do not correlate. During certain times on certain days of the year, the antennas become suitably aligned with the speckle trajectory, which is tied to the rotation of the observed planet/object.

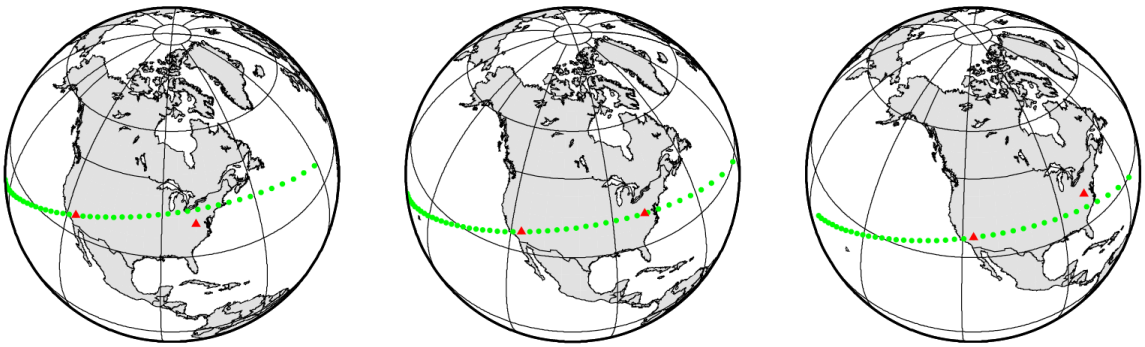

Figure 25. Figure extracted from [32]. Radar echoes from Mercury sweep over the surface of the Earth during the 2002 May 23 observations. Diagrams show the trajectory of the speckles one hour (left) before, (middle) during, and (right) one hour after the epoch of maximum correlation. Echoes from two receive stations (red triangles) exhibit a strong correlation when the antennas are suitably aligned with the trajectory of the speckles (green dots shown with a 1 s time interval).

For example, in fig. 25, there are two receiving stations, DSN - Goldstone (also the transmitter) and Green Bank Telescope – West Virginia and then the trajectory of the speckles of the signal coming from Mercury is marked with green dots. There is just a short time period when the receiving antennas baseline becomes aligned to the speckle's trajectory (center panel). The time when this happens is usually around 10 – 20 seconds, when the correlation yields to a high score at a certain value of the time lag (between 5 and 10 seconds). The epoch[9] at which the high correlation occurs provides a strong constraint on the orientation of the spin axis (α). The time lag (δt_{max}) at which the high correlation occurs provides a direct measurement of the spin rate (Ω), according to Green's equation (eq. 3 in [19]):

$$|\delta x| = 2r\Omega cos(\alpha)\delta t_{max} \tag{12}$$

Where δx corresponds to the distance between the two receiving antennas and r corresponds to the distance to the target object.

- The space-time positions of the two receiving stations at the epochs of correlation maxima are used to solve for the spin axis orientation that generates similar speckles at both receiving stations. A least-squares approach is then used to minimize the residuals between the predicted epochs and the observed epochs. Various subsets of epoch measurements are combined to identify the best-fit spin axis orientation referred to the epoch J2000. For the particular example of Mercury, the precession model for the spin axis assumes that the orbital precession rates are applicable, which is expected if Mercury closely follows the Cassini state[10].
- Once the spin axis is determined each time lag measurement is used to determine the instantaneous spin rate at the corresponding epoch (based on the similarity of the speckles).

Example of findings:

❖ Determination of the spin vector of Earth's sister planet Venus was the first application of the Goldstone radar. The direction of the spin axis was found to be nearly aligned with the orbital axis, but the surprising discovery was that Venus rotates in the retrograde direction, unlike Earth, with a spin period of -243 days.

[9] Epoch is defined as a moment in time used as a reference point for the celestial coordinates or orbital elements of a celestial body.

[10] The Cassini three empirical laws from Moon observations are: the rotation rate and the orbital mean motion are synchronous; the angle between Moon's equator and the ecliptic is constant; and Moon's spin axis and the normal to its orbital plane and ecliptic remain coplanar. A system obeying these laws is said to be in a Cassini state. Cassini state 1: both spin axis and orbital normal are on the same side of the normal to the Laplace plane. Cassini state 2 spin axis and orbit normal are on opposite sides of the normal to the Laplace plane.

- The first proper radar measurement of 59 days for Mercury's spin period was performed using Arecibo radio telescope, [33] . Radar was used since the proximity of Mercury to the Sun makes it a difficult target for optical studies.
- The GSSR is being used to measure the spin vectors of many asteroids during their closest approaches to Earth.

Following there is an example of the results presented by [34], where the authors presented the results for Venus spin vector obtained from Goldstone radar observations.

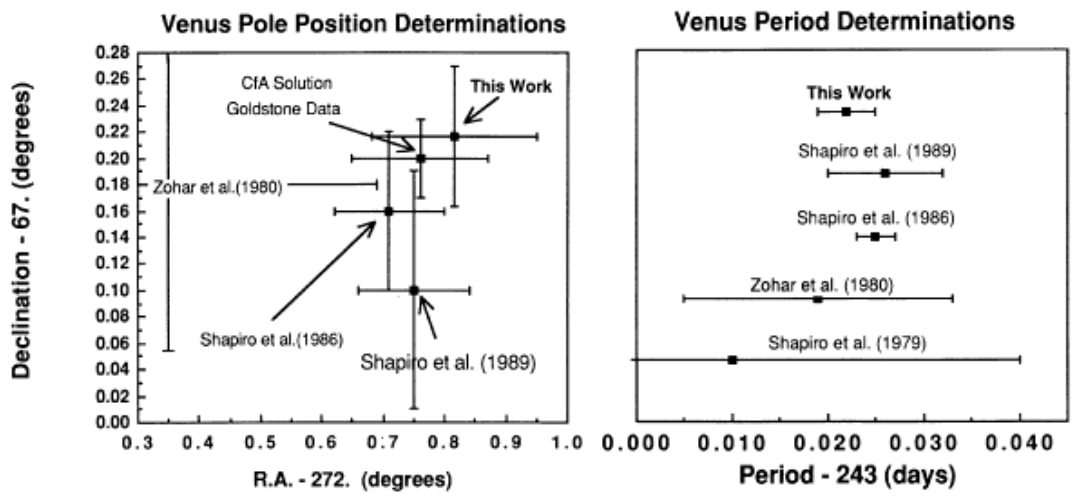

Figure 26. Venus pole position and period solutions compared. Obtained from [34].

Following there is an example of the results presented by [33], where the authors presented the results for Mercury spin period, with the Arecibo radio telescope.

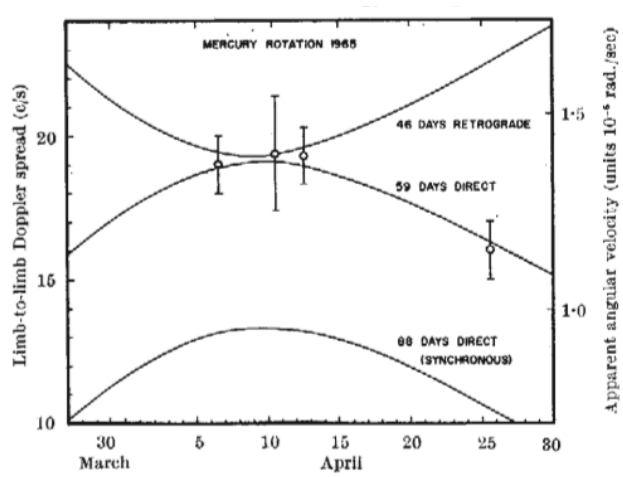

Figure 27. Plot of the apparent rotational angular velocity of the planet Mercury versus data for several values of rotation during the inferior conjunction of April 1965. The values inferred from the measurements are shown with their estimated errors, [33].

Following there is an example of the results presented by [32], where the authors presented the results for Mercury spin axis orientation using the RSD technique

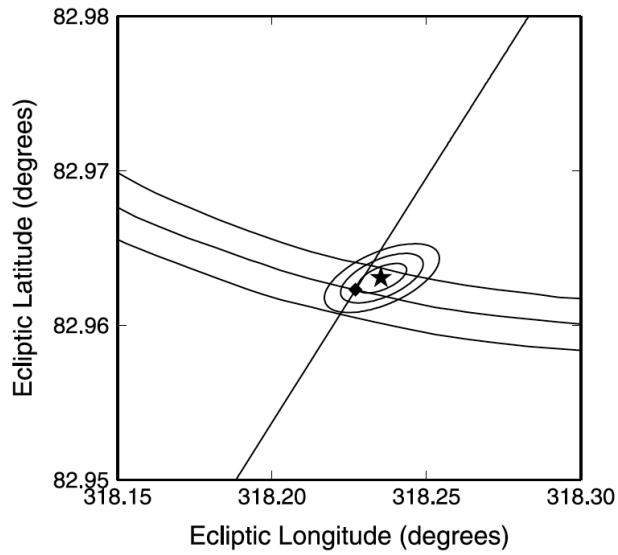

Figure 4. Figure extracted from [32]. Orientation of the spin axis of Mercury obtained by a least-squares fit to a subset of epochs that are minimally affected by atmospheric refraction. Contours representing 1-, 2-, and 3-s uncertainty regions surrounding the best-fit solution (star) are shown. The contours are elongated along the general direction of the constraints shown in Figure 3. The best-fit obliquity is (2.04 _ 0.08) arc min. The diamond and curved lines show the solution and obliquity uncertainties of [19], The oblique line shows the predicted location of Cassini state 1 based on the analysis of [35].

Multiparticle systems

The rings of Saturn and comet tails are multiparticle systems.

- Saturn rings consist of concentric rings A, B, C and D. The rings of Saturn are greatly overspread (the product of the time dispersion and the frequency dispersion is > 1). For this reason, a continuous wave frequency -stepping scheme is used. [11]

[11] A target is overspread to radar if the product of time dispersion (τ) and frequency dispersion (B) is greater than 1:

- Mars and the rings of Saturn are overspread.
- Most asteroids, Venus, and Mercury are not overspread.

Table shows the typical overspreading factors for various solar system bodies.

Typical overspreading factor F for various solar system bodies at 8.56 GHz. Obtained from [30].

Target	Overspread factor $F = \tau B$	Target	Overspread factor $F = \tau B$
NEA 2004-BL86	2.2e-6	Io	103.8
Mercury	5.6	Europa	37.9
Venus	8.3	Ganymede	53.7
Mars	617.4	Callisto	19.3

- The long tail of the comets contains gases and myriad particles. Detection is difficult when they are far from Earth, since they are small. The radio telescope is very useful for unambiguous identification of the nucleus.

The size and spatial distributions of the particle in both systems have been investigated using radar.

Example of findings:

- The Goldstone experiments showed the Saturn ring system to be a good reflector at 3.5 cm. Before it was thought the rings consisted of much smaller particles as small ice crystals 0.1 to 1 mm in size, but after the experiments, it was certain that the particles were greater than 1 cm, a radar wavelength or larger. The particles reflectivity for rings A and B are the ones reflecting most of the radar signal.
- The Doppler dispersion of the ring system is about 600 kHz at 12.6 cm wavelength, and the delay dispersion is 1600 ms [36].
- In 1985, Halley's comet was observed. A large broad-band component and no narrow-band component was measured in the echo. The absence of a central peak in the echo may be the result of the low dielectric constant that would result from the theorized very low bulk density of the nucleus.
- IRAS-Araki-Alcock was observed in May 1983 by Goldstone at 3.5 cm wavelength and 12.9 cm wavelength with a high signal-to-noise ratio during its closest approach to Earth (0.03 AU). It was found that the echo had a narrow-band component and a weaker broad-band component. The broad-band component corresponded to echoes from particles that probably had been ejected from, and are not gravitationally bound to, the active 7 km diameter nucleus. The spin period was measured at 2 or 3 days.

Following there is an example of the results presented by [36], where the authors presented the Doppler and delay dispersions of Saturn ring system.

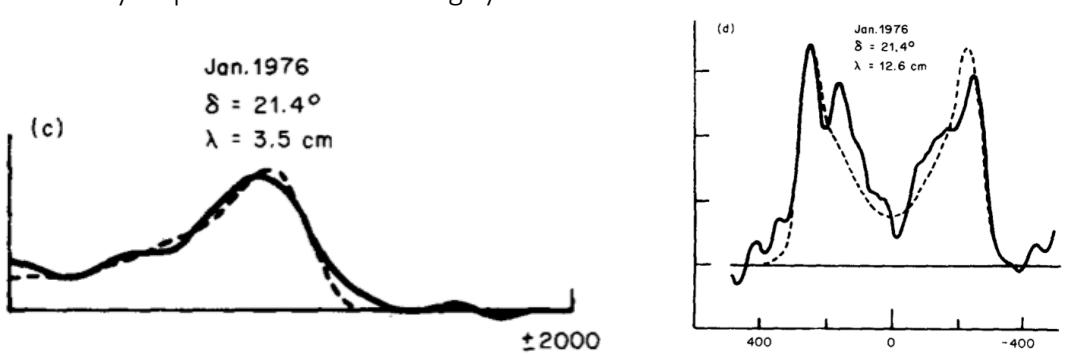

(a) Delay dispersion (b) Doppler dispersion

Figure 28. Saturn's ring echo power spectra obtained at ring plate tilt angle 21.4 deg and various wavelengths. The figure shows that the Doppler dispersion of the ring system is about 600 kHz at 12.6 cm wavelength, and the delay dispersion is 1600 ms. [36]

Chapter 5. Modes of operation

This information has been extracted mainly from [1] and [2].

The main differences between planetary radar and other radar systems operating on various platforms as ships or aircrafts is the modulation applied to the phase of the transmitted signal, as opposed to pulsing the transmitted power. A continuous wave can be coded using a sequence of 180 degrees phase reversals resulting in a pulse train. The signal received is then cross-correlated with a copy of this code in order to retrieve the echo, thereby synthesizing a pulse train with the desired settings. With this approach, one optimizes SNR because it is much cheaper to transmit the same average power continuously than to pulse the transmitter. Most modern ground-based radar astronomy observations employ continuous wave or repetitive, phase-coded continuous wave waveforms [37]. Because there is a wide divergence in the radar observables of targets and the certainties of the target's ephemerides, GSSR modes of operation must be tailored to the specifics of the target and the investigation; one radar mode would not be suitable for the goals of all experimenters. A mode for radar operation can be categorized according to the subsystem interconnections, the signal flow, and the specific values of several variable parameters. Among these parameters are the selected transmit waveform and the receiver bandwidth, and configuration of the DAS required to demodulate this selected waveform.

Regarding selected waveform, the different modes include:

- continuous wave (CW),
- binary phase-coded (BPC), or
- chirping.

Regarding the different transmitter/receiver configurations, measurements can be made:

- monostatic,
- bistatic, or
- multistatic.

Finally, a new capability was recently added to the GSSR, which is based on a new ranging method known as long code [38]. It is described at the end of this section.

Different modes regarding the selected waveform

Continuous Wave (CW)

A continuous-wave (CW) mode transmits a constant radio frequency signal that has no time modulation. Note that in the past it was usually frequency hopped but currently radar passbands are quite linear and hopping is no longer required. The amplitude and phase of the returned signal

in this mode are used to determine such target characteristics as radar cross section, rotation rate, and surface structure. Doppler shift and frequency spread of the received CW echo will vary greatly according to the radar scattering function of the target, and this function is related to the radius and rotation rate of the target. The radio frequency energy of an echo from a planet of relatively large radius or rapid rotation will spread over a proportionately greater range of frequencies (bandwidth) than that from a planet of lesser radius or slower rotation. Three different radar receiver bandwidths provide selectable frequency resolutions and allow optimum tailoring of the receiving and DAS functions to the target's radar bandwidth. A matched filter implementation, wherein the receiver's frequency response matches that of the echo, is the goal. Frequency hopping can be used in CW mode to reduce the effects of noise, but as mentioned above due to the linearity of the passband filters it is no longer required. CW signals are transmitted at two different carrier frequencies near the selected radar frequency[12].

1. Continuous Wave (CW): Narrow bandwidth
   Narrow-bandwidth targets have relatively small radii and/or small rotation rates. The main targets of this mode include:
   - Mercury,
   - asteroids,
   - comets,
   - Saturn's moon Titan, and Jupiter's Galilean satellites.

   Orbital predictions (ephemerides) of the observed object must be accurately known to successfully use this mode. If the Doppler correction applied to the receiver (or the exciter) is not exact, the radar echo will not appear in the narrow receiver bandwidth, and no signal will be detected.

   The continuous-wave echo is limited to roughly 40 kHz at the receiver in the narrow bandwidth mode. The bandwidth of the signal is divided into a number of frequency bins. Each bin can be made narrower by reducing the total receive bandwidth while keeping the number of samples constant, or alternatively taking a larger number of samples. A narrower bin gives high resolution in frequency. A recent addition to the radar DAS is the Orbital Debris[13] Radar

[12] For example, the CW signals might be 5 kHz less than the selected frequency for the first period of time and then hop to 5 kHz more than the selected frequency during the second time period. The radar echoes at the two hop frequencies are Fourier-transformed (a mathematical process) into the frequency domain and integrated to provide power spectral densities, i.e., a spectrograph is produced. The power spectral densities corresponding to the different frequency carriers are then subtracted to cancel some noise while leaving the signals.

[13] Orbital debris (duh BREE) is "junk" that is circling Earth. It is pieces from spacecraft. Humans have been launching objects into space for more than 50 years. Most of those objects have fallen back to Earth. A piece of debris falls back to Earth about once a day. These objects either land or burn up in the atmosphere. Most objects that return to Earth end up in water, since it makes up 70 percent of Earth's surface. But many of the objects sent into space are still in orbit around Earth. https://www.nasa.gov/audience/forstudents/5-8/features/nasa-knows/what-is-orbital-debris-58.html

Processor, which is based on a personal computer and array processor; it has up to 150-kHz bandwidth.

The information available using CW includes:

- radar cross sections,
- surface roughness,
- and rotation rates.
- Also, it is useful to check antenna pointing accuracy and Doppler tracking during ranging experiments.

Next figure shows an example of the echo received while performing CW for asteroid 1999FN19 during May 2018 observations.

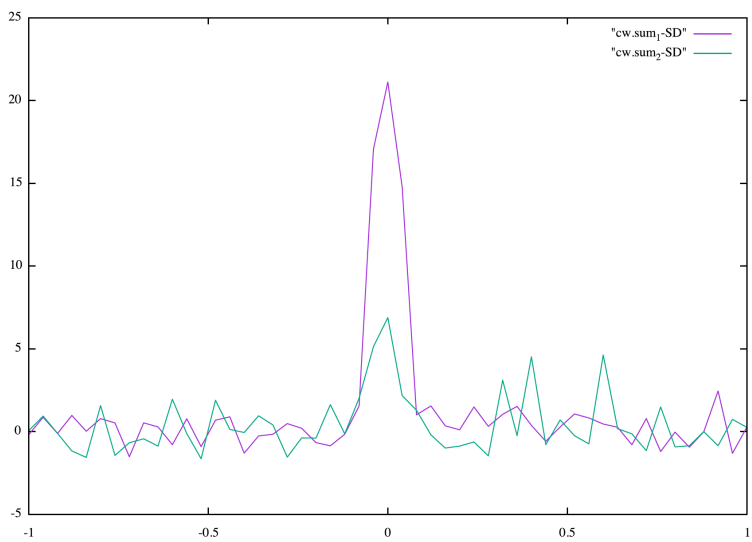

Figure 29. 1999FN19 NEO was observed on May 11, 2018. The figure shows the echo spectrum (for two channels) after adding 20 CW runs. Frequency resolution is 0.4 Hz, frequency offset of 500 Hz. Ephemerides solution used was s69.

The echo observed in both channels contains information about the object:

⇒ The amplitude is related to the radar cross-section.

⇒ Narrow bandwidth indicates slow rotator.

⇒ The amplitude of the echo in the second channel (SC) indicates that the surface has some degree of roughness.

⇒ The echo is well centered at 0 Hz, which means there is no additional offset to correct in the ephemerides.

Next figure shows the results recently obtained with CW for asteroid 2017 YE5 during June 2018 observations. A little bit of information of 2017 YE5 since it is a rare object.

2017 YE5 is an Apollo-type potentially hazardous asteroid with a diameter of 430-960 meters. It made a close approach on June 21st, at a distance of 0.04 AU (6.0 million km), its closest encounter with Earth for at least the next 200 years. 2017 YE 5 makes frequent close encounters with Jupiter, and its orbit suggests that it might be an extinct Jupiter-family comet. Many NEAs in comet-like orbits have been found to be optically dark, so it is suspected that will also be true with 2017 YE5. Assuming a dark surface albedo of 0.05, 2017 YE5 could be about 860 meters in diameter. Radar observations were scheduled at Goldstone on June 17-25, and at Arecibo on June 23-24.

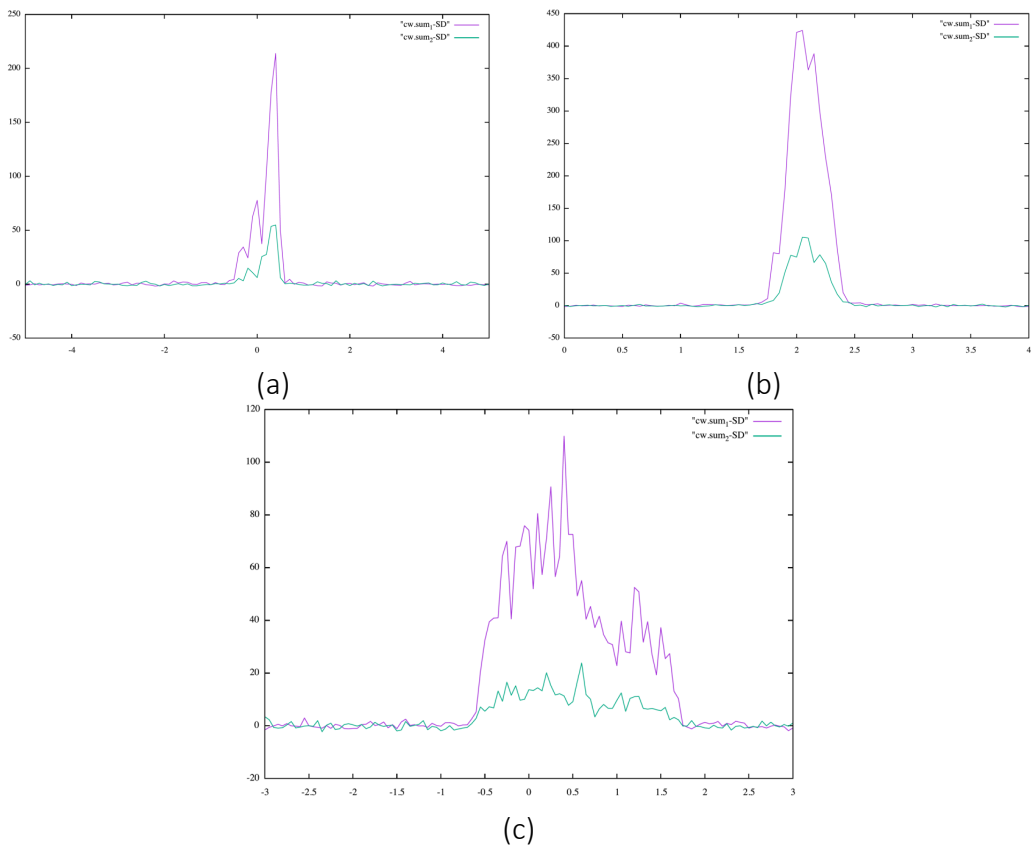

Figure 30. CW spectra obtained for 2017YE5 observations on June (a) 22, (b) 23 and (c) 24, 2018. The object resulted to be a contact binary. Particularly (c) shows the echo spectrum (for two channels) after adding 9 CW runs. Frequency resolution is 0.05 Hz, frequency offset of 500 Hz. Ephemerides solution used was s30.

The echo observed in both channels contains information about the object:

⇒ The amplitude is related to the radar cross-section.

⇒ The object resulted to be a contact binary.

2. Continuous Wave (CW): Medium bandwidth

This radar mode supports signals with wider bandwidths than the first mode, and operates at up to 8 MHz. The CW medium band is used for radar measurements of:

- Saturn's rings.

This is a low-resolution mode-less than or equal to 56 frequency (spectrograph) bins with two (left and right circular) polarization channels and cross power spectra.

3. Continuous Wave (CW): Wide bandwidth
   The CW wide-band mode is used to observe:
   - near-Earth asteroids,
   - comets with poorly known ephemerides, and
   - Mars, which has a wide frequency spectrum due to its size and high spin rate.

   If the target's ephemerides are not highly accurate, the Doppler shift cannot be predicted and removed to ensure that the signal is within the receiver's passband. Therefore, a sufficiently wide range of frequencies is processed. This mode is in transition to an upgraded configuration. The CW wide band has supported a maximum bandwidth of 20 MHz. A 65,536-channel spectrum analyzer has been used to process the wide-band signal and provide high resolution. This instrument was developed for SET1 (Search for Extra-Terrestrial Intelligence) and used for microwave surveillance at the Goldstone complex. In the future, a multimillion-channel spectrum analyzer may be used.

Binary Phase Coded (BPC)

The binary phase-coded (BPC) mode is used for ranging measurements. A pseudonoise (PN) code is modulated onto the carrier. The code is made long enough to prevent ambiguities in calculating the range to the target. These ambiguities can also be reduced by transmitting pairs of codes with slightly different baud (sub pulse time duration) periods. This mode is used to produce delay-Doppler maps of such targets as:

- Venus,
- Mercury,
- the Moon,
- and asteroids.

Binary phase coding can be used in any of several configurations:

- monostatic single
- monostatin dual polarization,
- bistatic single,
- bistatic dual polarization,
- tristatic single polarization

1. Generation of BPC signals

   Binary phase-coded signals are used only when making ranging measurements. To obtain the distance to the target, the radar system measures the round-trip travel time of the radar signal,

from which the distance can be calculated. Generally, to make ranging measurements, a time modulation has to be applied FROM LOCAL to the transmitted waveform. A simple system would switch the high-power transmitter carrier on and then off creating a pulse; during the time the transmitter is shut off the receiver listens for the echo. Then the process is repeated. The delay time from transmission to reception of the radar echo is then measured to give range to the target. The important parameters of the transmitted periodic waveform are the pulse:

- repetition frequency and
- time duration (pulsewidth).

Transmitting repetitive pulses allows the energy of many received pulses to be added (integration), thus improving the signal strength over noise.

The range resolution depends on the time duration of one baud, not the overall pulse. A subpulse is made short to give high range resolution, while keeping the overall transmitted pulse longer, resulting in high average transmitted power. Because power is transmitted continuously during the subpulses rather than being gated (i.e., the transmitter is shut off), there are fewer klystron switching problems, longer klystron life, and greater echo energy. The number of subpulses per long pulse is called the compression ratio or code length. A code zero (or +) corresponds to 0-deg phase of the transmitter carrier, and a one (or -) corresponds to a 180-deg phase change, or phase reversal. Figure 28 shows a simple example of a binary phase-coded transmit modulation, with five subpulses.

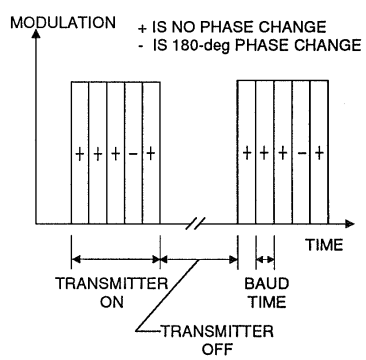

Figure 31. Transmitter modulation.

2. Demodulation (ranging)

When using BPC, energy is present away from the central peak of the range profile in the received signal. These unwanted range sidelobes are small with a well-designed code. Codes with long lengths are typically used; they are called pseudo-noise codes because their frequency spectrum is similar to that of noise. Demodulation of the received signal is performed through autocorrelation, where the correlation process is based on eqn.

$$\Phi_i(\tau) = \int_{iT}^{(i+1)T} x(t)BPC(t+\tau)dt \tag{9}$$

where:

- $\Phi_i(\tau)$ is the correlated output.
- BPC is the transmitted binary phase code.
- $x(t)$ is the echo signal.

In this process, one sample of the incoming code is multiplied by one subpulse or element of the transmitted or reference code and then accumulated; this is done for each element in the code (N multiplications). The calculation is repeated with the received signal advancing one subpulse with each sample time. When $x(t)$ matches BPC at each of N sample times, the correlator output $\Phi_i(\tau)$ reaches a maximum. By repeating this entire correlation process at incrementally greater time delays, data from a range of radar depths (the difference between limb and subradar point) can be
gathered to provide information on the entire surface of the object.

Currently different configurations are used if objects' echoes permit them. Usually ranging starts with 10 μs and 11 μs. If the echo is received successfully 1 μs s, 0.5 μs, 0.25 μs and 0.125 μs are used consecutively. For example, the resolution obtained from a 1 μs range gate size is about 150 m. With 0.125 μs the resolution is about 18.75 meters.

Next figure shows the results obtained with ranging (BPC) for asteroid 1999FN19 during May 2018 observations.

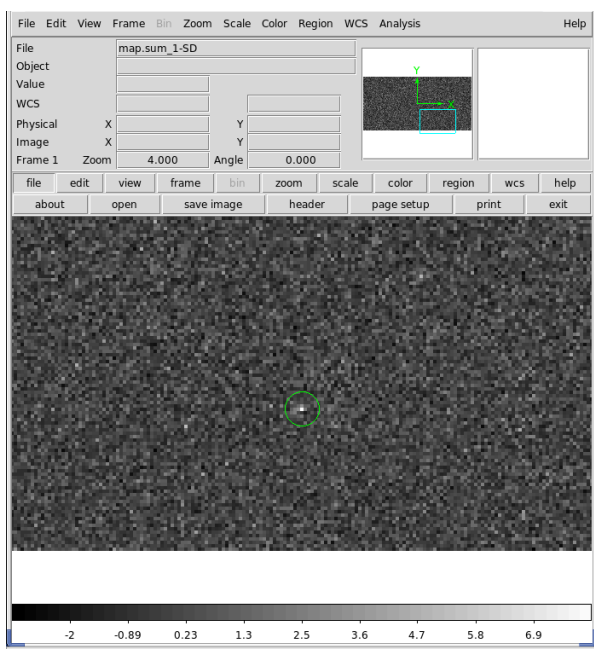

Figure 32. 1999FN19 NEO was observed on May 4, 2018. The figure shows the ranging measurements after adding 26 BPC runs. Baud rate is 0.125 μs, code length is 255 and fft size is 512, frequency resolution is 10 Hz. Ephemerides solution used was s69.

The object looked 2 bins deep and 2 bins wide. Might be smaller than scientist thought, or possibly elongated and seen in an orientation that isn't very deep.

Following with the example on 2017YE5 above, next figure shows the results obtained with BPC for asteroid 2017YE5 during June 2018 observations.

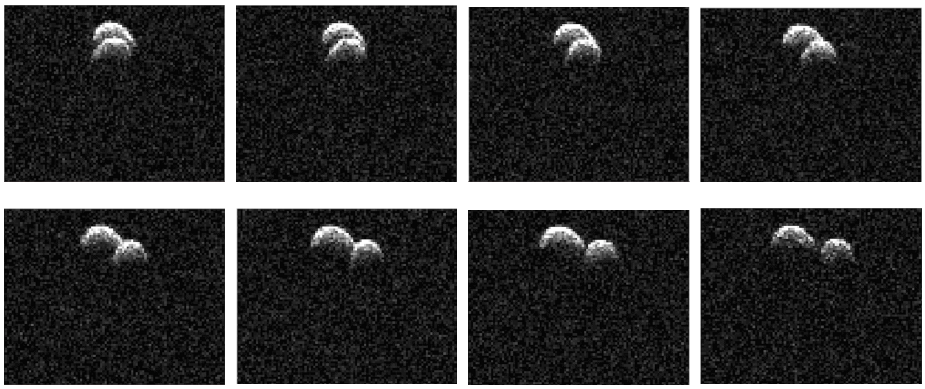

Figure 33. BPC ranging for asteroid 2017YE5. The figure shows the ranging measurements after adding 86 BPC runs. Baud rate is 0. 25 μs, code length is 255 and fft size is 2048, frequency resolution is 10 Hz. Ephemerides solution used was s28.

The observed object looked like a possible contact binary for the first set of observations made at Goldstone, first days from June 22 to June 24. During the next day, on June 25, Arecibo clearly observed that the two objects were not in contact. They were two asteroids really close to each other traveling in the same orbit.

Linear Frequency Modulation (LFM or chirp)

NEO observations by the GSSR up to 2009 have used only binary phase coded (BPC) waveforms to deliver the range resolution (also known as PN coded) (see, for example, [39]). The best range resolution at Goldstone using BPC waveforms has been limited to 18.75-m resolution (1/8 s), since any finer resolution violates the frequency license. GSSR's license from the National Telecommunications and Information Administration (NTIA) is between 8500 and 8620 MHz However, a change in waveform can achieve higher resolution without violating the GSSR license: the linear frequency modulation (LFM or chirp) waveform, which is widely used in synthetic aperture radar (SAR) applications (see, e.g., [40]). Using a chirp waveform for GSSR ranging is based on an informal report [41]. An internal JPL study [42] found that the practical bandwidth limit for the current Goldstone klystrons is 40 MHz when using chirp waveforms, which leads to an imaging system with 3.75-m resolution - an improvement of a factor of five. A sequence of images obtained in January 2010 with 3.75-m range resolution of NEO 2010 AL30 is shown in fig. 34.

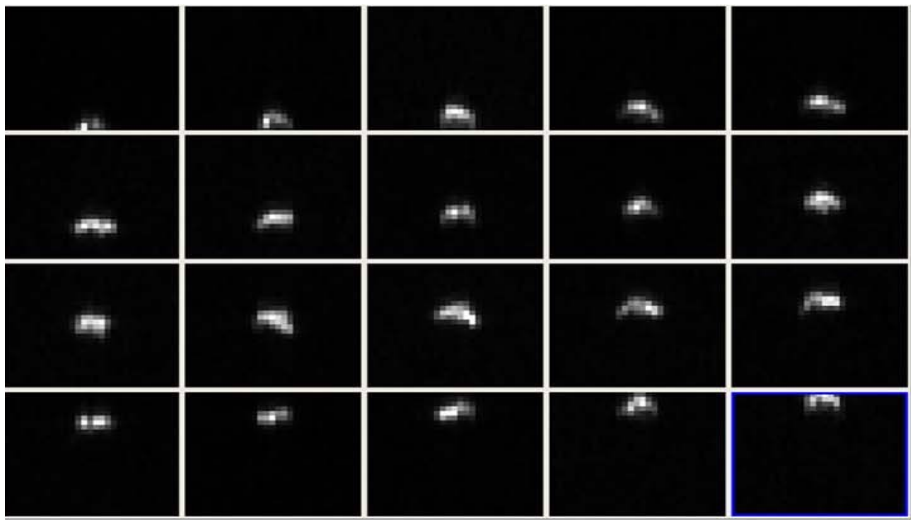

Figure 34. Goldstone delay-Doppler imagery of NEO 2010 AL30 on January 13, 2010, was using the highest resolution chirp waveform. Each frame represents 30 s of integration. Range increases downward; 1.875 m separate each row of pixels. Doppler increases to the right; each pixel column is separated by 0.5 Hz in each frame of the montage. The vertical drift of the echo in the images is due to uncertainties in the ephemerides.

By using both a broadband transmitter and a chirp waveform with 150-MHz bandwidth, the range resolution could be as fine as 1 m. With such fine scale imaging, this ground-based radar observatory could produce "spacecraft- encounter-quality" images of NEOs several times per year, providing an extremely low-cost means for NASA to explore a sizable fraction of the NEO population.

As mentioned above, the resolution of NEO imaging at the Goldstone radar could be improved to significantly finer than the current 3.75-m range resolution. Even though this is a factor of five higher than the previous best range resolution at Goldstone (see fig. 35 for a pictorial version of what a factor of five can gain), this could be improved to about 1-m range resolution with no difficulty in principle.

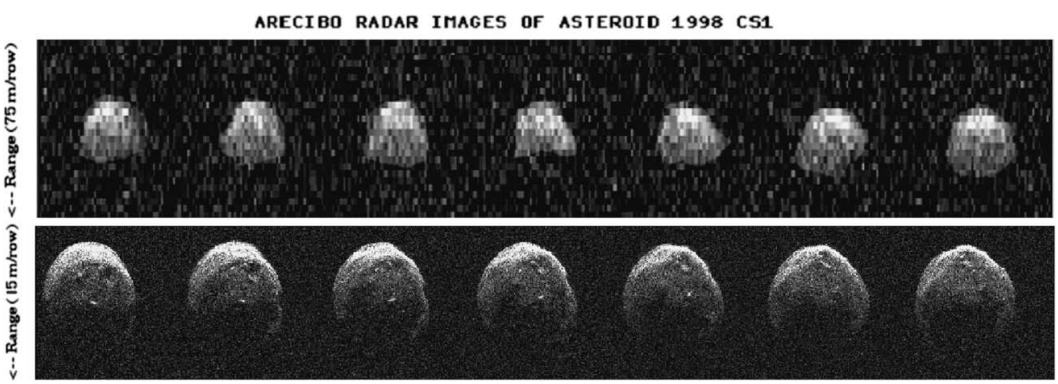

Figure 35. The chirp ranging system increases the GSSR ranging resolution by a factor of five, from 18.75 to 3.75 m. This figure shows the significance of a factor of five improved resolution for NEO 1998 CS1 from 75 m per row at the top to 15 m per row at the bottom.

The fundamental limitation to the range resolution is the bandwidth of the klystron power amplifiers through which the "chirp" waveform passes. The spectrum allocation of the Goldstone radar is from 8500 to 8620 MHz (120-MHz bandwidth). The range resolution of the Goldstone radar could be improved most simply by procuring power amplifiers that would safely pass a broader bandwidth chirp than the 40-MHz bandwidth amplifiers currently in use. If power amplifiers could be obtained with 150-MHz of usable bandwidth, then 1-m range resolution could be achieved. However, to achieve 1-m resolution in cross range (Doppler shift), longer coherent integration times would be required. Only then could images with (1 m)2 pixel sizes be made.

Delay-Doppler radar NEO images with 3.75-m range resolution will lead to dramatic improvement in our knowledge of NEO sizes, shapes, and detailed surface structure. Finer details for NEO surfaces will facilitate much improved insight into NEO geology and collisional evolution. The detection of asteroid satellites will be significantly enhanced by the increase in resolution. For many NEOs, the higher resolution will permit much finer fractional precision Goldstone radar ranging astrometry than was previously possible, which will improve long-term orbital prediction for such objects. Next figure shows the results obtained with chirping for asteroid 1999FN19 during May 2018 observations.

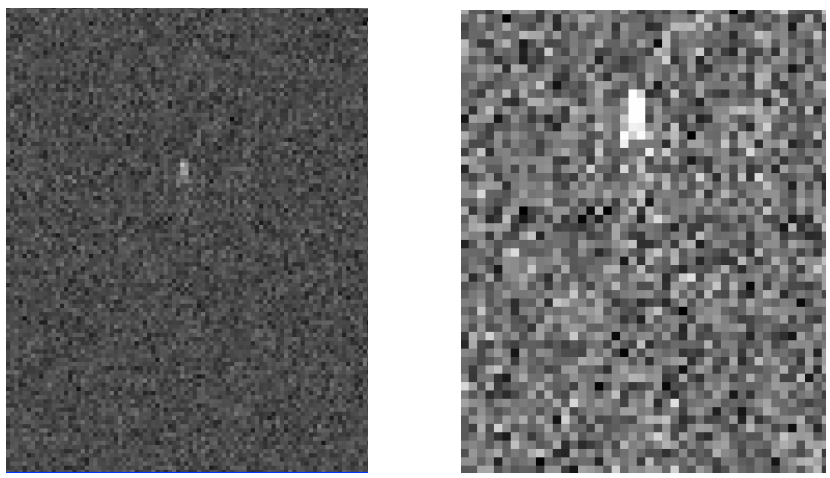

Figure 36. 1999FN19 NEO was observed on May 11, 2018. The figure shows the delay-Doppler map after adding 114 runs. Chirp at 40 MHz, sample clock at 80 MHz, pulse repetition period (prp) 25 μs, resolution 0.025 μs, range 1000, FFT 1000, offset +10 Hz, number coherent integration 1000 and frequency resolution 0.04 Hz. Ephemerides solution used was s69.

The conclusions for this object are:

- ⇒ Visible extent about 22.5 m. The object turned to be small compared to data from the first observation in 1999.
- ⇒ The rotation period is estimated to be around 50 h.
- ⇒ It is unusual for a small object to be a slow rotator.
- ⇒ Orbital correction end up being 0.375 μs to ephemerides solution .s69.

Resolution and range coverage

The different selected waveforms translate into different resolution and range coverage. For example, for PBC with a baud period of 11 us a range coverage of 209 km with a 1.65 km resolution is obtained. This is why 11 us and 10 us baud rates are used to find the object and then lower baud rates are used to re-fine its orbit. A baud period of 0.25 us gives a range coverage of 4.76 km with a 37.5 m resolution. The finer is obtained for 0.1 us, with a range coverage of 15.34 km at a 15 m resolution. If instead a LFM waveform is used range coverages of 18.75 km at 3.75 m resolutions are obtained. Changing the pulse repetition period from 125 us to 5 us range coverages of 0.75 km are obtained at 3.75 m. The following table shows a summary of this values.

Table 6. BPC waveform settings, resolution and range coverage. Table developed by Clement Lee

Baud period (us)	Baud rate (MHz)	Code length	PRP (us)	Resolution (m)	Range coverage (km)
11	0.090909091	127	1397	1650	209.55
10	0.1	127	1270	1500	190.5
1	1	127	127	150	19.05
0.5	2	255	127.5	75	19.125
0.5	2	127	63.5	75	9.525
0.25	4	255	63.75	37.5	9.5625
0.25	4	127	31.75	37.5	4.7625
0.125	8	255	31.875	18.75	4.78125
0.125	8	127	15.875	18.75	2.38125
0.125	8	1023	127.875	18.75	19.18125
0.1	10	1023	102.3	15	15.345

Table 7. Chirp (LFM) procedure (CW + Chirp): settings, resolution and range coverage. Table developed by C. Lee.

Equivalent baud period (us)	Bandwidth (MHz)	Range bins	PRP (us)	Resolution (m)	Range coverage (km)	# rep/sec
4	0.25	250	1000	600	150	1000
5	0.2	250	1250	750	187.5	800
8	0.125	125	1000	1200	150	1000
10	0.1	125	1250	1500	187.5	800
1	1	1000	1000	150	150	1000
1	1	500	500	150	75	2000
1	1	250	250	150	37.5	4000
1	1	200	200	150	30	5000
0.5	2	250	125	75	18.75	8000
0.5	2	200	100	75	15	10000
0.2	5	250	50	30	7.5	20000
0.2	5	200	40	30	6	25000
0.1	10	400	40	15	6	25000
0.05	20	800	40	7.5	6	25000

0.1	10	250	25	15	3.75	40000
0.1	10	200	20	15	3	50000
0.05	20	400	20	7.5	3	50000
0.025	40	5000	125	3.75	18.75	8000
0.025	40	4000	100	3.75	15	10000
0.025	40	800	20	3.75	3	50000
0.025	40	400	10	3.75	1.5	100000
0.025	40	200	5	3.75	0.75	200000

Different modes regarding the different transmitter/receiver configurations

Monostatic

Monostatic operation means the transmit and receive antennas are collocated (i.e., there is only one receive antenna); it is the most basic type of radar operation. Monostatic planetary radar experiments are done at the 70-m antenna (the Mars Station) since the radar control room and high-power transmitters are located there.

Bistatic and multistatic

Bistatic operation means that more than one antenna is used to receive the radar signal. The type of selected waveforms for this configuration can be:

- CW, usually narrow band, and
- BPC

Particularly, bistatic and tristatic configurations are used to:

- resolve the hemisphere ambiguity associated with monostatic delay-Doppler maps,
- provide high resolution, and
- perfom altimetry of targets, at or away from the subradar region.

Although signals are always transmitted from the Mars antenna site, either the 26-m or the 34-m antenna at the Venus site or the 34-m antenna at the Echo site can be used as a receiver along with the 70-m antenna in bistatic or tristatic mode. The combined signals from two or more antennas can then be used as interferometer measurements, whereby a fringe (or interferometric) pattern is produced. The pattern consists of multiple lobes that span much smaller angles than the single main lobe of a monostatic antenna pattern, [43]. The number of fringes spanned by the planet depends on the distance between the antennas relative to the size of the wavelength. Figure 35 shows an interferometer configuration.

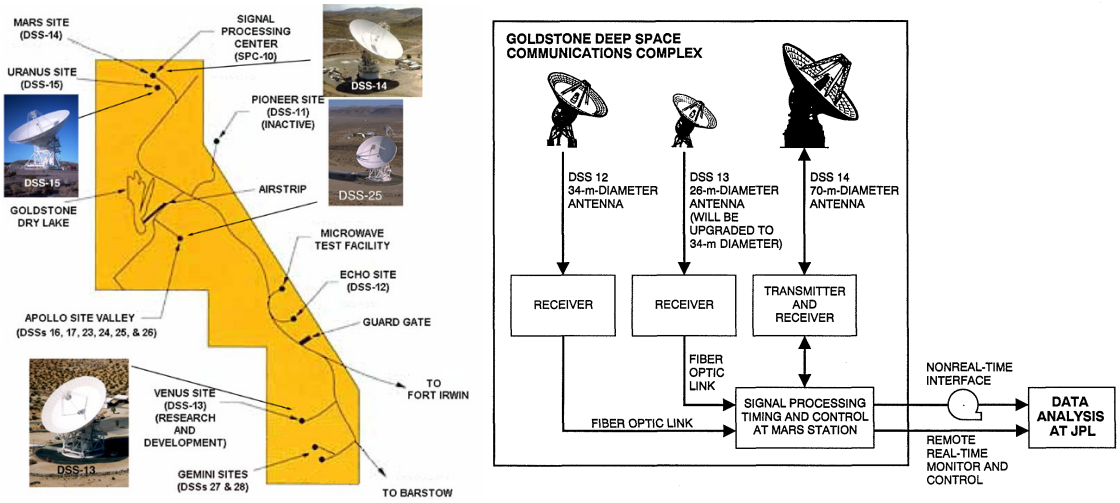

Figure 37. Goldstone DSN stations. (a)Map of the different sites, showing Venus, Echo and Mars stations, and (b) interferometry sketch.

Also, not only the antennas within the Goldtone complex can serve this purpose. Other radio observatories can be used in conjunction with Goldstone's high-power radar station to form a bistatic radar, for example:

- the Owens Valley, California, Observatory;
- the Arecibo Observatory at Arecibo, Puerto Rico; or
- the Very Large Array at Socorro, New Mexico.

Because the Goldstone system can handle up to four channels of signal processing, several modes with bistatic or tristatic configurations are possible, including bistatic single or dual polarization, or tristatic single polarization. Both the 34-m Echo antenna and the 34-m Venus antenna can simultaneously receive both right and left polarizations at both 12.9-cm wavelength and at 3.5-cm wavelength. Tables 8 and 9 show the properties for the Echo and Venus stations within the Goldstone complex.

Table 8. Echo Station Performance (34-m Antenna)

Parameter	Value	
	12.9 cm	3.5 cm
Polarization	RC, LC	
Frequency range, MHz.	2320 +/- 10	8510 +/- 10
Antenna gain, dB	56.1	66.2
Antenna beamwidth, deg.	0.27	0.075
Ellipticity, dB	0.6	0.8
Low-noise amplifier	Block III Maser	Block IIA Maser
Center frequency, MHz	2320	8510
Bandwidth, MHz	30	> 100
Gain, dB	45	44.5

Noise temperature, K	8	4
Receiver bandwidth, MHz	20	20
Dynamic range, dB	> 60	
System noise temperature, K	< 20	25

Table 9. Venus Station Performance (34-m Antenna)

Parameter	Value	
	12.6 cm	3.5 cm
Polarization	RC, LC	
Frequency range, MHz.	2380	8510 +/- 10
Antenna gain, dB	54.5 +/- 0.15	
Antenna beamwidth, deg.	0.36	0.030
Ellipticity, dB	0.7	
Low-noise amplifier		
Center frequency, MHz	2380	8510
Bandwidth, MHz	12	20
Gain, dB	37.6	50
Receiver bandwidth, MHz	14	20
Dynamic range, dB	> 60	
System noise temperature, K	30	

New capability added to GSSR to perform ranging measurements: the long code [38], [44].

The long code benefits DSN science because it enables ranging of targets that are aliased in range or Doppler (e.g. the Galilean satellites). This also allows for Goldstone radar observations of Venus, Mercury, and Mars. The long code capability at Goldstone can be used for determining the ranges of newly discovered NEO that have range uncertainties of tens of thousands of kilometers. The uncertainties of this size are too large for the standard ranging code to resolve unambiguously. Currently the use of two different setups at Goldstone is needed in order to obtain a unique range estimate with the "short" code, but the long code requires only a single setup, and thus saves time.

Origin of the long-code processing

In 1986, long-code was developed by Sulzer at Arecibo Observatory for ionospheric radar observations. In 1992, the method was applied to planetary radar observations by [45] at Arecibo. In 1994, the first successful radar range measurements to Ganymede and Callisto were achieved and published by [45] at Arecibo. In 2001, [46] carry out long-code observations of Mercury from GSSR using equipment borrowed from Arecibo. This capability later lost during hardware upgrades. In 2015, long-code was implemented on next generation of radar hardware at GSSR.

The capability was verified through successful range measurements of Galilean satellites, Mercury, Venus, and NEOs and confirmed though detections in bistatic configuration with GBT.

Motivation to develop the long code

The main motivation is to implement the capability to unambiguously measure range and to generate unaliased delay-Doppler imagery of planetary targets. Its main advantages are:

- allows for rapid ranging estimation in a single observation,
- enables ranging of overspread targets not previously measurable, such as Galilean satellites, and
- alleviates delay and Doppler folding of overspread targets.

This capability particularly supports science effort to detect subtle orbital changes due to tidal dissipation of Jupiter:

- the fully-steerable Goldstone 70-meter antenna allows long-term ranging to the Galilean satellites for ephemerides refinement, and
- improved orbit accuracy may allow Europa Clipper to skip initial distant flybys (1000 km).

In addition, it is beneficial to the determination of newly discovered NEO.

Limitations of the standard "short-code"

There are some limitations associated to the standard "short-code" as:

- waveforms with high repetition rates used for NEO observations are insufficient for resolving overspread targets,
- backscatter images of terrestrial planets and the Galilean satellites are both Doppler aliased and wrapped in range, fig. 38, and
- multiple measurements are required to resolve inherent range ambiguities.

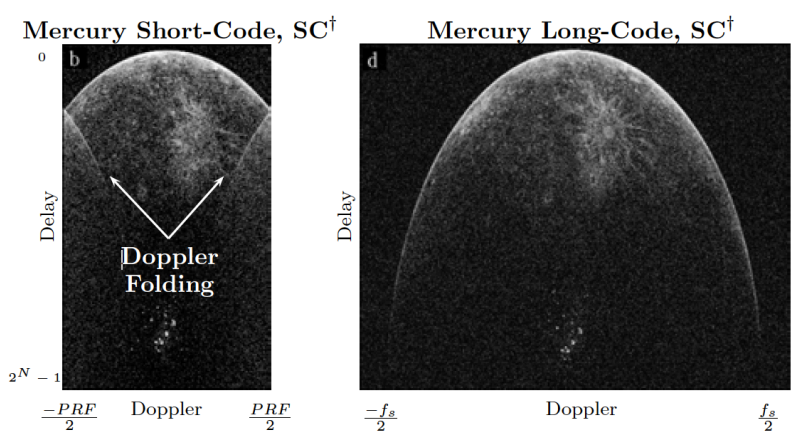

Figure 38. Example of the observations obtained using short code and long code for the same target (Mercury). Observations made by J. Harmon at Arecibo Observatory, [38], [44].

Long-code processing

The long-code method eliminates range ambiguities by transmitting non-repeating pseudo-noise waveform and forming a separate matched filter for each delay. Doppler aliasing issues are alleviated by performing spectral analysis at full sample rate. There are three main drawbacks of this technique with respect the "short-code" processing:

- the computational complexity is increased,
- requires precise knowledge of hardware latency, linear feedback shift register (LFSR) state, and target delay, and
- introduces elevated self-clutter interference from different target regions.

Long-code modification requirements

There are a number of modifications required in order to be able to implement the long-code processing, as the need to modify the GSSR waveform generator and the control software to support binary phase code (BPC) modulation of length $2^{63} - 1$, and the need to build a long-code correlation images processor in order to be able to form delay-Doppler imagery, [46].

Chapter 6. Summary of Radar Science Services Support Types

This information has been extracted from internal communications.

Summary

The DSN Radar Science Services are provided to scientists to enable them to use the DSN for direct scientific observations. The GSSR is nowadays a science research instrument used for a variety of radar experiments, primarily in the inner solar system. Its greatest use is the study of NEOs; another application is the characterization of orbital dynamics of Jupiter's Galilean moons, for example. Some of these can be done with continuous wave (CW) transmission at a fixed (or nearly fixed) frequency, but many require a modulated signal. The ones most commonly used are described briefly here, but as a research instrument, other possibilities should not be precluded.

NEO observations may either be bistatic, meaning that one antenna continuously transmits, while a second antenna continuously receives, or monostatic, in which a single antenna alternates between transmitting and receiving. In a monostatic track, the antenna transmits for one round-trip light-time (RTLT), disables the transmitter and enables the receiver, receives for an RTLT, is reconfigured for transmit again, and repeats. The RTLT is typically about 90 seconds but may be as short as about 5 seconds (limited by how fast the equipment can be reconfigured between transmit and receive modes), or as long as several hours for the Jovian moons.

The modes of operation of the GSSR are again summarized here. These modes fall into three broad categories, all at both 3.5-cm and 12.5-cm:

1. Continuous Wave (CW)
   Initial characterization of an asteroid is typically done with CW transmission, at 8560 MHz, usually with an offset of 500 Hz to displace it from the zero-frequency when the received signal is down-converted to complex baseband. Often a second offset is also applied, of no more than a few kHz, to pre-compensate for Doppler shifts from motion of the target object, and motion of the antenna as the Earth rotates.

2. Binary Phase Coding (BPC)
   The transmitter operates at 8560 MHz, usually with an offset of some tens of Hz, as well as a Doppler correction offset. As shown in the figure below, the phase of this signal is periodically set to +90° or –90° (inverted), according to a pseudo-random pattern.

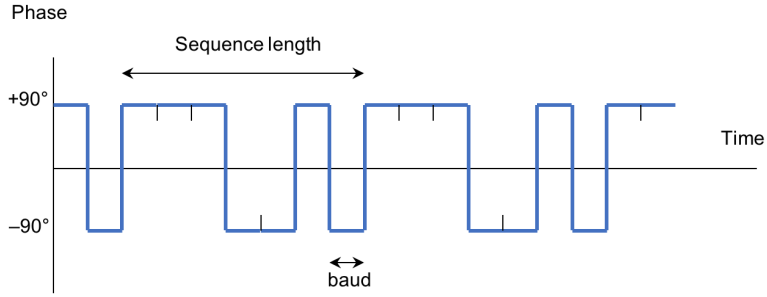

Figure 39. BPC scheme showing the phase of the signal set to +90° and -90° according to a pseudo-random pattern.

In the communications community, this is known as Binary Phase Shift Keying (BPSK) at a given baud rate, with a maximum-length binary sequence generated by a Linear Feedback Shift Register (LFSR). While a wide range of alternatives are possible, the following combinations have been the most commonly used in the last few months:

Baud rate	Sequence length
11 usec	127
10 usec	127 and 511
1 usec	127, 255, and 1023
0.5 usec	127 and 255
0.25 usec	255

Offsets have been 10 Hz, 40 Hz, 50 Hz, 100 Hz, and 150 Hz.

3. Linear Frequency Modulation (LFM or "chirp")
   As shown in the figure, the transmitter's frequency is swept from $f_0+f_{ofs}-\Delta f/2$ to $f_0+f_{ofs}+\Delta f/2$ over a time interval Δt, where f_0=8560 MHz, f_{ofs} is a small offset frequency, and Δf is the chirp bandwidth. The frequency then snaps back instantaneously, but in a phase-continuous way, and the chirp is repeated.

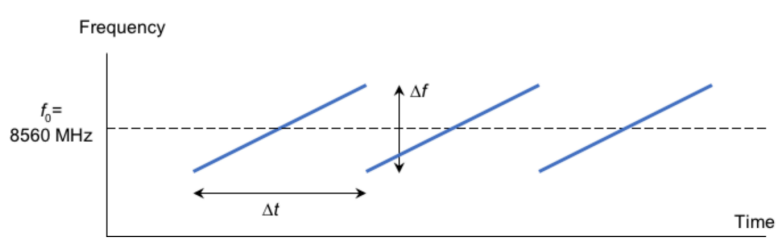

Figure 40. LFM scheme showing the frequency swept every Δt.

As with BPC, a wide range of alternatives are possible, but the following combinations have been the most commonly used in the last few months:

Bandwidth	Sweep rate
20 MHz	50 usec
40 MHz	25 usec

Offsets of 250 Hz and 500 Hz have been used.

Current and past observations of planets and planetary objects

The Planetary Radar Astronomy Program currently uses - or has used in the past - the GSSR to conduct scientific observations of the following planets and planetary objects:

- Mercury
  - Construct dual-polarization radar maps at a resolution as fine as ~ 10 km, with special emphasis of the polar regions and the unimagined hemisphere.
  - Conduct a series of closure-point ranging measurements for use in testing gravitational theories, including general relativity. Some of this work is coordinated with Arecibo observations, as part of a cooperative effort to minimize systematic sources of error.
  - Refine estimates of Mercury's pole direction to constrain theoretical explanations for the planet's spin/orbit resonance, and to measure the radius of Mercury's fluid core.
- Venus
  - Obtain radar images that improve on Magellan data in terms of their resolution of topographic maps.
  - Using the new Radar Speckle Displacement technique at Venus, it is expected that the detection of seasonal changes due to atmospheric dynamics, in addition to spin excitations due to core-mantle interactions, as well as other Venus interior processes will be determined. These observations would be in support of the science for the proposed ESA mission "Venus Express."
  - RSD tracks of Venus to understand the drivers of the variations in its spin rotation and the evolution of its orbit about the Sun.
- Moon
  - Measure lunar topography. There are three main reasons:
    a) Identify permanently shadowed regions near the poles which may harbor H2O ice (and also nearby polar areas in permanent sunlight to supply power to human or robotic investigations of the ice). H2O ice could be used to provide energy and fuel (hydrogen, oxygen) for spacecraft and habitats, as well as human consumables (oxygen) for HEDS missions.
    b) Identify hazards on the lunar near-side for robotic or human landing sites.
    c) Geological studies: Construct images of selected regions at a resolution as fine as 15m in each component of the Stokes vector to elucidate the scattering mechanism and the nature of near-surface structure and to constrain the electrical properties of the regolith. Measure topography in selected areas to refine geologic interpretation of lunar landforms. The Goldstone (radar) interferometer (DSS-14, 13, 15, 24, 25, 26 - only

need DSS-14, DSS-13 or 12 (GAVRT) and one other antenna) is uniquely suited for measuring lunar topography.

- Mars
  - Maintain the accuracy of the Mars orbital ephemerides.
  - Determine the surface reflectivity and effective slope for multiple ground tracks within the tropics.
  - Use dual-polarization, continuous-wave measurements, random-code delay-Doppler imaging, and Goldstone-VLA observations to elucidate the global variations in the surface's small-scale structural complexity.
  - Use these observations to constrain the surface's gross geometry at scales (~ 1 cm to ~ 10 m) relevant to the safe landing and maneuverability of Mars surface rovers.
- Near-Earth Asteroids

  GSSR high resolution characterization is a key element in near-Earth asteroid (NEA) hazard reduction, since knowing whether an object is a chunk of metal or a "rubble pile" would demand very different orbit modification strategies. Radar observations can determine the density of NEA binary objects- an important parameter for asteroids known accurately only for Eros and soon Ceres.

  Science objectives:
  - Secure recovery of newly discovered objects and refine orbits of previously observed objects.
  - Use delay-Doppler (and possibly interferometric) imaging to obtain information about dimensions, shapes, and spin vectors.
  - Determine dual-polarization scattering properties and elucidate near-surface characteristics at cm-to-km structural scales.
  - Measure the radar cross-section, estimate the radar albedo, and use it to bound the regolith bulk density, porosity, and metal concentration.
- Main belt Asteroids
  - Using time-delay measurements, shrink the line-of-sight component of the positional-error ellipsoid.
  - Use power spectra to constrain pole direction and diameter.
  - Estimate surface slope at topographic scales and near-surface roughness at small scales.
  - Measure the radar cross-section, estimate the radar albedo, and use it to bound the regolith bulk density, porosity, and metal concentration.
- Comets
  - Search for clouds of large (≥ cm) particles near the nucleus, such as those discovered around Halley and IRAS-Araki-Alcock. Use the G-VLA system to image those clouds.
  - Image the nucleus and determine its size, shape, spin properties, and surface characteristics.
  - Refine estimates of orbital elements to clarify the dynamical history of long-period comets and to assist spacecraft navigation during missions to short-period comets.
- Europa, Ganymede, and Callisto

- Use the G-VLA system to make global maps of radar features.
- Seek correlations with features in Voyager and Galileo images.
- Use random-code ranging to make (North-South ambiguous) images for each satellite, especially Callisto, to help in understanding the coherent backscatter phenomenon discovered in radar observation of the icy Galilean satellite.
- RSD tracks of the Galilean satellites (Europa, Ganymede and Io) to study the resonance[14] in their orbitals motions. The spin states of those three is of relevance for future missions.
- Radar ranging measurements of the Galilean satellites in order to estimate tidal dissipations of Jupiter and the satellites, and to improve the accuracy of their orbits. the radar ranging measurements of the Galilean satellites are several times more precise than optical astrometry. GSSR in a bistatic experiment with Green Bank Telescope (GBT) becomes a powerful system, more than twice as sensitive as GSSR by itself, and as such is capable of providing high-resolution ranging detections of Europa, Ganymede, and Callisto. The innermost Galilean satellite Io has the strongest tidal interaction with Jupiter, so obtaining high-precision ranging measurements of Io is particularly important. Io is the only non-icy Galilean satellite and has the smallest radar albedo, hence the lowest signal strength. Arecibo was used in order to obtain the first radar measurements of Io's line-of-sight position to date. The new ranging capability obtained from these studies is known as the long code [38]. DSN will have access to radar ranging of Galilean satellites after 2016 when Jupiter leaves Arecibo's declination window until 2022. These measurements will contribute to the maintenance of highly accurate ephemerides of the Galilean satellites that could support Europa Clipper and future missions.

❖ Saturn's Rings
- Use delay-Doppler images in each Stokes vector component to constrain the manner in which radar waves are backscattered from the classical ring sections and to infer the physical properties of ring particles.
- Use G-VLA observations to image the ring system at 1200-km resolution.

❖ Saturn's Icy Satellites
- Detect the first radar echoes from Iapetus, and possibly Rhea, to ascertain whether these objects, whose surfaces contain non-water ices, share the unusual radar properties of Jupiter's icy moons.

❖ Titan
- Refine estimates of Titan's radar properties.

The GSSR provides Flight Project support, explores targets for future spacecraft missions (e.g., the poles of Mercury, near-Earth asteroids), makes observations in response to peer-reviewed P.I.

[14] Three of the Galilean moons (Europa, Ganymede and Io) exhibit Laplace resonance (three-body resonance with a 1:2:4 orbital period). There are two Io-Europa conjunctions and three Io-Ganymede conjunctions for each Europa-Ganymede conjunction. In other words, for each Ganymede orbital period there are two Europa orbital periods and four Io orbital periods.

requests, and obtains important science results as collateral benefits from the above. Funding of the DSN Deep Space Stations (DSS) operations is funded by NASA. Funding of GSSR data analysis is supported through various U.S. and international sponsors.

Although the GSSR experiments do not involve spacecraft tracking and, hence, their importance is not driven by the mission critical events, the allocation of time for them is not free from some constraints. The criticality of the GSSR task events determined by three factors:

- use of global resources (non-DSN antennas in bi-static experiments) in conjunction with the DSN,
- time of the astronomical events (e.g., asteroid's closest approach),
- flight project request (e.g., radar mapping of landing sites on Mars).

All DSS-14 high power, >110KW, tracks require a clearance. If the track is below 27.5 degrees for DSS-13 a clearance is required. All high transmitter ops require a DSN/JPL engineer on site to operate the local equipment. Goldstone DSN DSS passes per month depend on astronomical events and P.I. requests. See GSSR User Loading Profile (ULP) for forecast:

- available at https://rapweb.jpl.nasa.gov/Requirements/GSSR.pdf

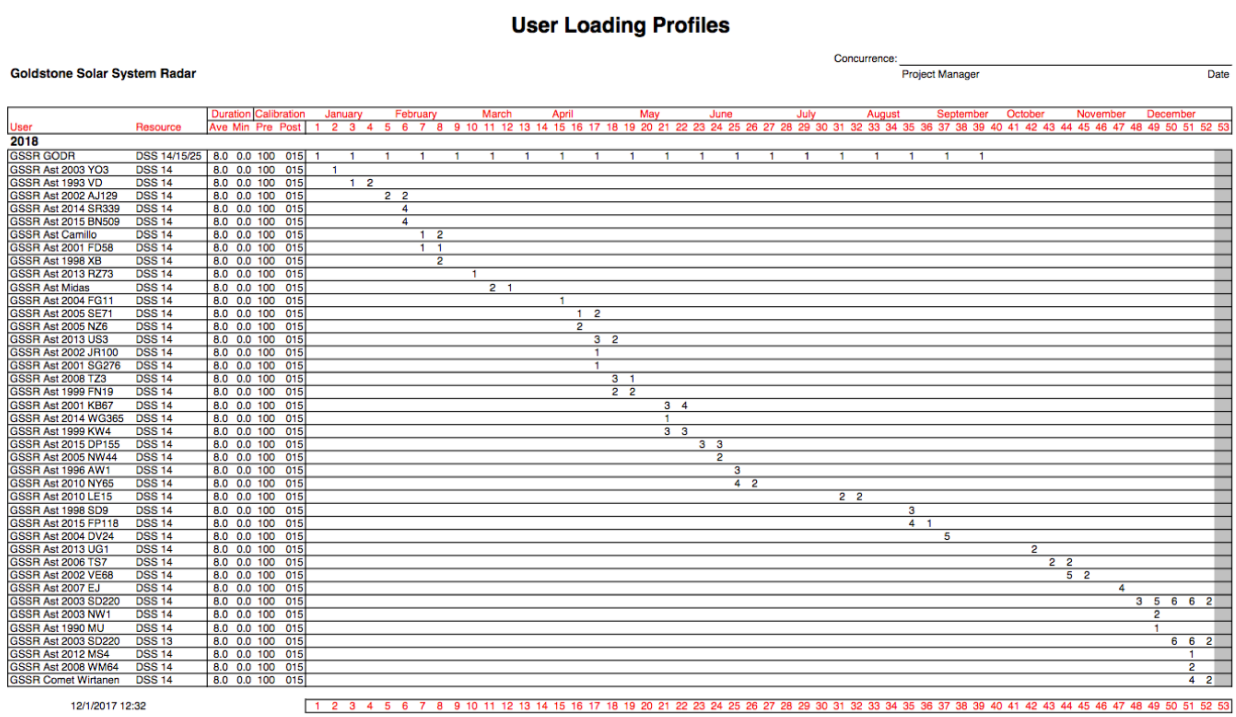

Resources

The official GSSR webpage: https://gssr.jpl.nasa.gov provides a summary of the most important discoveries.
The calendar for general planned events/tracks: https://gssr.jpl.nasa.gov/Calendar/month.php provides link to the official schedule.
Planets and planetary objects observations:

- History of attempted measurements of the spin state of Venus. http://mel.ess.ucla.edu/groupwiki/index.php/VenusRSD
- History of attempted measurements of the spin state of Europa and Ganymede. http://mel.ess.ucla.edu/groupwiki/index.php/GalSatsMasterlog

Asteroid Radar Research webpage:
https://echo.jpl.nasa.gov

- Goldstone asteroid schedule: https://echo.jpl.nasa.gov/asteroids/goldstone_asteroid_schedule.html provides the schedule for the asteroids tracks and links to the information of each asteroid. This information includes:
  - background,
  - discovery M.P.E.C link,
  - SNR calculations,
  - track assignments,
  - uncertainties,
  - setups
- Arecibo asteroid schedule: http://www.naic.edu/~pradar/ provides the schedule for the asteroids tracks and CW spectra images of recently observed objects as:

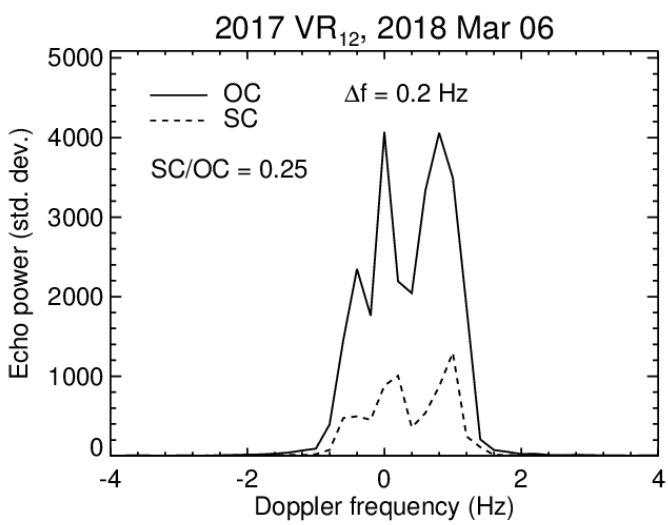

Figure 41. Image extracted from Arecibo asteroid schedule webpage for measurements of 2017VR12 on March 6, 2018

Chapter 7. Post-processing of Near-Earth Objects

This section is dedicated to learning how the signal processing of NEO's is done. It is composed of several practices that go over the different modes of operation and the process to set up the configuration file:

- Practice 1: Setting up the environment
- Practice 2: Post-processing of CW data
- Practice 3: Post-processing of BPC data
- Practice 4: Post-processing of Chirp data
- Practice 5: Post-processing of CW, BPC and Chirp data on bistatic configuration
- Practice 6: Understanding the configuration file.

Each one of these practices makes use of the examples accessible through camazotz. If you still don't have access to this machine please refer to your group supervisor and ask to have the machine added to your CAR. If foreign national expect some delays.

Once you have access to camazotz, you can start working on your practices.

PRACTICE 1: Setting up the environment

Log into your user:

```
ssh -X username@camazotz.jpl.nasa.gov
```

Create the working directories for all the practices.

```
mkdir  CW_practice
mkdir  BPC_practice
mkdir  Chirp_practice
```

Be aware that data is accessible at /run/media/username/565c4e8f-90b7-4520-9669-e0a6cdcf8b83/.
Let's make a symbolic link to the data

```
ln -s /run/media/username/565c4e8f-90b7-4520-9669-e0a6cdcf8b83/ HD
```

Run the following command to see what NEOs are available to you:

```
ls HD/ -ltr
```

Currently, the above command will list:

```
drwxr-xr-x. 3 jao gssr 35 Feb  3 17:15 2002AJ129_34
drwxr-xr-x. 3 jao gssr 35 Feb  6 14:07 2002AJ129_37
drwxr-xr-x. 3 jao gssr 35 Feb  6 19:24 2014SR339_37
drwxr-xr-x. 3 jao gssr 35 Feb  7 15:18 2018CB_38
drwxr-xr-x. 4 jao gssr 47 Feb  7 16:54 2002AJ129_36
drwxr-xr-x. 3 jao gssr 35 Feb  7 17:01 2014SR339_36
drwxr-xr-x. 3 jao gssr 35 Feb  7 17:04 2014SR339_38
drwxr-xr-x. 3 jao gssr 35 Feb  8 15:55 2014SR339_39
drwxr-xr-x. 3 jao gssr 35 Feb  9 12:57 2014SR339_40
drwxr-xr-x. 3 jao gssr 35 Feb 10 14:26 2015BN509_39
drwxr-xr-x. 3 jao gssr 35 Feb 10 14:30 2015BN509_41
drwxr-xr-x. 3 jao gssr 35 Feb 10 14:33 2014SR339_41
drwxr-xr-x. 3 jao gssr 35 Feb 19 00:13 Camillo_49
drwxr-xr-x. 3 jao gssr 35 Feb 19 00:17 2001FD58_49
drwxr-xr-x. 4 jao gssr 47 Mar  5 18:19 2017VR12_64
drwxr-xr-x. 4 jao gssr 47 Mar  7 19:50 2017VR12_66
drwxr-xr-x. 3 jao gssr 35 Mar 21 15:07 Midas_80
drwxr-xr-x. 3 jao gssr 35 Mar 21 15:10 Midas_78
drwxr-xr-x. 3 jao gssr 35 Mar 25 13:12 2018DH1_84
drwxr-xr-x. 3 jao gssr 35 Mar 26 11:47 2018DH1_85
drwxr-xr-x. 3 jao gssr 35 Apr  7 10:44 2018EB_97
drwxr-xr-x. 4 jao gssr 50 Apr 20 15:59 2018CB_40
```

In order to see what is done for each NEO, the contents of readme.1st files need to be examined. Those files are stored in each satellite folder.

For example, for 2018DH1_84:

```
cat /HD/2018DH1_84/readme.1st
```

This command lists the contents of the file:

```
033034 - 034707
17 runs CW     s19

034847 - 035907
11 runs CW     s21

040539 - 040845
 4 runs 10us   s21

041348 - 043020
17 runs 11us   s21

043202 - 043406
 3 runs 11us   s23

043806 - 044521
 8 runs 1us    s23

044925 - 051025
22 runs 0.25us s23

051609 - 061509
60 runs 0.125us s25
```

During this observation of 2018DH1_84 the following was performed:

- First 17 CW runs were performed and the ephemerides solution was updated from s19 to s21 and verified for 11 CW runs.
- Then the operation mode was switched to BPC ranging and there were 4 runs at baud 10 μs and 17 runs at baud 11 μs.
- The ephemerides solution was updated from s21 to s23 and 3 more runs of BPC ranging at 11 μs were performed to verify the change.
- Then the resolution was increased to 1 μs for 8 runs, increased again to 0.25 μs for 22 runs and finally the ephemerides solution was updated from s23 to s25.
- The resolution was finally increased to 0.125 μs for 60 runs.

If we look now to 2018DH1_85, same NEO but the following day, we can see what the scientist decided to do with this object.

```
cat HD/2018DH1_85/readme.1st

041529 - 041949
  6 runs CW    s25

042347 - 042859
  7 runs 1us   s25

043405 -
  1 run 20 MHz s25

043729 - 061436
```

```
113 runs 20 MHz s27
```

During this observation of 2018DH1_85 the following was performed:

- First 6 CW runs were performed using previous solution s25.
- Then the operation mode was switched to BPC ranging and there were 7 runs at baud 1 μs.
- Probably, as everything looked the same and SNR was strong enough, scientist decided to switch to another mode of operation: chirping.
- Chirping at 20MHz was performed for 1 run and then they switch ephemerides solutions. 1 run is too little, so probably they forgot to updated in the previous step.
- The ephemerides solution was updated from s25 to s27 and 113 runs at 20 MHz chirp were performed.

2018DH1 is then a good NEO to practice since all modes were covered. For this reason, next practices are based on 2018DH1, either 2018DH1_84 or 2018DH1_85, depending on the operation mode for the practice.

PRACTICE 2: Post-processing of CW data

Go to the CW_practice folder and create a directory for 2018DH1_84.

```
cd CW_practice/
mkdir 2018DH1_84
cd 2018DH1_84
```

Copy readme.1st and cw.cfg files.

```
cp ../../HD/2018DH1_84/readme.1st .
cp ../../HD/2018DH1_84/dss14/proc/cw.cfg .
```

cw.cfg is the configuration file.

Part 1: Loopback file

The loopback file in CW mode gives information of the system, harmonics should be at least 20 dB weaker that the main echo. The loopback file is usually before the CW runs and is of shorter length. If the files are listed:

```
ls ../../HD/2018DH1_84/dss14/ -ltr


-rw-r--r--. 1 jao gssr      87318 Mar 25 01:29 PUNCH.OUT.14v-14-14.s19
-rw-r--r--. 1 jao gssr   41000000 Mar 25 02:03 data20180325020342.000
-rw-r--r--. 1 jao gssr  113000000 Mar 25 03:31 data20180325033034.000
-rw-r--r--. 1 jao gssr  113000000 Mar 25 03:32 data20180325033136.000
-rw-r--r--. 1 jao gssr  113000000 Mar 25 03:33 data20180325033238.000
-rw-r--r--. 1 jao gssr  113000000 Mar 25 03:34 data20180325033340.000
-rw-r--r--. 1 jao gssr  113000000 Mar 25 03:35 data20180325033442.000
-rw-r--r--. 1 jao gssr  113000000 Mar 25 03:36 data20180325033544.000
-rw-r--r--. 1 jao gssr  113000000 Mar 25 03:37 data20180325033646.000
-rw-r--r--. 1 jao gssr  113000000 Mar 25 03:38 data20180325033748.000
-rw-r--r--. 1 jao gssr  113000000 Mar 25 03:39 data20180325033850.000
-rw-r--r--. 1 jao gssr  113000000 Mar 25 03:40 data20180325033952.000
-rw-r--r--. 1 jao gssr  113000000 Mar 25 03:41 data20180325034054.000
-rw-r--r--. 1 jao gssr  113000000 Mar 25 03:42 data20180325034156.000
-rw-r--r--. 1 jao gssr  113000000 Mar 25 03:43 data20180325034259.000
-rw-r--r--. 1 jao gssr  113000000 Mar 25 03:44 data20180325034401.000
-rw-r--r--. 1 jao gssr  113000000 Mar 25 03:45 data20180325034503.000
-rw-r--r--. 1 jao gssr  113000000 Mar 25 03:46 data20180325034605.000
-rw-r--r--. 1 jao gssr  113000000 Mar 25 03:47 data20180325034707.000
.
.
```

As expected, there are:

```
 033034 - 034707
17 runs CW     s19
```

PUNCH.OUT.14v-14-14.s19 is the ephemerides solution file (defined in the Appendix B), data20180325020342.000 is the loopback file and from data20180325033034.000 to data20180325034707.000 we have the 17 CW runs.

Let's process the loopback file using cw_p.pl, but first of all let's investigate what are the options for the source code.

```
cw_p.pl -h

cw_p.pl [-A | -a] [-f | -F <file>] [-e <cfg>] [-w <dir>] [-l] [-b <skp sec> | -B <skp blk>]
[-o <frqofst>] [-i <bw>] [-n <fft>] [-s | -S] [-d | -D] [-X] [-M | -m] [-G | -g] [-r] [-q]
where: -A | -a      : autorun on [all | 1st] data file
       -f <file>    : specify data file from local disk
       -F <file>    : specify data file from Fiber Channel
       -e <cfg>     : use different config file (default: cw.cfg)
       -w <dir>     : change working directory
       -l           : loopback data
       -B <FCB blk> : elapsed FCB blocks to be skipped
       -b <sec>     : elapsed time to be skipped
       -c <sec>     : elapsed time to be processed
       -o <frqofst> : frequency offset
       -i <bw>      : spectrum bandwidth
       -n <fft>     : FFT for PSD
       -s | -S      : add to summation (-S to restart summation)
       -d | -D      : gnuplot() display on single rum or summation
       -x | -X      : calculate cross-section (accumulation or final run)
       -G | -g      : Retrieve | use this Ephemerides file
       -z | -Z      : DRCV configuration (mode:-7; swap:NO; F(s):5MHz
       -q           : quit when error
       -r           : replace spectrum file if it exists
       -v           : calculate Mean/Variance
       -M | -m      : mute mode - msg to /tmp/debug file (-M to flush content)
```

Let's use:

- -f and specify the file to process, including path,
- -r to overwrite exixting files,
- -a for automathic, which uses the stored cw.cfg values, and
- -l to indicate we are processing loopback data.

```
cw_p.pl -f ../../HD/2018DH1_84/dss14/data20180325020342.000 -r -l -a
```

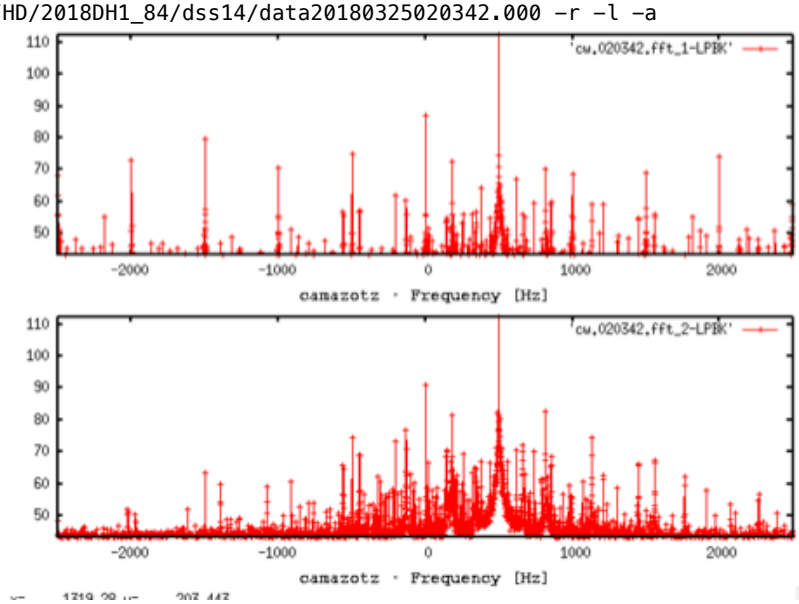

Figure 42. Loopback processing for 2018DH1_84/dss14/data20180325020342.000

The principal harmonic is at 500 Hz offset and is about 112 dB, while the harmonics are below 85 dB for one channel and 90 dB for the second channel, which makes a difference of about 27 and 22 dB, respectively.

Part 2: CW runs

Looking back at the contents of the readme.1st file:

```
033034 - 034707
17 runs CW     s19

034847 - 035907
11 runs CW     s21

040539 - 040845
 4 runs 10us   s21

041348 - 043020
17 runs 11us   s21

043202 - 043406
 3 runs 11us   s23

043806 - 044521
 8 runs 1us    s23
044925 - 051025
22 runs 0.25us s23

051609 - 061509
60 runs 0.125us s25
```

There are two pieces of data to process, one is using solution s19 and the other one is using the updated solution to s21.

```
033034 - 034707
17 runs CW     s19

034847 - 035907
11 runs CW     s21
```

So let's start processing the first 17 runs. To do this we can make use of autocw.pl.

```
autocw.pl -h

* * * * * * * * * * * * * * * * * * * * * * * * * * * * * * * * *
*                                                               *
* autocw.pl [-p] <dir>/<1st file> <dir>/<last file> ["options"] *
* where  -p : pause between processing                          *
*        <dir> : data files directory                           *
*        <1st file> <lst file> : "data."YYYYMMDDhhmmss          *
*        ["options"] : (optional) parameters                    *
*              e.g. "-d" for gnuplot() display                  *
*                                                               *
* * * * * * * * * * * * * * * * * * * * * * * * * * * * * * * * *
```

That is:

```
autocw.pl ../../HD/2018DH1_84/dss14/data20180325033034.000
../../HD/2018DH1_84/dss14/data20180325034707.000 -r
```

If successful it will show a final message:

```
*** Totally 17 files processed ***
```

Next step is to sum those runs together reducing the noise. To do that we use: mapssum.pl.

```
mapssum.pl -h

* * * * * * * * * * * * * * * * * * * * * * * * * * * * * * * * * * * * * *
*
* mapssum.pl <dir>/<1st map> [<last map> | -1 | #maps] [options]
* where  <dir> : files directory
*        <1st file>, <lst file> : "{map}."yyyymmddhhmmss
*
*        <options> :
*            -n <cnt>         - number of summation
*            -t <tmspan>      - duration of summation
*            -f               - auto scaling
*            -v <frqlo:frqhi> - normalization for CW to the (low:high) freq
*            -v <col:row>     - normalization for map w/ Doppler and range bins
*            -q               - don't save any incomplete sum
*            -s <fname>       - filename for incomplete sum (e.g. map.sum_1)
*            -m '<flag>'      - mirrormap w/ parameter
*        e.g. mapssum.pl <1st file> -1 -t 350 -v 128:255 -m "-f 511" -q
*
* * * * * * * * * * * * * * * * * * * * * * * * * * * * * * * * * * * * * *
```

Following the options of mapssum.pl we will:

```
mapssum.pl ./cw.033034.fft_1 ./cw.034707.fft_1 -v 200:2495
mapssum.pl ./cw.033034.fft_2 ./cw.034707.fft_2 -v 200:2495
```

When processing the autocw.pl messages like the following appear on your terminal:

```
FFT length                    : 10000
Frequency resolution          : 5.000000e-01 Hz
Processed bandwidth           : 5.000000e+03 Hz
```

Processed bandwidth = 10000*0.5 = 5000, means your frequency span goes from -2500 to 2500. So we normalize for CW to the (low:high) frequency by setting -v from 200 to 2495. Also we sum both channels, the opposite sense (1) and same sense (2).

Finally we plot those sums using gnuplot. So, type `gnuplot` in your terminal and:

```
plot [-40:40] 'sum.cw-fft_1-033034-034707-17-SD' w line, 'sum.cw-fft_2-033034-
034707-
17-SD' w line
```

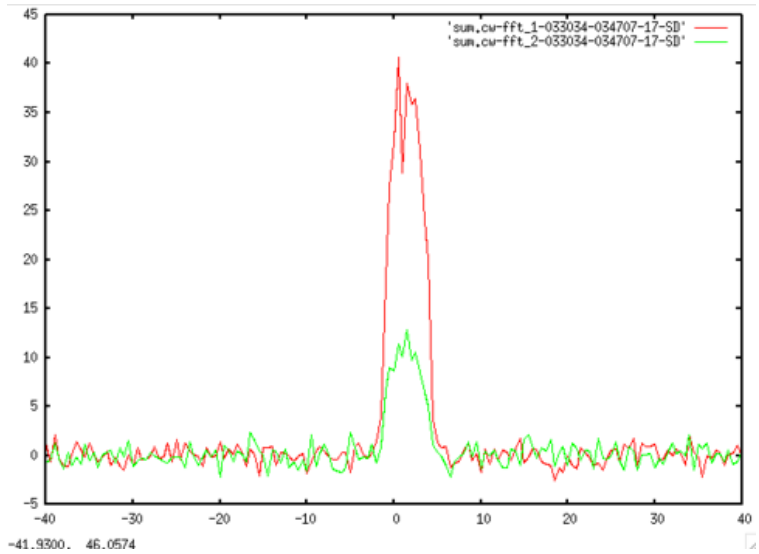

Figure 43. CW data processed for channels 1 and 2 from 2018DH1_84/dss14/data20180325033034.000 to 2018DH1_84/dss14/data20180325034707.000

Looking at fig. 44 we can get some information about the object:

- Center frequency is a little bit shifted to the right. This means the ephemerides solution can be updated.
- The object is narrow which indicates it is a slow rotator.
- Channel 2 is noticeable but it is less powerful than channel 1. The object has some degree of rugosity.

Following with the track, the solution was updated from s19 to s21, and there were 11 CW runs.

```
034847 – 035907
11 runs CW     s21
```

Let's repeat the processing by:

```
autocw.pl ../../HD/2018DH1_84/dss14/data20180325034847.000
../../HD/2018DH1_84/dss14/data20180325035907.000 -r

        *** Totally 11 files processed ***

mapssum.pl ./cw.034847.fft_1 ./cw.035907.fft_1 -v 200:2495
        File Created: sum.cw-fft_1-034847-035907-11-SD

mapssum.pl ./cw.034847.fft_2 ./cw.035907.fft_2 -v 200:2495
        File Created: sum.cw-fft_2-034847-035907-11-SD

gnuplot
plot  [-40:40]  'sum.cw-fft_1-034847-035907-11-SD  w  line,  'sum.cw-fft_2-034847-
035907-11-SD'
w line
```

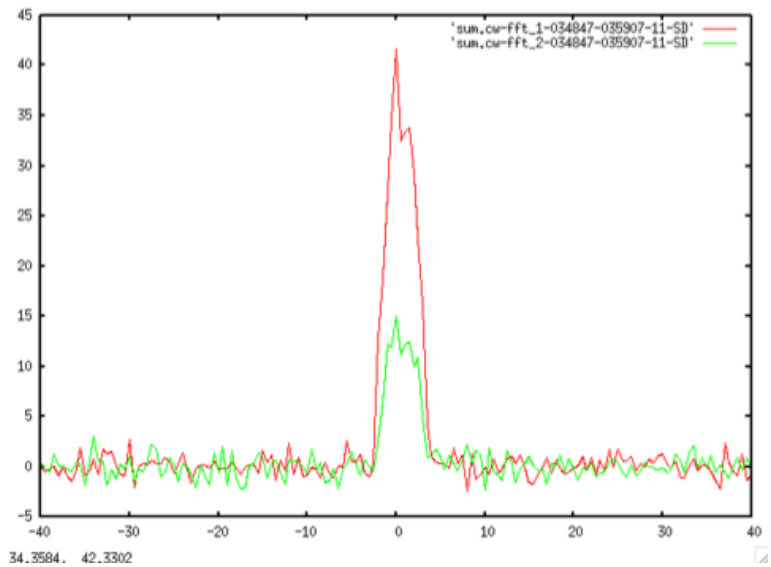

Figure 44. CW data processed for channels 1 and 2 from 2018DH1_84/dss14/data20180325034847.000 to 2018DH1_84/dss14/data20180325035907.000

Solution s21 has been updated and the echo center frequency has moved toward 0 Hz.

Before going to ranging in practice 3 let's modify the configuration file to reduce the frequency resolution and see how this impacts the echo in fig. 38.

To do this, run a single file and go through the configuration file and set parameters manually by not using -a.

```
cw_p.pl -f ../../HD/2018DH1_84/dss14/data20180325034847.000 -r -d
```

The following parameters to set or modify will appear, just hit enter until you reach frequency resolution, which is set to 0.5 Hz and we will modify to 0.25 Hz.

```
cw_p.pl Ver. 6.00
Target                                  : [2018DH1]
Directory                                : [/run/media/nalvarez/565c4e8f-90b7-4520-
9669-
                                         e0a6cdcf8b83/2018DH1_84/dss14/]
Mode                                    : [6]
    Channel to Use                      : []
    Swapping I & Q                      : [Y]
Recording Time                          : [20180325034847]
Sample Frequency (in MHz)               : [2]
Data-taking duration                    : [28]
   Sec Worth of Data to Skip            : []
   (opt) FCB Block (8KB) to Skip        : []
   Sec Worth of Data to Process         : []
No. of Hops                             : [] 1
    Freq Shifting (Y or N)              : [Y]
    Freq Offset                         : [-500]
Calculate Round-Trip time               : [N]
    Round Trip Time                     : []
```

```
Remove Doppler? (RG|DR|N)            : [N]
Spectrum bandwidth                   : [5000]
Freq Resolution                      : [0.5] 0.25
    (FFT Length)                     : [20000]
Remove DC (Y or N)                   : [Y]
Limit No. of Transfer to Add         : []
FFT BW Limit (Y or N)                : [N]
FFT in Time Series                   : [N]
FFT in dB (Y or N)                   : [N]
Standard Deviation(Y or N)           : []
Save Unp File (Y or N)               : []

Re-configure Gnuplot  : [N]
      Save This Configuration?  [ cw.cfg ]

         Configuration Saved to cw.cfg!

Limit data unpacking to the 1st block? .....[N] ^C
```

Once you see: `"Configuration Saved to cw.cfg!"` You can skip by ctrl+C. Let's repeat the processing one more time by:

```
autocw.pl ../../HD/2018DH1_84/dss14/data20180325034847.000
../../HD/2018DH1_84/dss14/data20180325035907.000 -r
mapssum.pl ./cw.034847.fft_1 ./cw.035907.fft_1 -v 200:2495
mapssum.pl ./cw.034847.fft_2 ./cw.035907.fft_2 -v 200:2495
gnuplot
plot  [-40:40]  'sum.cw-fft_1-034847-035907-11-SD'  w  line,  'sum.cw-fft_2-034847-035907-11-SD'
w line
```

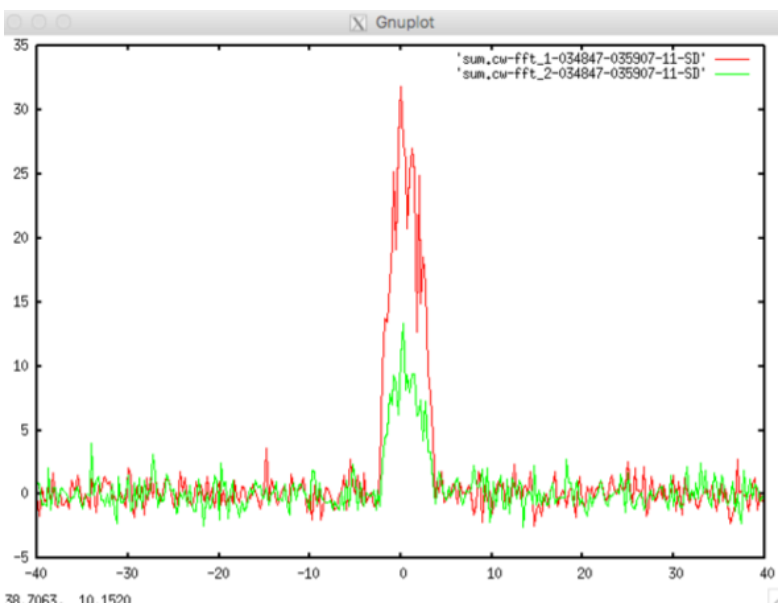

Figure 45. CW data processed for channels 1 and 2 wit frequency resolution modified to 0.25 Hz: from 2018DH1_84/dss14/data20180325034847.000 to 2018DH1_84/dss14/data20180325035907.000

As it can be seen by comparing fig. 39 and fig. 38, the frequency resolution has been increased to 0.25 Hz, and the echoes look much less smooth.

PRACTICE 3: Post-processing of BPC data

Go to the BPC_practice folder and create a directory for 2018DH1_84.

```
cd BPC_practice/
mkdir 2018DH1_84
cd 2018DH1_84
```

Copy readme.1st and cw.cfg files.

```
cp ../../HD/2018DH1_84/readme.1st .
cp ../../HD/2018DH1_84/dss14/proc/bpc.* .
```

bpc.10us, bpc.11us, bpc.1us, bpc.0.25us and bpc.0.125us are the configuration files for each one of the following:

```
040539 - 040845
 4 runs 10us   s21

041348 - 043020
17 runs 11us   s21

043202 - 043406
 3 runs 11us   s23

043806 - 044521
 8 runs 1us    s23

044925 - 051025
22 runs 0.25us s23

051609 - 061509
60 runs 0.125us s25
```

Part 1. BPC at 10 us

For BPC configuration file, we need to modify the location of the ephemerides solution file. For doing this we can run a single file and use rng_p.pl.

```
rng_p.pl -h

rng_p.pl [-A | -a] [-f | -F <file>] [-e <drv>] [-l] [-b <skp sec> | -B <skp blk>] [-c
<proc sec> | -C <proc blk>] [-1 <fst bin> -2 <lst bin>] [-k code] [-i <fft>] [-n ncoh]
[-u <chn>] [-g <efile>] [-p] [-w <dir>] [-s | -S] [-d | -D] [-t <dst>} [-z <mode>] [-M
| -m] [-q]
where: -A | -a   : autorun on [all | 1st] data file
       -b <sec>  : elapsed time to be skipped
       -B <blk>  : blocks to be skipped (Fiber Channel only)
       -c <sec>  : elapsed time to be processed
       -C <blk>  : blocks to be procssed (Fiber Channel only)
       -d | -D   : start saoimage display [current run | sum]
       -e <drv>  : use different than the default <bpc|lfm>.cfg file
       -f <file> : specify file name from local drive
       -F <file> : specify file from Fiber Channel
       -l        : process as loopback data
       -o        : option - for Chirp processing
       -k <code> : code length (BPC)
```

```
        -i <fft>  : FFT length
        -n <ncoh> : coherent average
        -g <efile>: Ephemerides file
        -z <mode> : DRCV mode (also set swapiq=N)
        -M | -m   : mute mode - msg to '/tmp/debug' file (-M to flush content)
        -r        : replace the map file if it exists
        -t <dst>  : transfer map file to <host:dir>; e.g. morag:/mnt/backups/gssr/tmp
        -p        : don't echo configuration to screen
        -q        : quit when error
        -s | -S   : add to summation (-S to restart summation)
        -u <chn>  : Channel (pol2use) to use
        -v        : calculate mean & variance
           -y       : print FFT I/Q components
        -w <dir>  : change working directory
        -1 <fst>  : override start of range bin (bin1)
        -2 <lst>  : override end of range bin
```

From all these options we are not going to use any since we only want to modify the configuration file.

```
rng_p.pl -f ../../HD/2018DH1_84/dss14/data20180325040539.000


rng_p.pl Version 9.02 09/23/16
    (0)     bpc.0.125us
    (1)     bpc.0.25us
    (2)     bpc.10us
    (3)     bpc.11us
    (4)     bpc.1us
    Select BPC Control File          : [0] 2
File Base (fbase)                    : [2018DH1]
Directory                            : [../../HD/2018DH1_84/dss14/]
Recording Time                       : [20180325040539]
data-taking duration                 : [28]
   Sec of Data to Skip               : []
   Sec of Data to Process            : []
Op Mode ("-" for 2's comp)           : [2]
   Swapping I & Q                    : [Y]
Hardware Sampling Rate (in MHz)      : [2]
Remove Doppler? (RG|DR|DP|DD|F(f)|N) : [N]
Time Drift? (RG|DR|N)                : [N]
Calculate Phase Delay?               : [Y]
   Ephemerides File Name               : [PUNCH.OUT.14v-14-14.s21]
 ../../HD/2018DH1_84/dss14/PUNCH.OUT.14v-14-14.s21
   XMT Station                       : [4]
   Sky Frequency                     : [8560000000]
   UpLink to station                 : [4]
   RCV Station                       : [4]
   Planet No.                        : [9]
   Satellite No.                     : [99]
Station/Site Delay (in usecs)        : [0]
Freq Offset (in Hz)                  : []
Range Offset (in bins)               : []
Baud (in uSec)                       : [10]
Downsample Size (pre-drift)          : [20]
Downsample Size (post-drift)         : [1]
Code Length (start w/ 'L':longcode)  : [127]
   Make sure offset < 393 Hz (<ok>)  : [Ok]
   FFT Length for Decoding           : [256]
   Frames to Skip                    : []
   Limit no. of Frames to Decode     : [99999999]
   1st Range Bin to Save             : [1]
   Num of Range Bins to Save         : [127]
Cross-range FFT Size (< 2113665)     : [256]
```

```
Freq Resolution (0.0357 to 3.08 Hz)  : [3.0757874015748]
   86 FFT frames, 0.0 sec wasted     : [Ok]
   Coherent Averaging                : [1]
   zeropadding ratio? (nopad = 1)    : []

<Optional Parameters>
Remove DC?                           : [Y]
Scale Image to Sigma?                : []
Compress Image file (Y or N)         : []
Image Rotation (C|R|F|c|r|f|N)       : [F]
Label Map File?                      : []
Display with ds9 or saoimage?        : [ds9]
   Center on target?                 : [Y]
   Set zoom level to?                : [4]
   Dsp scale? (linear|log|histequ)   : []
Sufix for File Extension             : [p?]
Sufix for FFT Output File            : [map]
Preserve unppacked data?             : [N]
Preserve decoded data?               : [N]

      Save This Configuration?  [ bpc.10us ]

         Configuration Saved to bpc.10us!
```

Important parameters are code length = 127 and fft size = 256.

Now let's process:

```
040539 - 040845
 4 runs 10us       s21
```

For this, we are going to use autorng.pl

```
autorng.pl -h

        dir = ../  start tm =  end tm = [options]

        options: nothing means bpc, -o means chirping.
```

Basically, the function needs initial and final file.

```
autorng.pl ../../HD/2018DH1_84/dss14/data20180325040539.000
../../HD/2018DH1_84/dss14/data20180325040845.000

        *** Totally 4 files processed ***
```

Now let's sum the files created, by using mapssum.pl. We are going to use option -v, that in bpc stands for:

```
-v <col:row>     - normalization for map w/ Doppler and range bins
```

Or in other words, -v fft_size: code_length, that are set to 256 and 127 respectively.

```
mapssum.pl ./map.20180325040539-p1 ./map.20180325040845-p1 -v 256:127

File Created: sum.map-p1-040539-040845-4-SD
```

To plot ranging mk_mpeg.pl is used:

```
mk_mpeg.pl -h

mk_mpeg.pl <w> <h> [-v <ptn1:ptn2:...>] [-n <ptn1:ptn2:...>] [-c <n>|-C {-1 | 0 |
<x:y>}] [-z <mag>] [-s dscale]
       {more options} = [-w <dir>] [-f <fname>] [-1 <fst>] [-l <lst>]

where  <w>                    : map width  (freq bin)
       <h>                    : map heigth (range bin)
       [-v <ptn...>]          : display files with matching patterns (default: map.)
       [-n <ptn...>]          : gnore files with matching patterns
       [-c <n>]               : all maps centered based on the nth map
        [-C {-1 | 0 | <x:y>}] : '0'- individual; '-1'- manual; otherwise- centered @
        [x,y]
                                 coordinates
       [-z <mag>]             : zone in w/ magnifier
       [-s  <dscale>]               :  display  scale,  e.g.  log,  sqrt,  squared,  etc
(default:linear)

       [-w <dir>]             : working directory (default: PWD)
       [-f <fname>]           : display <fname> file
       [-1 <fst>]             : first sorted maps to display (default: 1)
       [-l <lst>]             : last sorted maps to display (default: 999)
```

Where <w> = fft_size = 256 and <h> = code_length = 127.

```
mk_mpeg.pl 256 127 -f sum.map-p1-040539-040845-4-SD -c 1 -z 4

                mappeak 256 127 sum.map-p1-040539-040845-4-SD
                Signal Strength:
                      0  @ frq   162, range bin    92 =        26.26
                      1  @ frq   161, range bin    92 =        16.82
                      2  @ frq    64, range bin    52 =         4.63
```

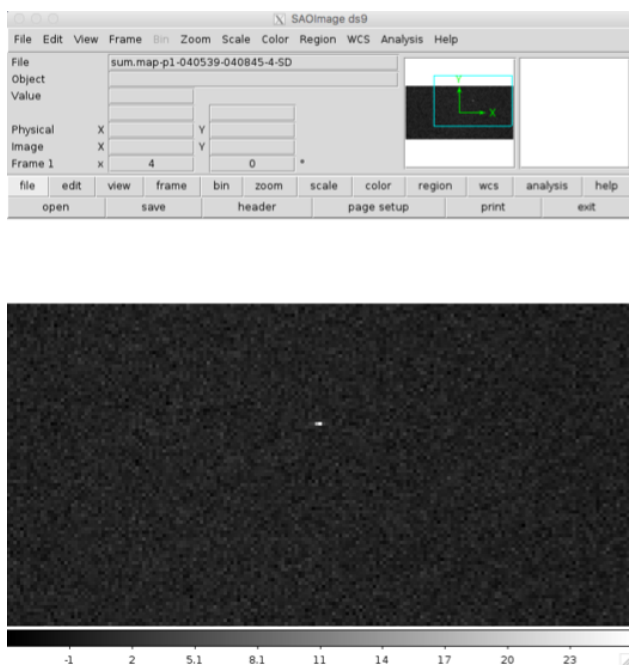

Figure 46. Ranging processing at 10 us for files from 2018DH1_84/dss14/data20180325040539.000 to 2018DH1_84/dss14/data20180325040845.000

The maximum is found at frq 162, range bin 92. Does it make sense?
The center is equal to the fft_size divided by 2, i.e. 128. Echo bin position needs to be always on the right side. In this case echo is located at bin 162. So the echo is 162 – 128 = 34 bins to the right. This implies an offset of 34 times frequency resolution (3.075 Hz in configuration file), which translates into a 104.75 Hz offset.

Part 2. BPC at 11 us

For BPC configuration file, we need to modify the location of the ephemerides solution file. For doing this we can run a single file and use rng_p.pl.

```
rng_p.pl -f ../../HD/2018DH1_84/dss14/data20180325041348.000

rng_p.pl Version 9.02 09/23/16
    (0)     bpc.0.125us
    (1)     bpc.0.25us
    (2)     bpc.10us
    (3)     bpc.11us
    (4)     bpc.1us
    Select BPC Control File          : [0] 3
File Base (fbase)                    : [2018DH1]
Directory                            : [../../HD/2018DH1_84/dss14/]
Recording Time                       : [20180325043406]
data-taking duration                 : [28]
   Sec of Data to Skip               : []
   Sec of Data to Process            : []
Op Mode ("-" for 2's comp)           : [2]
   Swapping I & Q                    : [Y]
Hardware Sampling Rate (in MHz)      : [2]
Remove Doppler? (RG|DR|DP|DD|F(f)|N) : [N]
Time Drift? (RG|DR|N)                : [N]
Calculate Phase Delay?               : [Y]
   Ephemerides File Name               : [../PUNCH.OUT.14v-14-14.s21]
 ../../HD/2018DH1_84/dss14/PUNCH.OUT.14v-14-14.s21
   XMT Station                       : [4]
   Sky Frequency                     : [8560000000]
   UpLink to station                 : [4]
   RCV Station                       : [4]
   Planet No.                        : [9]
   Satellite No.                     : [99]
Station/Site Delay (in usecs)        : [0]
Freq Offset (in Hz)                  : []
Range Offset (in bins)               : []
Baud (in uSec)                       : [11]
Downsample Size (pre-drift)          : [22]
Downsample Size (post-drift)         : [1]
Code Length (start w/ 'L':longcode)  : [127]
   Make sure offset < 357 Hz (<ok>)  : [Ok]
   FFT Length for Decoding           : [256]
   Frames to Skip                    : []
   Limit no. of Frames to Decode     : [99999999]
   1st Range Bin to Save             : [1]
   Num of Range Bins to Save         : [127]
Cross-range FFT Size (< 2113665)     : [256]
Freq Resolution (0.0357 to 2.80 Hz)  : [2.796170365068]
   78 FFT frames, 0.1 sec wasted     : [Ok]
   Coherent Averaging                : [1]
   zeropadding ratio? (nopad = 1)    : []

<Optional Parameters>
```

```
Remove DC?                          : [Y]
Scale Image to Sigma?               : []
Compress Image file (Y or N)        : []
Image Rotation (C|R|F|c|r|f|N)      : [F]
Label Map File?                     : []
Display with ds9 or saoimage?       : [ds9]
   Center on target?                : [Y]
   Set zoom level to?               : [4]
   Dsp scale? (linear|log|histequ)  : []
Sufix for File Extension            : [p?]
Sufix for FFT Output File           : [map]
Preserve unppacked data?            : [N]
Preserve decoded data?              : [N]

      Save This Configuration?  [ bpc.11us ]
         Configuration Saved to bpc.11us!
```

Now let's process like we did for 10 us. Remember that we are now using files:

```
041348 - 043020
17 runs 11us       s21

autorng.pl ../../HD/2018DH1_84/dss14/data20180325041348.000
../../HD/2018DH1_84/dss14/data20180325043020.000 -r

       *** Totally 17 files processed ***

mapssum.pl ./map.20180325041348-p1 ./map.20180325043020-p1 -v 256:127

       File Created: sum.map-p1-041348-043020-17-SD

       mk_mpeg.pl 256 127 -f sum.map-p1-041348-043020-17-SD -c 1 -z 4

              mappeak 256 127 sum.map-p1-041348-043020-17-SD
              Signal Strength:
                    0  @ frq   165, range bin    96 =        64.97
                    1  @ frq   164, range bin    96 =        23.16
                    2  @ frq   166, range bin    96 =        14.86
```

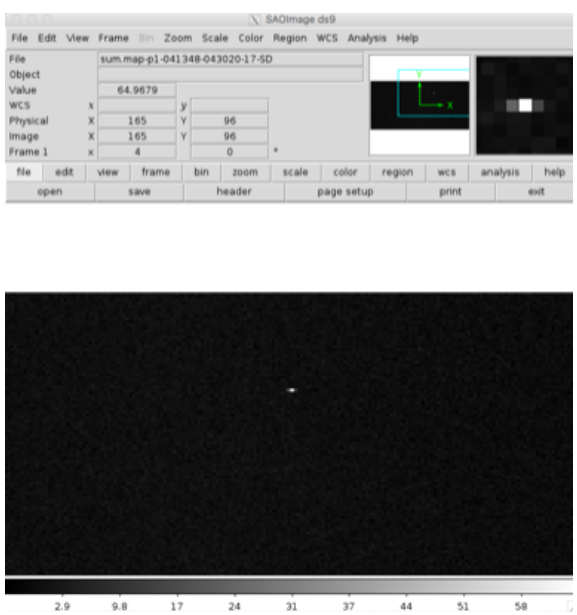

Figure 47. Ranging processing at 11 us for files from 2018DH1_84/dss14/data20180325041348.000 to 2018DH1_84/dss14/data20180325043020.000

The center is equal to the fft_size divided by 2, i.e. 128. In this case echo is located at bin 165. So the echo is 165 – 128 = 37 bins to the right. This implies an offset of 37 times frequency resolution (2.8 Hz in configuration file), which translates into a 103.6 Hz offset.

Based on 10 us and 11 us ranging, the solution is updated. It appears the scientist requested for 3 more runs after updating the solution from s21 to s23.

```
043202 - 043406
 3 runs 11us       s23
```

Let's quickly process those files.

First modify ephemerides file into configuration file:

```
rng_p.pl Version 9.02 09/23/16
    (0)     bpc.0.125us
    (1)     bpc.0.25us
    (2)     bpc.10us
    (3)     bpc.11us
    (4)     bpc.1us
    Select BPC Control File          : [0] 3
File Base (fbase)                    : [2018DH1]
Directory                            : [../../HD/2018DH1_84/dss14/]
Recording Time                       : [20180325043202]
data-taking duration                 : [28]
   Sec of Data to Skip               : []
   Sec of Data to Process            : []
Op Mode ("-" for 2's comp)           : [2]
   Swapping I & Q                    : [Y]
Hardware Sampling Rate (in MHz)      : [2]
Remove Doppler? (RG|DR|DP|DD|F(f)|N) : [N]
Time Drift? (RG|DR|N)                : [N]
Calculate Phase Delay?               : [Y]
   Ephemerides File Name                : [../../HD/2018DH1_84/dss14/PUNCH.OUT.14v-14-
14.s21]
 ../../HD/2018DH1_84/dss14/PUNCH.OUT.14v-14-14.s23

autorng.pl ../../HD/2018DH1_84/dss14/
data20180325043202.000 ../../HD/
2018DH1_84/dss14/data20180325043406.000 -r

        *** Totally 3 files processed ***

mapssum.pl ./map.20180325043202-p1 ./map.20180325043406-p1 -v 256:127

        File Created: sum.map-p1-043202-043406-3-SD

mk_mpeg.pl 256 127 -f sum.map-p1-043202-043406-3-SD -c 1 -z 4

                    Signal Strength:
                      0  @ frq   165, range bin   127 =        28.51
                      1  @ frq   166, range bin   127 =        12.01
                      2  @ frq   164, range bin   127 =         8.01
```

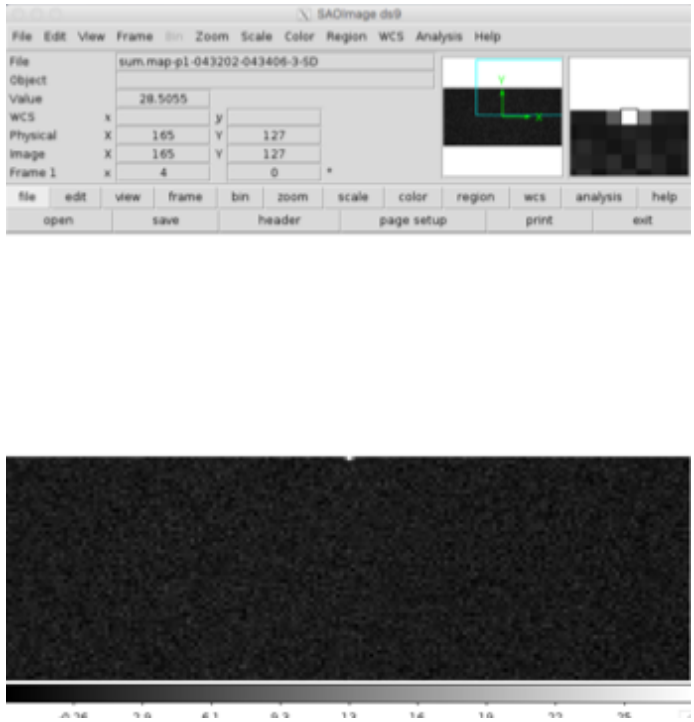

Figure 48. Ranging processing at 11 us with updated solution for files from 2018DH1_84/dss14/data20180325043202.000 to 2018DH1_84/dss14/data20180325043406.000

Part 3. BPC at 1 us

Let's modify the location of the ephemerides' solution file. Remember we are going to process:

```
043806 - 044521
8 runs 1us     s23


rng_p.pl -f HD/2018DH1_84/dss14/
data20180325043806.000

rng_p.pl Version 9.02 09/23/16
    (0)     bpc.0.125us
    (1)     bpc.0.25us
    (2)     bpc.10us
    (3)     bpc.11us
    (4)     bpc.1us
    Select BPC Control File          : [0] 4
File Base (fbase)                    : [2018DH1]
Directory                            : [../../HD/2018DH1_84/dss14/]
Recording Time                       : [20180325043806]
data-taking duration                 : [28]
   Sec of Data to Skip               : []
   Sec of Data to Process            : []
Op Mode ("-" for 2's comp)           : [3]
   Swapping I & Q                    : [Y]
Hardware Sampling Rate (in MHz)      : [8]
Remove Doppler? (RG|DR|DP|DD|F(f)|N) : [N]
Time Drift? (RG|DR|N)                : [N]
Calculate Phase Delay?               : [Y]
```

```
   Ephemerides File Name                : [../PUNCH.OUT.14v-14-14.s23]
 ../../HD/2018DH1_84/dss14/PUNCH.OUT.14v-14-14.s23
   XMT Station                        : [4]
   Sky Frequency                      : [8560000000]
   UpLink to station                  : [4]
   RCV Station                        : [4]
   Planet No.                         : [9]
   Satellite No.                      : [99]
Station/Site Delay (in usecs)         : [0]
Freq Offset (in Hz)                   : []
Range Offset (in bins)                : []
Baud (in uSec)                        : [1]
Downsample Size (pre-drift)           : [8]
Downsample Size (post-drift)          : [1]
Code Length (start w/ 'L':longcode)   : [255]
   Make sure offset < 1960 Hz (<ok>) : [Ok]
   FFT Length for Decoding            : [512]
   Frames to Skip                     : []
   Limit no. of Frames to Decode      : [99999999]
   1st Range Bin to Save              : [1]
   Num of Range Bins to Save          : [255]
Cross-range FFT Size (< 1052688)      : [256]
Freq Resolution (0.0357 to 15.32 Hz) : [3.8296568627451]
   107 FFT frames, 0.1 sec wasted     : [Ok]
   Coherent Averaging                 : [4]
   zeropadding ratio? (nopad = 1)     : []

<Optional Parameters>
Remove DC?                            : [Y]
Scale Image to Sigma?                 : []
Compress Image file (Y or N)          : []
Image Rotation (C|R|F|c|r|f|N)        : [F]
Label Map File?                       : []
Display with ds9 or saoimage?         : [ds9]
   Center on target?                  : [Y]
   Set zoom level to?                 : [4]
   Dsp scale? (linear|log|histequ)    : []
Sufix for File Extension              : [p?]
Sufix for FFT Output File             : [map]
Preserve unppacked data?              : [N]
Preserve decoded data?                : [N]

      Save This Configuration?  [ bpc.1us ]

         Configuration Saved to bpc.1us!
```

Note that now code_length is 255, fft_size is 256.

```
autorng.pl ../../HD/2018DH1_84/dss14/data20180325043806.000
../../HD/2018DH1_84/dss14/data20180325044521.000 -r

       *** Totally 8 files processed ***


mapssum.pl ./map.20180325043806-p1 ./map.20180325044521-p1 -v 256:255

       File Created: sum.map-p1-043806-044521-8-SD

mk_mpeg.pl 256 255 -f sum.map-p1-043806-044521-8-SD -c 1 -z 4
```

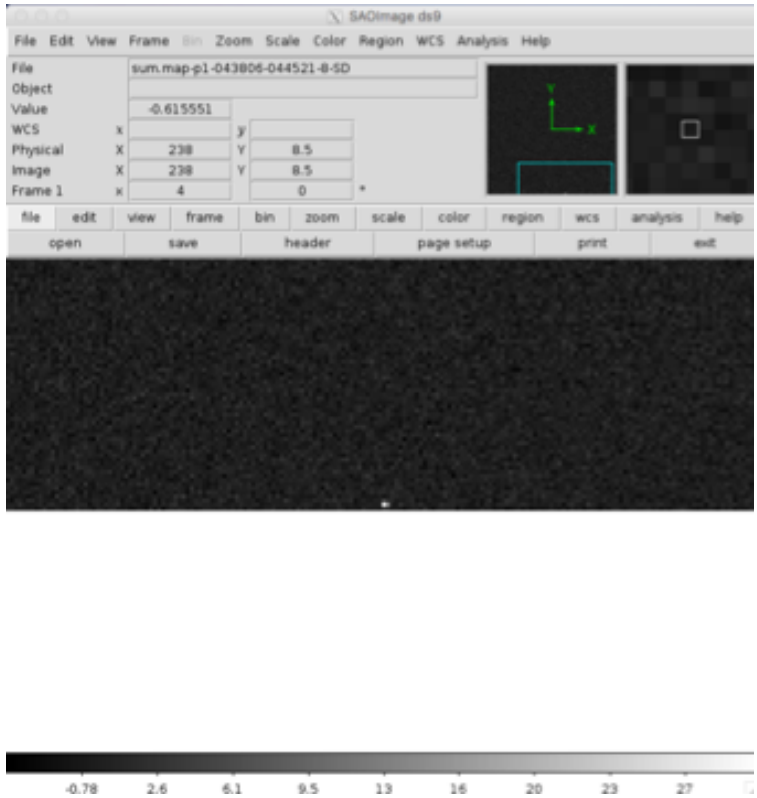

Figure 49. Ranging processing at 1 for files from 2018DH1_84/dss14/data20180325043806.000 to 2018DH1_84/dss14/data20180325044521.000

The center is equal to the fft_size divided by 2, i.e. 128. In this case echo is located at bin 155. So the echo is 155 – 128 = 27 bins to the right. This implies an offset of 27 times frequency resolution (3.83 Hz in configuration file), which translates into a 103.6 Hz offset.

Part 4. BPC at 0.25 us

Let's modify the location of the ephemerides solution file. Remember we are going to process:

```
044925 - 051025
22 runs 0.25us s23


rng_p.pl -f ../../HD/2018DH1_84/dss14/data20180325044925.000 -r

rng_p.pl Version 9.02 09/23/16
    (0)     bpc.0.125us
    (1)     bpc.0.25us
    (2)     bpc.10us
    (3)     bpc.11us
    (4)     bpc.1us
    Select BPC Control File          : [0] 1
File Base (fbase)                    : [2018DH1]
Directory                            : [../../HD/2018DH1_84/dss14/]
```

```
Recording Time                        : [20180325044925]
data-taking duration                  : [27]
   Sec of Data to Skip                : []
   Sec of Data to Process             : []
Op Mode ("-" for 2's comp)            : [3]
   Swapping I & Q                     : [Y]
Hardware Sampling Rate (in MHz)       : [20]
Remove Doppler? (RG|DR|DP|DD|F(f)|N)  : [N]
Time Drift? (RG|DR|N)                 : [N]
Calculate Phase Delay?                : [Y]
   Ephemerides File Name                : [../PUNCH.OUT.14v-14-14.s23]
 ../../HD/2018DH1_84/dss14/PUNCH.OUT.14v-14-14.s23
   XMT Station                        : [4]
   Sky Frequency                      : [8560000000]
   UpLink to station                  : [4]
   RCV Station                        : [4]
   Planet No.                         : [9]
   Satellite No.                      : [99]
Station/Site Delay (in usecs)         : [0]
Freq Offset (in Hz)                   : []
Range Offset (in bins)                : []
Baud (in uSec)                        : [0.25]
Downsample Size (pre-drift)           : [5]
Downsample Size (post-drift)          : [1]
Code Length (start w/ 'L':longcode)   : [255]
   Make sure offset < 7843 Hz (<ok>)  : [Ok]
   FFT Length for Decoding            : [512]
   Frames to Skip                     : []
   Limit no. of Frames to Decode      : [99999999]
   1st Range Bin to Save              : [1]
   Num of Range Bins to Save          : [255]
Cross-range FFT Size (< 1052688)      : [1024]
Freq Resolution (0.0370 to 15.32 Hz)  : [0.957414215686274]
   25 FFT frames, 0.9 sec wasted      : [Ok]
   Coherent Averaging                 : [16]
   zeropadding ratio? (nopad = 1)     : []

<Optional Parameters>
Remove DC?                            : [Y]
Scale Image to Sigma?                 : []
Compress Image file (Y or N)          : []
Image Rotation (C|R|F|c|r|f|N)        : [F]
Label Map File?                       : []
Display with ds9 or saoimage?         : [ds9]
   Center on target?                  : [Y]
   Set zoom level to?                 : [4]
   Dsp scale? (linear|log|histequ)    : []
Sufix for File Extension              : [p?]
Sufix for FFT Output File             : [map]
Preserve unppacked data?              : [N]
Preserve decoded data?                : [N]

      Save This Configuration?  [ bpc.0.25us ]

         Configuration Saved to bpc.0.25us!
```

Note that for those runs fft_size = 1024 and code_length = 255.

Let's finish processing:

```
autorng.pl ../../HD/2018DH1_84/dss14/data20180325044925.000
../../HD/2018DH1_84/dss14/data20180325051025.000 -r
```

```
        *** Totally 22 files processed ***

mapssum.pl ./map.20180325044925-p1 ./map.20180325051025-p1 -v 1024:255

        File Created: sum.map-p1-044925-051025-21-SD

mk_mpeg.pl 1024 255 -f sum.map-p1-044925-051025-21-SD -c 1 -z 4

               mappeak 1024 255 sum.map-p1-044925-051025-21-SD
               Signal Strength:
                     0  @ frq   618, range bin     5 =        32.28
                     1  @ frq   617, range bin     6 =        25.06
                     2  @ frq   619, range bin     5 =        19.86
```

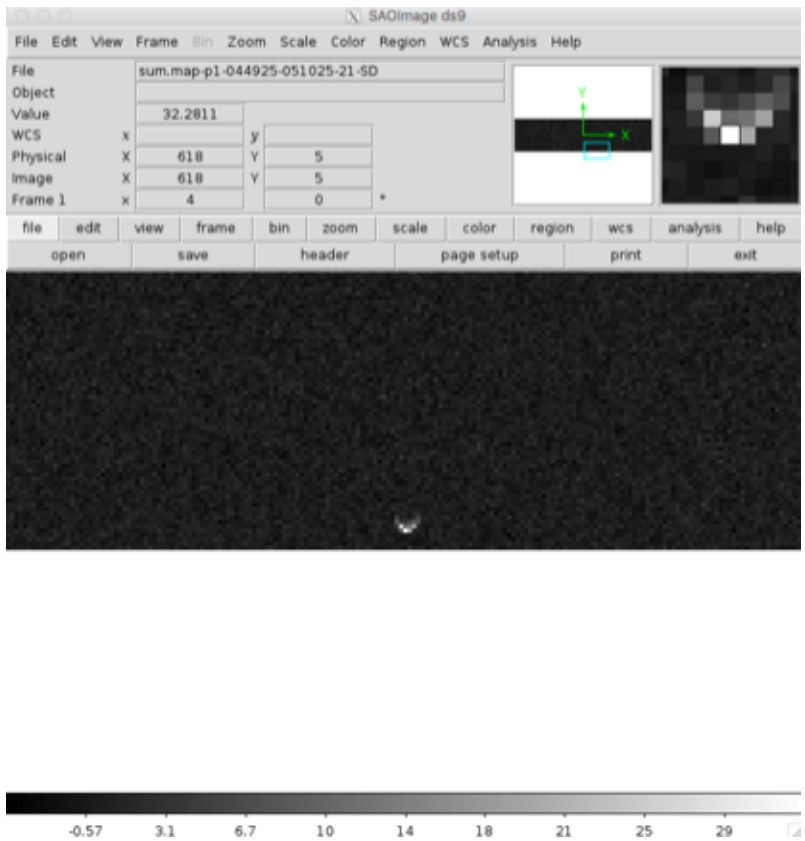

Figure 50. Ranging processing at 1 for files from 2018DH1_84/dss14/data20180325044925.000 to 2018DH1_84/dss14/data20180325051025.000

The center is equal to the fft_size divided by 2, i.e. 512. In this case echo is located at bin 618. So the echo is 618 – 512 = 106 bins to the right. This implies an offset of 106 times frequency resolution (0.96 Hz in configuration file), which translates into a 101.76 Hz offset. The object is about 6 x 4 bins.

Part 5. BPC at 0.125 us

With all previous results scientists updated solution file from s23 to s25. Let's modify the location and the ephemerides solution file in the configuration file for 0.125 us. Remember we are going to process:

```
051609 - 061509
60 runs 0.125us s25

rng_p.pl -f ../../HD/2018DH1_84/dss14/data20180325051609.000 -r


rng_p.pl Version 9.02 09/23/16
    (0)     bpc.0.125us
    (1)     bpc.0.25us
    (2)     bpc.10us
    (3)     bpc.11us
    (4)     bpc.1us
    Select BPC Control File          : [0] 0
File Base (fbase)                    : [2018DH1]
Directory                            : [../../HD/2018DH1_84/dss14/]
Recording Time                       : [20180325051609]
data-taking duration                 : [27]
   Sec of Data to Skip               : []
   Sec of Data to Process            : []
Op Mode ("-" for 2's comp)           : [3]
   Swapping I & Q                    : [Y]
Hardware Sampling Rate (in MHz)      : [32]
Remove Doppler? (RG|DR|DP|DD|F(f)|N) : [N]
Time Drift? (RG|DR|N)                : [N]
Calculate Phase Delay?               : [Y]
   Ephemerides File Name               : [../PUNCH.OUT.14v-14-14.s25]
../../HD/2018DH1_84/dss14/PUNCH.OUT.14v-14-14.s25
   XMT Station                       : [4]
   Sky Frequency                     : [8560000000]
   UpLink to station                 : [4]
   RCV Station                       : [4]
   Planet No.                        : [9]
   Satellite No.                     : [99]
Station/Site Delay (in usecs)        : [0]
Freq Offset (in Hz)                  : []
Range Offset (in bins)               : []
Baud (in uSec)                       : [0.125]
Downsample Size (pre-drift)          : [4]
Downsample Size (post-drift)         : [1]
Code Length (start w/ 'L':longcode)  : [511]
   Make sure offset < 7827 Hz (<ok>) : [Ok]
   FFT Length for Decoding           : [1024]
   Frames to Skip                    : []
   Limit no. of Frames to Decode     : [99999999]
   1st Range Bin to Save             : [1]
   Num of Range Bins to Save         : [511]
Cross-range FFT Size (< 525314)      : [2048]
Freq Resolution (0.0370 to 7.64 Hz)  : [0.382216242661448]
   10 FFT frames, 0.8 sec wasted     : [Ok]
   Coherent Averaging                : [20]
   zeropadding ratio? (nopad = 1)    : []

<Optional Parameters>
Remove DC?                           : [Y]
Scale Image to Sigma?                : []
Compress Image file (Y or N)         : []
```

```
Image Rotation (C|R|F|c|r|f|N)       : [F]
Label Map File?                      : []
Display with ds9 or saoimage?        : [ds9]
   Center on target?                 : [Y]
   Set zoom level to?                : [4]
   Dsp scale? (linear|log|histequ)   : []
Sufix for File Extension             : [p?]
Sufix for FFT Output File            : [map]
Preserve unppacked data?             : [N]
Preserve decoded data?               : [N]

      Save This Configuration?  [ bpc.0.125us ]

         Configuration Saved to bpc.0.125us!
```

Note that for those runs fft_size = 2048 and code_length = 511.
Let's finish processing:

```
autorng.pl ../../HD/2018DH1_84/dss14/data20180325051609.000
../../HD/2018DH1_84/dss14/data20180325061509.000 -r

mapssum.pl ./map.20180325051609-p1 ./map.20180325061509-p1 -v 2048:511

mk_mpeg.pl 2048 511 -f sum.map-p1-051609-061509-60-SD -c 1 -z 4

               mappeak 2048 511 sum.map-p1-051609-061509-60-SD
               Signal Strength:
                     0  @ frq  1285, range bin    23 =        24.41
                     1  @ frq  1286, range bin    23 =        24.32
                     2  @ frq  1287, range bin    22 =        19.17
```

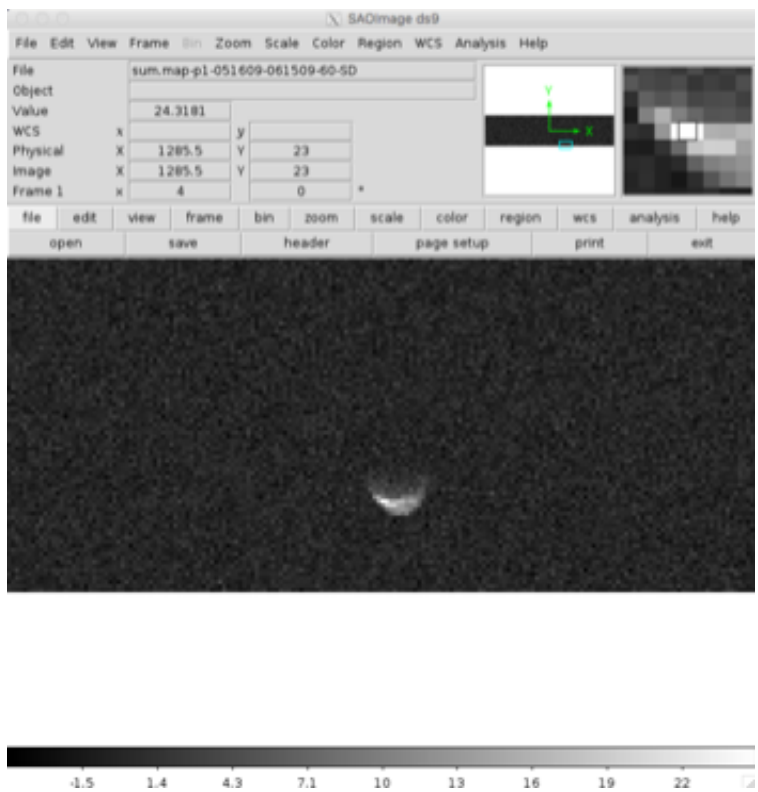

Figure 51. Ranging processing at 1 for files from 2018DH1_84/dss14/data20180325051609.000 to 2018DH1_84/dss14/data20180325061509.000

The center is equal to the fft_size divided by 2, i.e. 1024. In this case echo is located at bin 1285 So the echo is 1285 – 1024 = 261 bins to the right. This implies an offset of 106 times frequency resolution (0.38 Hz in configuration file), which translates into a 99.18 Hz offset. The object is about 15 x 10 bins.

PRACTICE 4: Post-processing of Chirp data

Go to the Chirp_practice folder and create a directory for 2018DH1_85.

```
cd Chirp_practice/
mkdir 2018DH1_85
cd 2018DH1_85
```

Copy readme.1st and cw.cfg files.

```
cp ../../HD/2018DH1_84/readme.1st .
cp ../../HD/2018DH1_84/dss14/proc/lfm.* .
cp ../../HD/2018DH1_84/dss14/proc/chirp.* .
```

Take a look at the contents of readme.1st file:

```
041529 - 041949
  6 runs CW    s25

042347 - 042859
  7 runs 1us   s25

043405 -
  1 run 20 MHz s25

043729 - 061436
113 runs 20 MHz s27
```

For this practice we are going to focus on chirp data.

```
043729 - 061436
113 runs 20 MHz s27

rng_p.pl -f ../../HD/2018DH1_85/dss14/data20180326043729.000 -o -r


rng_p.pl Version 9.02 09/23/16
File Base (fbase)                    : [2018DH1]
Directory                            : [../../HD/2018DH1_85/dss14/]
Recording Time                       : [20180326043729]
data-taking duration                 : [23]
   Sec of Data to Skip               : []
   Sec of Data to Process            : []
Op Mode ("-" for 2's comp)           : [3]
   Swapping I & Q                    : [Y]
Hardware Sampling Rate (in MHz)      : [40]
Remove Doppler? (RG|DR|DP|DD|F(f)|N) : [N]
Time Drift? (RG|DR|N)                : [N]
Calculate Phase Delay?               : [Y]
   Ephemerides File Name               : [../PUNCH.OUT.14v-14-14.s27]
 ../../HD/2018DH1_85/dss14/PUNCH.OUT.14v-14-14.s27
   XMT Station                       : [4]
   Sky Frequency                     : [8560000000]
   UpLink to station                 : [4]
   RCV Station                       : [4]
   Planet No.                        : [9]
   Satellite No.                     : [99]
Station/Site Delay (in usecs)        : [0]
Freq Offset (in Hz)                  : []
```

```
Range Offset (in bins)               : []
LFM Definition File (C=gen)          : [chirp.20M_50u]
Downsample Size (pre-drift)          : [2]
Downsample Size (post-drift)         : [1]
Duty Cycle                           : [1]
   << Chirp / FFT Length: 1000 / 1000 >>
   << Pulse Repetition Time: 25 (usec) >>
   Make sure offset < 20000 Hz (<ok>) : [Ok]
   Frames to Skip                    : []
   Limit no. of Frames to Decode     : [99999999]
   1st Range Bin to Save             : [1]
   Num of Range Bins to Save         : [1000]
Cross-range FFT Size (< 268435)      : [1000]
Freq Resolution (0.0435 to 20.00 Hz) : [0.2]
   4 FFT frames, 3.0 sec wasted      : [Ok]
   Coherent Averaging                : [100]
   zeropadding ratio? (nopad = 1)    : []

<Optional Parameters>
Remove DC?                           : [Y]
Scale Image to Sigma?                : []
Compress Image file (Y or N)         : [N]
Image Rotation (C|R|F|c|r|f|N)       : [N]
Label Map File?                      : []
Display with ds9 or saoimage?        : [ds9]
   Center on target?                 : [Y]
   Set zoom level to?                : [2]
   Dsp scale? (linear|log|histequ)   : []
Sufix for File Extension             : [p?]
Sufix for FFT Output File            : [map]
Preserve unppacked data?             : [N]
Preserve decoded data?               : [N]

      Save This Configuration?  [ lfm.20M_50u ]

         Configuration Saved to lfm.20M_50u!
```

Important parameters are Chirp / FFT Length: 1000 / 1000

```
autorng.pl ../../HD/2018DH1_85/dss14/data20180326043729.000
../../HD/2018DH1_85/dss14/data20180326061436.000 -r -o

mapssum.pl ./map.20180326043729-p1 ./map.20180326061436-p1 -v 1000:1000 -n 200

        File Created: sum.map-p1-043729-061436-113-SD

mk_mpeg.pl 1000 1000 -v sum.map-p1-043729-061436-113-SD -c 1 -z 4

mappeak 1000 1000 sum.map-p1-043729-061436-113-SD
Signal Strength:
      0  @ frq   741, range bin   941 =        14.03
      1  @ frq   746, range bin   947 =        12.53
      2  @ frq   748, range bin   950 =        12.25
```

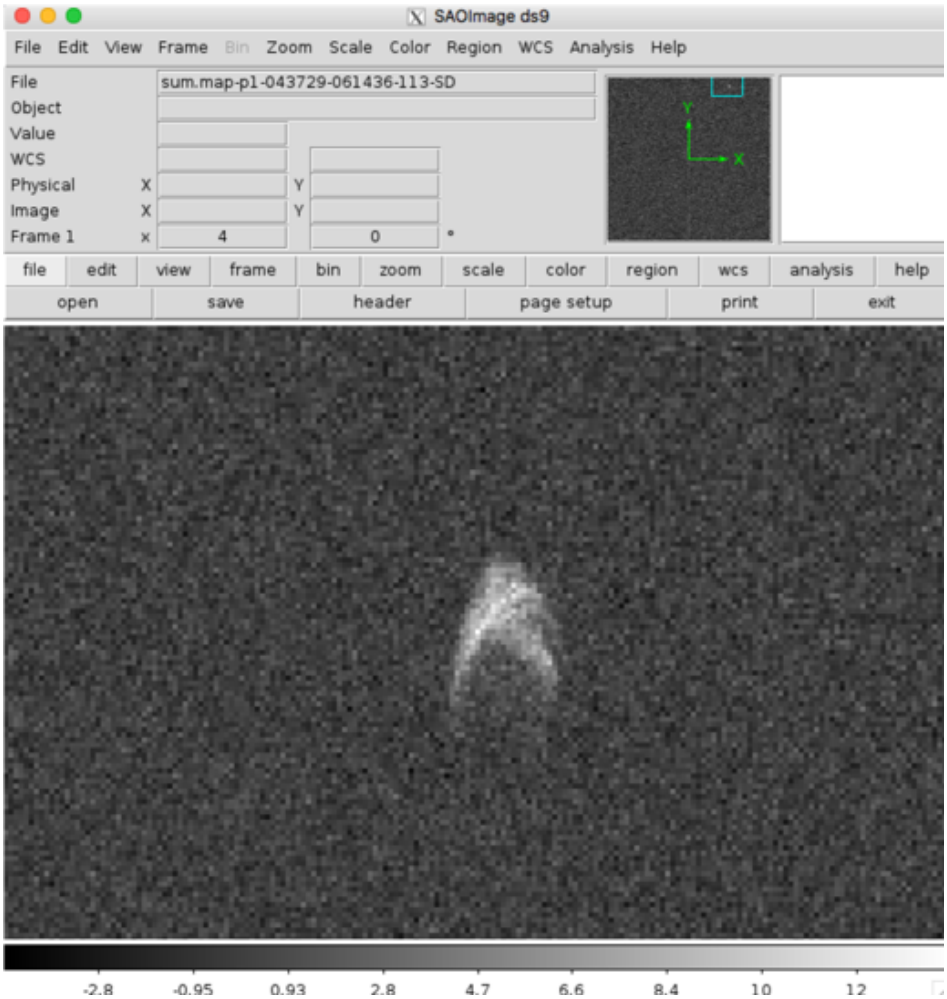

Figure 52. Chirp processing at 1 for files from 2018DH1_84/dss14/data20180326043729.000 to 2018DH1_84/dss14/data20180326061436.000

PRACTICE 5: Post-processing of CW and Chirp data on bistatic configuration.

In this practice we are going to process bistatic data from asteroid 2012TC4_285. The measurements were made in bistatic configuration between Goldstone and Green Bank Telescope. Both CW and chirping measurements were taken.

Go to the Bistaticpractice folder and create a directory for 2012TC4_285.

```
cd Bistaticpractice/
mkdir 2012TC4_285
cd 2012TC4_285
```

Copy readme.1st and configuration files.

```
cp ../../HD/2012TC4_285/GBT/readme.1st .
cp ../../HD/2012TC4_285/GBT/proc/cw.cfg .
cp ../../HD/2012TC4_285/GBT/proc/lfm.cfg .
cp ../../HD/2012TC4_285/GBT/proc/chirp* .
```

If we cat the contents in readme.1st file:

```
Recap:
=====

1245-1305 CW +500 fixed (40 kW)
1305-1340 80 MHz Chirp fixed (40 kW)
1340-1900 80 MHz Chirp fixed (72 kW)
1900-1930 CW +500 fixed (70 kW)

Outages:
=======

134015-134106 Beam trip
134258-134328 Beam trip
1434-1436     GBT stopped for new scan (off target)
1720-172240   DSS-13 Azimuth brake set due to counter-torque
1740 GBT radardas completed 9000 seconds at, restarted.


  62138613760 Oct 12 03:02 data20171012022118.000   CW
 377835487232 Oct 12 03:23 data20171012031402.000   LFM 2 chns

  29905387520 Oct 12 13:05 data20171012124531.000   CW
1607936770048 Oct 12 14:33 data20171012130944.000   LFM 1 chn
2880000000000 Oct 12 17:05 data20171012143551.000   LFM 1 chn
1616537116672 Oct 12 18:30 data20171012170640.000   LFM 1 chn
 237410189312 Oct 12 19:00 data20171012184802.000   LFM 1 chn
  39044775936 Oct 12 19:30 data20171012190406.000   CW
```

We can see that both CW and chirp measurements were performed for this track. Let's start processing CW and then chirp data.

PART A. CW data in bistatic mode.

We are going to focus on data20171012124531.000. As you can see this is one large file and it needs to be process in segments. That is the main difference when processing bistatic data.

First make sure that the ephemerides directory is well set in your cw.cfg by:

```
cw_p.pl -f ../../HD/2012TC4_285/GBT/data20171012124531.000 -c 20 -r
```

And edit your config file:

```
cw_p.pl Ver. 6.00
Target                                : [2012TC4]
Directory                             : [../../HD/2012TC4_285/GBT/]
Mode                                  : [7 ]
    Channel to Use                    : []
    Swapping I & Q                    : [Y]
Recording Time                        : [20171012124531]
Sample Frequency (in MHz)             : [6.2500]
Data-taking duration                  : [9000]
   Sec Worth of Data to Skip          : []
   (opt) FCB Block (8KB) to Skip      : []
   Sec Worth of Data to Process       : [20]
No. of Hops                           : [1]
    Freq Shifting (Y or N)            : [Y]
    Freq Offset                       : [-500]
Calculate Round-Trip time             : [N]
    Round Trip Time                   : []
Remove Doppler? (RG|DR|N)             : [RG]
    Process in Real-time? (Y|N)       : []
    Base Frequency                    : [7190000000]
    Special paramter (rarely)         : []
    Doppler Specification File        : [cw.cfg]
                   Ephemerides File Name            : [../PUNCH.OUT.13f-09-09.s71]
               ../../HD/2012TC4_285/GBT/PUNCH.OUT.13f-09-09.s71
    XMT Station                       : [3]
    UpLink to station                 : [9]
    RCV Station                       : [9]
    Planet No.                        : [9]
    Satellite No.                     : [99]
Spectrum bandwidth                    : [6250]
Freq Resolution                       : [0.2]
Remove DC (Y or N)                    : [N]
Limit No. of Transfer to Add          : []
FFT BW Limit (Y or N)                 : [N]
FFT in Time Series                    : [N]
FFT in dB (Y or N)                    : [N]
Standard Deviation(Y or N)            : [Y]
    Lower Freq Bound                  : [1400]
    Higher Freq Bound                 : [4000]
Save Unp File (Y or N)                : []

Re-configure Gnuplot  : [N]

      Save This Configuration?  [ cw.cfg ]

         Configuration Saved to cw.cfg!
```

In order to run consecutive segments of 20 seconds we are going to use segmcw.pl.

```
segmcw.pl -h
* * * * * * * * * * * * * * * * * * * * * * * * * * * * * * * * * * * *
*                                                                     *
* segmcw.pl [-p] <datafile> <skip tm> <proc tm> <cnt> ["options"]     *
* where  -p : pause between processing                                *
*        <datafile> : "data."YYYYMMDDhhmmss                           *
*        <skip tm> <proc tm> : secs                                   *
*        <cnt> : segments to process "(start):(end)"                  *
*        ["options"] : (optional) parameters                          *
*              e.g. "-d" for gnuplot() display                        *
*                                                                     *
* * * * * * * * * * * * * * * * * * * * * * * * * * * * * * * * * * * *
```

We need then the name of the file followed by the number of samples to skip and the number of samples to process per segment, followed by the number of segments to process.

```
segmcw.pl ../../HD/2012TC4_285/GBT/data20171012124531.000 20 20 1:20
```

The values `<skip tm>` defines the window size in seconds and the value `<proc tm>` defines the number of seconds processed within the window. Next table graphically shows what those variables represent.

Table 10. Example scheme for values <skip tm> and <proc tm> defining how the data is processed. The typical scheme is having both set to the same value, in the example 20 20.

10 20	20 20	40 20
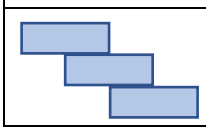		

When processing the autocw.pl messages like the following appear on your terminal:

```
FFT length                    : 31250
Frequency resolution          : 2.000000e-01 Hz
Processed bandwidth           : 6.250000e+03 Hz
```

Processed bandwidth = 31250*0.2 = 6250, means your frequency span goes from -3125 to 3125. So we normalize for CW to the (low:high) frequency by setting -v from 200 to 3100. Also we sum both channels, the opposite sense (1) and same sense (2).

Let's now sum the created files:

```
mapssum.pl ./cw.124531.fft_1 ./cw.125151.fft_1 -v 200:3100
mapssum.pl ./cw.124531.fft_2 ./cw.125151.fft_2 -v 200:3100
```

Finally we plot those sums using gnuplot. So, type `gnuplot` in your terminal and:

```
plot [-40:40] 'sum.cw-fft_1-124531-125151-20-SD' w line, 'sum.cw-fft_2-124531-125151-20-SD' w line
```

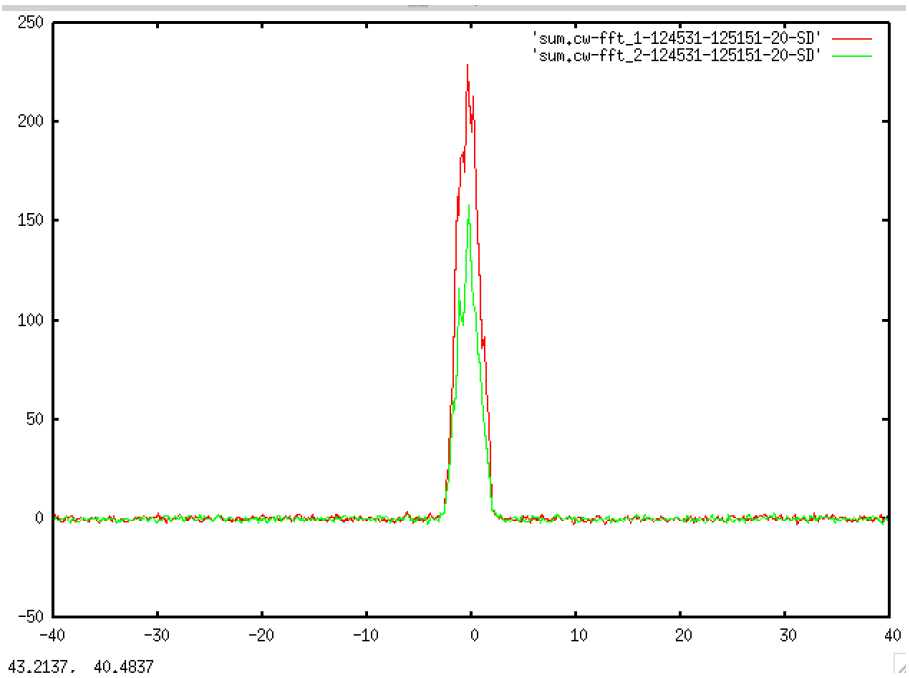

Figure 53. CW spectra processed for bistatic measurements taken of NEO 2012TC4_285.

Looking at fig. 54 we can get some information about the object:

- The object is narrow which indicates it is a slow rotator.
- Channel 2 is quite powerful compared to channel 1 (a little bit less). The object surface is probably quite rough.

PART B. Chirp data in bistatic mode.

Now we are going to process the chirp data available for 2012TC4_285 taken in bistatic mode. Let's cat again readme.1st file:

```
Recap:
=====

1245-1305 CW +500 fixed (40 kW)
1305-1340 80 MHz Chirp fixed (40 kW)
1340-1900 80 MHz Chirp fixed (72 kW)
1900-1930 CW +500 fixed (70 kW)

Outages:
=======
```

```
134015-134106 Beam trip
134258-134328 Beam trip
1434-1436     GBT stopped for new scan (off target)
1720-172240   DSS-13 Azimuth brake set due to counter-torque
1740 GBT radardas completed 9000 seconds at, restarted.



  62138613760 Oct 12 03:02 data20171012022118.000   CW
 377835487232 Oct 12 03:23 data20171012031402.000   LFM 2 chns

  29905387520 Oct 12 13:05 data20171012124531.000   CW
1607936770048 Oct 12 14:33 data20171012130944.000   LFM 1 chn
2880000000000 Oct 12 17:05 data20171012143551.000   LFM 1 chn
1616537116672 Oct 12 18:30 data20171012170640.000   LFM 1 chn
 237410189312 Oct 12 19:00 data20171012184802.000   LFM 1 chn
  39044775936 Oct 12 19:30 data20171012190406.000   CW
```

We are going to process data20171012130944.000 which is LFM 1 chn, 80 MHz Chirp fixed (72 kW).

```
rng_p.pl Version 9.02 09/23/16
File Base (fbase)                    : [2012TC4]
Directory                            : [../../HD/2012TC4_285/GBT/]
Recording Time                       : [20171012130944]
data-taking duration                 : [9000]
   Sec of Data to Skip               : [9000]
   Sec of Data to Process            : [20]
    *** Invalid proc time constraint ***
data-taking duration                 : [9000]
   Sec of Data to Skip               : [9000] 20
   Sec of Data to Process            : [20] 8000
Op Mode ("-" for 2's comp)           : [3 ]
   Swapping I & Q                    : [Y]
Hardware Sampling Rate (in MHz)      : [160.0000]
Remove Doppler? (RG|DR|DP|DD|F(f)|N) : [RG]
Time Drift? (RG|DR|N)                : [RG]
   Process in Real-time? (Y|N)       : []
Calculate Phase Delay?               : [N]
    Hardcoded delay (in sec)?        : [N]
   Ephemerides  File  Name                         :  [../PUNCH.OUT.13f-09-09.s71]
../../HD/2012TC4_285/GBT/PUNCH.OUT.13f-09-09.s71
   XMT Station                       : [3]
   Sky Frequency                     : [7190000000]
   UpLink to station                 : [3]
   RCV Station                       : [9]
   Planet No.                        : [9]
   Satellite No.                     : [99]
Station/Site Delay (in usecs)        : []
Freq Offset (in Hz)                  : []
Range Offset (in bins)               : []
LFM Definition File (C=gen)          : [80MHz_25us]
Downsample Size (pre-drift)          : [1]
Downsample Size (post-drift)         : [2]
Duty Cycle                           : [1]
   << Chirp / FFT Length: 2000 / 2000 >>
   << Pulse Repetition Time: 12.5 (usec) >>
   Make sure offset < 40000 Hz (<ok>) : [Ok]
   Frames to Skip                    : []
   Limit no. of Frames to Decode     : []
   1st Range Bin to Save             : [1]
   Num of Range Bins to Save         : [2000]
Cross-range FFT Size (< 134217)      : [1000]
```

```
Freq Resolution (0.0001 to 40.00 Hz) : [0.2]
   1800 FFT frames, 0.0 sec wasted   : [Ok]
   Coherent Averaging                : [200]
   zeropadding ratio? (nopad = 1)    : []

<Optional Parameters>
Remove DC?                           : [N]
Scale Image to Sigma?                : [Y]
   Sufix for Scaled Output File      : [maps]
   Fst Column                        : []
   Last Column                       : []
   Fst Row                           : []
   Last Row                          : []
Compress Image file (Y or N)         : []
Image Rotation (C|R|F|c|r|f|N)       : []
Label Map File?                      : []
Display with ds9 or saoimage?        : [ds9]
   Center on target?                 : [Y]
   Set zoom level to?                : []
   Dsp scale? (linear|log|histequ)   : []
Sufix for File Extension             : [a?]
Sufix for FFT Output File            : [map]
Preserve unppacked data?             : [N]
Preserve decoded data?               : [N]

      Save This Configuration?  [ lfm.cfg ]

         Configuration Saved to lfm.cfg!
```

Let's process by segments.

```
segmrng.pl -o ../../HD/2012TC4_285/GBT/data20171012130944.000  20 20 1:f lfm.cfg "-
d -r"
```

Since file is 5024 and we are processing segments of 20 seconds, this will generate 252 files. Here we are summing the first two generated maps for illustration.

```
mapssum.pl  ./maps.20171012130944-a1 ./maps.20171012131004-a1 -v 2000:1000 -n 300
```

Remember that -n sets the max number of files to process (99 by default) and -v 2000:1000 corresponds to the following settings in the config file:

```
Num of Range Bins to Save         : [2000]
Cross-range FFT Size (< 134217)      : [1000]
```

And then we are ploting the resulting sum by:

```
mk_mpeg.pl 2000 1000 -v sum.maps-a1-130944-131004-2-SD -c 1 -z 4
```

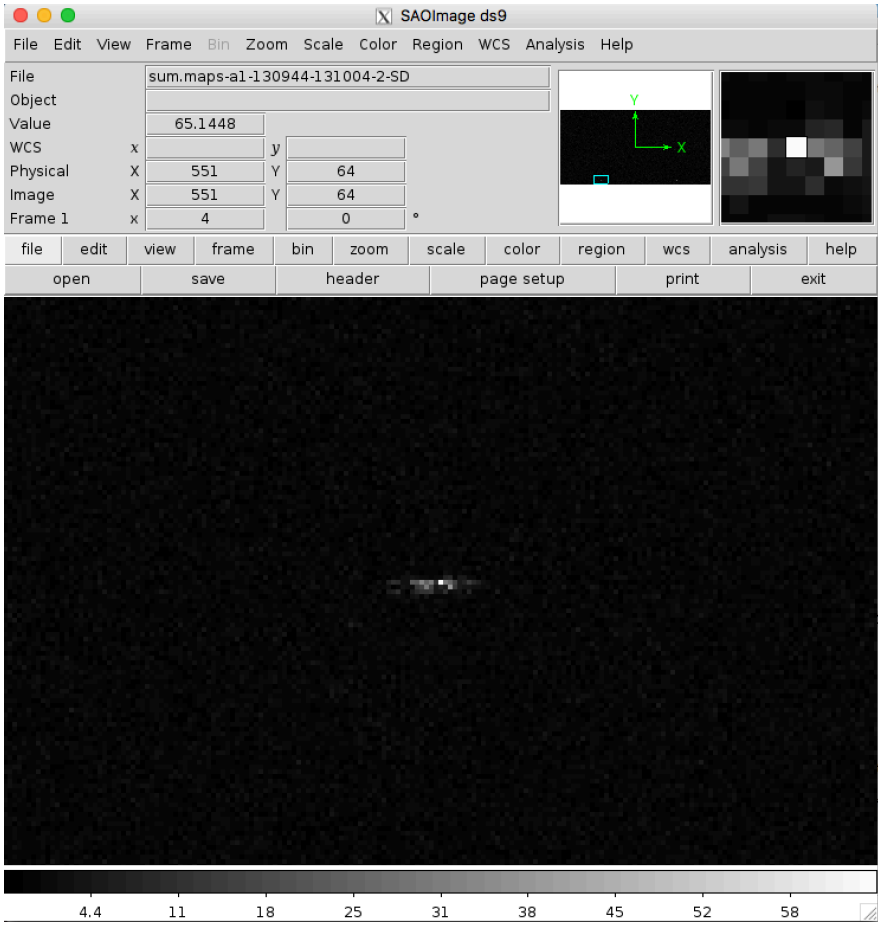

Figure 54. Chirp processing at 1 for files from 2012TC4_285/GBT/data20171012130944.000

PRACTICE 6: Understanding the configuration file.

At this point, we have learned what are the main steps to post-process CW, BPC and Chirp data and what is expected as a result of the processing. Regarding the configuration file, so far, we have only modified the frequency resolution in the configuration file to see the effects on CW data (at the end of practice 2), but we haven't really went through it to understand each of the variables. The configuration file has a lot of variables that are already set once you copy the stored file along the data named as cw.cfg, bpc.xxus, or lfm.x.xus but the understanding of those variables is relevant and crucial to be able to process the data on your own. Some of the parameters are defined by the recorder mode and configuration, other are defined by the scientist.

Note that GSSR has three different back-end receivers: portable fast samplers (PFS), digital receiver (DRCV) and dual channel agilent receiver (DCAR).

The variables are now described.

- Mode: the mode defines the the packaging scheme of the recorder used and depends on who is providing the data.

  a) PFS. It has multiple quantization bits and 1 or 2 channels option. The possible combinations are defined as mode in the following table.

Table 11. Mode setting

Mode	Channels	Quantization bits
1	1	2
2	1	4
3	1	8
5	2	2
6	2	4
7	2	8

  b) DRCV. It has 8 quantization bits and 1 or 2 channels.
  c) DCAR. It has 8 quantization bits and 1 or 2 channels.

- Sampling frequency (Fs): the sampling frequency is given by the recorder configuration. It is decided based on ranging resolution and recording receiver. Here is a table of all samples rates for each configuration (unless otherwise specified). Note that PFS and DCAR are operator selectable because of the external clock. Typical set-ups are:

  a) PFS

Table 12. PFS recorder main configuration.

Type	Sample rate

CW	2 MHz
BPC 10 us	2 MHz
BPC 11 us	2 MHz
BPC 1 us	2 MHz
BPC 0.5 us	4 MHz
BPC 0.25 us	8 MHz
BPC 0.125 us	16 MHz
Chirp 5 MHz	10 MHz
Chirp 10 MHz	20 MHz
Chirp 20 MHz	40 MHz
Chirp 40 MHz	40 MHz

b) DRCV

Table 13. DRCV recorder main configuration.

Type	Sample rate	Channels
CW	10 MHz	2
BPC 10 us	10 MHz	1
BPC 11 us	10 MHz	1
BPC 1 us	10 MHz	1
BPC 0.5 us	10 MHz	1
BPC 0.25 us	20 MHz	1
BPC 0.125 us	40 MHz	1
BPC 0.1 us	40 MHz	1
Chirp 10 MHz	20 MHz	1
Chirp 20 MHz	40 MHz	1
Chirp 40 MHz	80 MHz	1
Chirp 80 MHz	160 MHz	1

c) DCAR

Table 14. DCAR recorder main configuration.

Type	Sample rate	Channels
CW	6.25 MHz	2
BPC 10 us	8 MHz	1
BPC 11 us	8 MHz	1
BPC 1 us	8 MHz	1
BPC 0.5 us	8 MHz	1
BPC 0.25 us	16 MHz/20 MHz	1
BPC 0.125 us	32 MHz	1
BPC 0.1 us	40 MHz	1
BPC 0.0625 us	64 MHz	1
BPC 0.05 us	80 MHz	1
BPC 0.0312 us	128 MHz	1

BPC 0.025 us	160 MHz	1
Chirp 10 MHz	20 MHz	1
Chirp 20 MHz	40 MHz	1
Chirp 30 MHz	60 MHz	1
Chirp 40 MHz	80 MHz	1
Chirp 50 MHz	100 MHz	1
Chirp 60 MHz	120 MHz	1
Chirp 70 MHz	140 MHz	1
Chirp 80 MHz	160 MHz	1

- Baud: The baud time is provided by scientist in the planning email and corresponds to the 10 us, 11us, 1 us, 0.25 us, 0.125 us modes used in practice 2, or shown in table above. Baud frequency is the inverse of baud value.
- FFT length: provided by the scientist in the planning email.
- Code length: provided by the scientist in the planning email.
- Downsampling value (ds): It is given by the is given by the recorder configuration. Usually is equal to Fs*Baud, but it can be otherwise specified.
- Number of coherent integrations (n_{coh}): It is given by the scientist in the planning email, and corresponds to the number of coherent summations. By integrating longer times (n_{coh} bigger) the Doppler resolution changes. Note that the range resolution is fixed based on the range resolution of the waveform.

Here there is an example of the plan for 2018 EB DOY 97 (2018EB97). The observation took place on April 7, 2018.

Hello all,

We are starting with 2018 EB this evening. We only have one track scheduled. 2018 EB was discovered on 2018 March 1 by NEOWISE. J. Masiero reported a diameter of about 240 m based on thermal observations obtained by the NEOWISE spacecraft. We do not know the rotation period, but there are some indications that it is slow.

Here is our plan:
-CW until a detection (s10 3-sigma Doppler is 300 Hz)
-10 us until a detection (s10 3-sigma delay is 19,000 us)
-11 us until a detection
-1 us until a detection
-decide what to do next based on the SNRs

Setups
==========

CW setup:
TX polarization RCP

RCV polarization LCP & RCP
Bandwidth: 5000 Hz
Frequency hops: no hopping
TX offset +500 Hz
Fourier Transform: 5000 for 1 Hz resolution.

10-usec
baud 10 usec
code 127
FFT 128
ncoh 1
bandwidth 787 Hz
resolution 6.15 Hz
TXOFF +100 Hz (echo in column 81)

11-usec
baud 11 usec
code 127
FFT 128
ncoh 1
bandwidth 716 Hz
resolution 5.59 Hz
TXOFF +100 Hz (echo in column 82)

1-usec
baud 1 usec
code 255
ncoh 10
bandwidth 392.2 Hz
FFT 256
resolution 1.5 Hz
TXOFF +50 Hz (echo is column 161)

2018 EB predicts on aardvark:
/export/data3/osod/ops/2018eb/EPH.OUT.s10
/export/data3/osod/ops/2018eb/PRDX.OUT.14v-14-14.s10
/export/data3/osod/ops/2018eb/PUNCH.OUT.14v-14-14.s10
/export/data3/osod/ops/2018eb/PRDX.OUT.14f-14-14.s10
/export/data3/osod/ops/2018eb/PUNCH.OUT.14f-14-14.s10

Pointing:

Date (UTC)	DOY	hhmmss	RA	Dec	Macro	LHA	Dec	RTT	OSOD	
2018 APR 07	97	034000	222.38140	35.62960	A	-4.400	4.500	34.7	s10	Please note the rise time
2018 APR 07	97	040000	222.40080	35.78370	A	-4.500	4.500	34.7	s10	
2018 APR 07	97	050000	222.45570	36.24190	A	-5.200	4.400	35.0	s10	
2018 APR 07	97	060000	222.50590	36.69320	A	-6.300	4.400	35.2	s10	

Transmit offsets are in millidegrees.

Let's process the data for this NEO knowing that PFS was used for CW for the recorder configurations. See what was done for 2018EB97:

```
cat ../../HD/2018EB_97/readme.1st

        033538 - 034238
         7 runs CW s10
        034524 - 035114
         6 runs CW s12
        035555 - 035923
         4 runs 10us s12
        040407 - 041547
        11 runs 1us s12
        042054 - 043934
        17 runs 0.25us s14
        044353 - 052441
        36 runs 0.125us s14
```

So, we have CW and BPC data to process.

CW data

Create a folder for 2018EB97 in your CWpractice directory.

Knowing that PFS was used for the recorder configuration and looking at the planning email, we know:

PFS recorder configuration (looking at table 10 and table 9):

- ⇒ the sampling frequency is set to SMPRATE = 2MHz (table 10).
- ⇒ it uses 2 channels (table 10 and also, according to planning email, two polarizations are received)
- ⇒ recorder receives I and Q (swap IQ, Y) and uses 4 quantization bits.
- ⇒ from table 9, we can see the appropriate mode is 6 (RCVMODE).

From planning email:

- ⇒ FFT length is FFT_LEN = 5000
- ⇒ The frequency resolution is FRQRESN = 1
- ⇒ No frequency hopping
- ⇒ Bandwidth is 5000 Hz, requires NUMHOPS = 1
- ⇒ Transmitter offset is 500 Hz, FRQOFST = -500, requires NUMHOPS = 1
- ⇒ Ephemerides files is PUNCH.OUT.14v-14-14.s10
- ⇒ Pointing is important to the operator only.

We also know:

- ⇒ Processing station is dss14 and we are observing a NEO:

xmtstation = 4
uplinkto = 4
rcvstation = 4
planet = 9
satellite = 99

Part 1. Loopback file

Let's process loopback file for CW data and set configuration file parameters to make sure everything looks ok. Loopback files is:

```
ls ../../HD/2018EB_97/dss14/ -ltr

        -rw-r--r--. 1 jao gssr      63504 Apr  7 00:42 PUNCH.OUT.14v-14-14.s10
        -rw-r--r--. 1 jao gssr   41000000 Apr  7 02:21 data20180407022118.000
        -rw-r--r--. 1 jao gssr  129000000 Apr  7 03:36 data20180407033538.000
        -rw-r--r--. 1 jao gssr  129000000 Apr  7 03:37 data20180407033648.000
        -rw-r--r--. 1 jao gssr  129000000 Apr  7 03:38 data20180407033758.000
        -rw-r--r--. 1 jao gssr  129000000 Apr  7 03:39 data20180407033908.000
        -rw-r--r--. 1 jao gssr  129000000 Apr  7 03:40 data20180407034018.000
        -rw-r--r--. 1 jao gssr  129000000 Apr  7 03:42 data20180407034128.000
        -rw-r--r--. 1 jao gssr  129000000 Apr  7 03:43 data20180407034238.000
        -rw-r--r--. 1 jao gssr      63504 Apr  7 03:43 PUNCH.OUT.14v-14-14.s12
        -rw-r--r--. 1 jao gssr  129000000 Apr  7 03:45 data20180407034524.000
        -rw-r--r--. 1 jao gssr  129000000 Apr  7 03:47 data20180407034634.000
        -rw-r--r--. 1 jao gssr  129000000 Apr  7 03:48 data20180407034744.000
        -rw-r--r--. 1 jao gssr  129000000 Apr  7 03:49 data20180407034854.000
        -rw-r--r--. 1 jao gssr  129000000 Apr  7 03:50 data20180407035004.000
        -rw-r--r--. 1 jao gssr  129000000 Apr  7 03:51 data20180407035114.000
        .
        .
        .
```

There is an empty configuration file named cw_empty.cfg at ../cw_empty.cfg. Copy this into your working folder by:

```
cp ../empty.cwf .
```

Now let's proceed by running cw_p.pl (remember to add -e option to use cw_empty.cfg):

```
cw_p.pl -f ../../HD/2018EB_97/dss14/data20180407022118.000 -l -e
cw_empty.cfg -r
```

Some parameters will appear automatically,

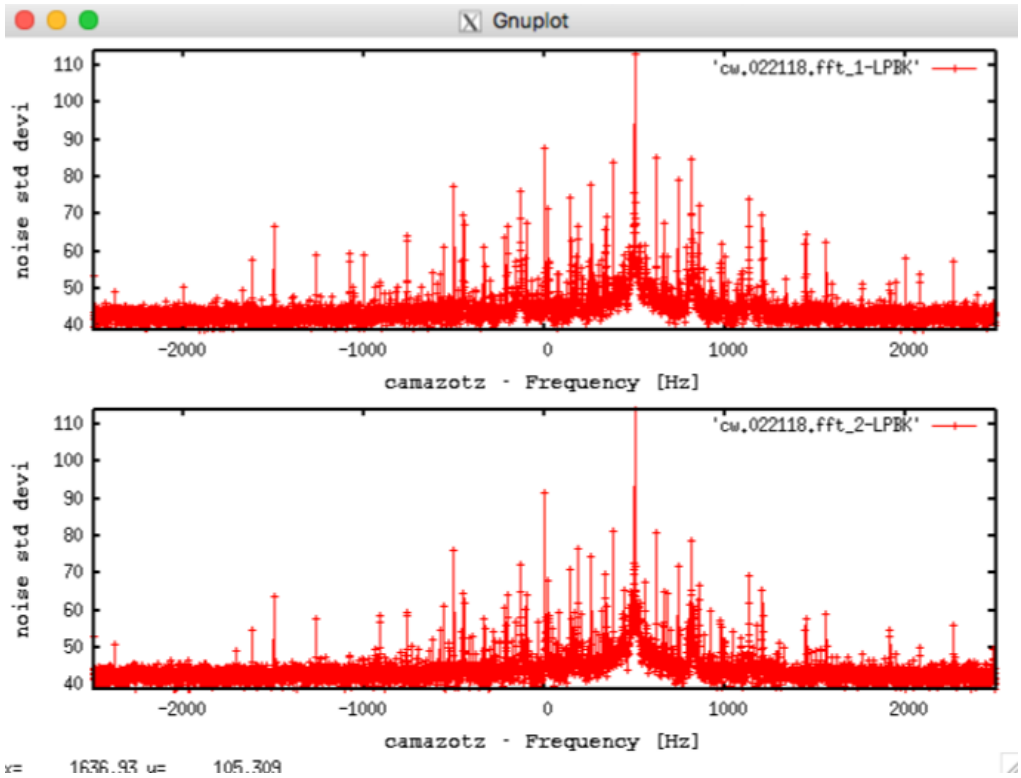

Figure 55. CW data loopback file processed for 2018EB97.

Part 2. CW data

Now, process the rest of the CW data, remember to modify the ephemerides file in the configuration file when you process the second batch of runs.

```
        033538 - 034238
         7 runs CW s10

        034524 - 035114
         6 runs CW s12

autocw.pl ../../HD/2018EB_97/dss14/data20180407033538.000
../../HD/2018EB_97/dss14/data20180407034238.000 -e cw_empty.cfg -r
mapssum.pl ./cw.033538.fft_1 ./cw.034238.fft_1 -v 200:2495
mapssum.pl ./cw.033538.fft_2 ./cw.034238.fft_2 -v 200:2495
gnuplot
plot  [-50:50]  'sum.cw-fft_1-033538-034238-7-SD'  w  line,  'sum.cw-fft_2-033538-
034238-7-SD' w line
```

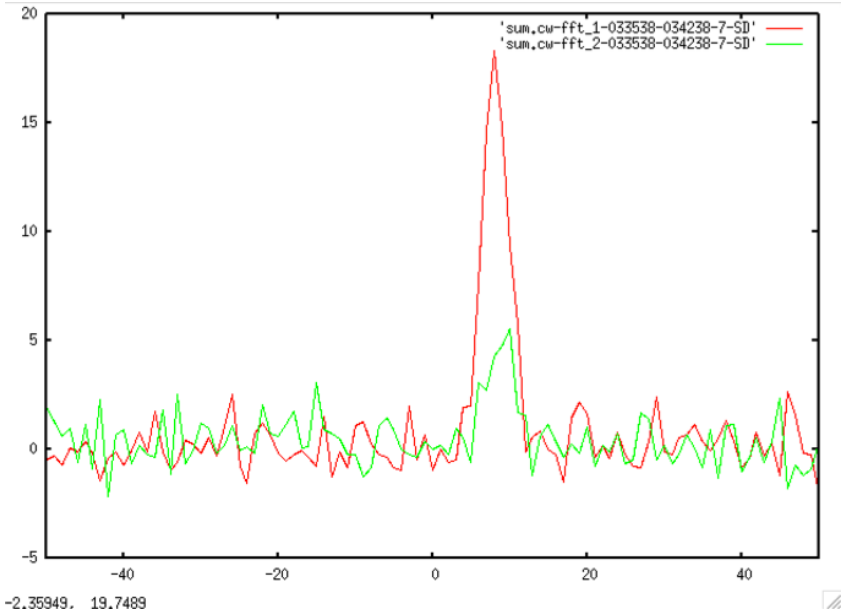

Figure 56. CW data files processed for 2018EB97.

```
autocw.pl ../../HD/2018EB_97/dss14/data20180407034524.000
 ../../HD/2018EB_97/dss14/data20180407035114.000  -r -e cw_empty.cfg
mapssum.pl ./cw.034524.fft_1 ./cw.035114.fft_1 -v 200:2495
mapssum.pl ./cw.034524.fft_2 ./cw.035114.fft_2 -v 200:2495

gnuplot
plot  [-50:50]  'sum.cw-fft_1-034524-035114-6-SD'  w  line,  'sum.cw-fft_2-034524-
035114-6-SD'  w line
```

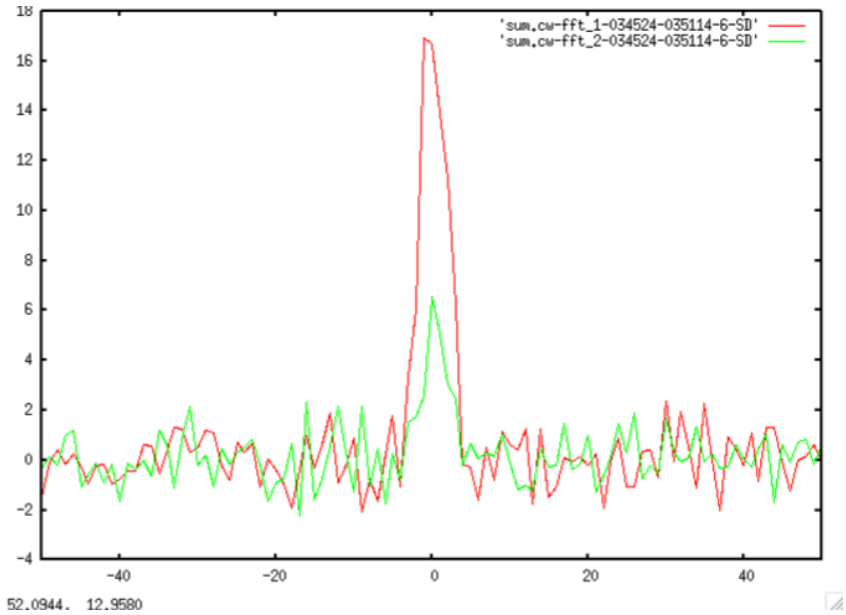

Figure 57. CW data files processed for 2018EB97.

BPC data

Create a folder for 2018EB97 in your BPCpractice directory.

Knowing that DCAR was used for the recorder configuration for BPC data and looking at the planning email, we know:

DCAR recorder configuration (looking at table 12 and table 9):

- ⇒ the sampling frequency is set to SMPRATE = 2MHz (table 12).
- ⇒ it uses 1 channels (table 10 and also, according to planning email, two polarizations are received)
- ⇒ recorder receives I and Q (swap IQ, Y) and uses 4 quantization bits.
- ⇒ from table 9, we can see the appropriate mode is 2 (RCVMODE).

From planning email:

- ⇒ Baud is 10 usec
- ⇒ The frequency resolution is 6.15
- ⇒ Number of coherent sums is 1
- ⇒ Code length is 127
- ⇒ FFT length is 128
- ⇒ Bandwidth is 787 Hz
- ⇒ Transmitter offset is 100 Hz
- ⇒ Ephemerides files is already updated to PUNCH.OUT.14v-14-14.s12

We also know:

⇒ Processing station is dss14 and we are observing a NEO:
xmtstation = 4
uplinkto = 4
rcvstation = 4
planet = 9
satellite = 99

Create a folder for 2018EB97 in your BPCpractice directory.

PART 1. Loopback file

Let's process loopback file for BPC 10 us data and set configuration file parameters to make sure everything looks ok. Loopback files is:

```
ls ../../HD/2018EB_97/dss14/ -ltr
```

.
.
.

```
-rw-r--r--. 1 jao gssr   21000000 Apr  7 03:53 data20180407035334.000
-rw-r--r--. 1 jao gssr   65000000 Apr  7 03:56 data20180407035555.000
-rw-r--r--. 1 jao gssr   65000000 Apr  7 03:57 data20180407035704.000
-rw-r--r--. 1 jao gssr   65000000 Apr  7 03:58 data20180407035814.000
-rw-r--r--. 1 jao gssr   65000000 Apr  7 03:59 data20180407035923.000
.
.
.
```

There is an empty configuration file named bpc_empty.xxus at ../. Copy this into your working folder by:

```
cp ../bcp_empty.xxus .
```

Now let's proceed by running cw_p.pl (remember to add -e option to use cw_empty.cfg):

```
rng_p.pl -f ../../HD/2018EB_97/dss14/data20180407035334.000 -l -e bpc_empty.xxus -r
```

Some parameters will appear automatically.

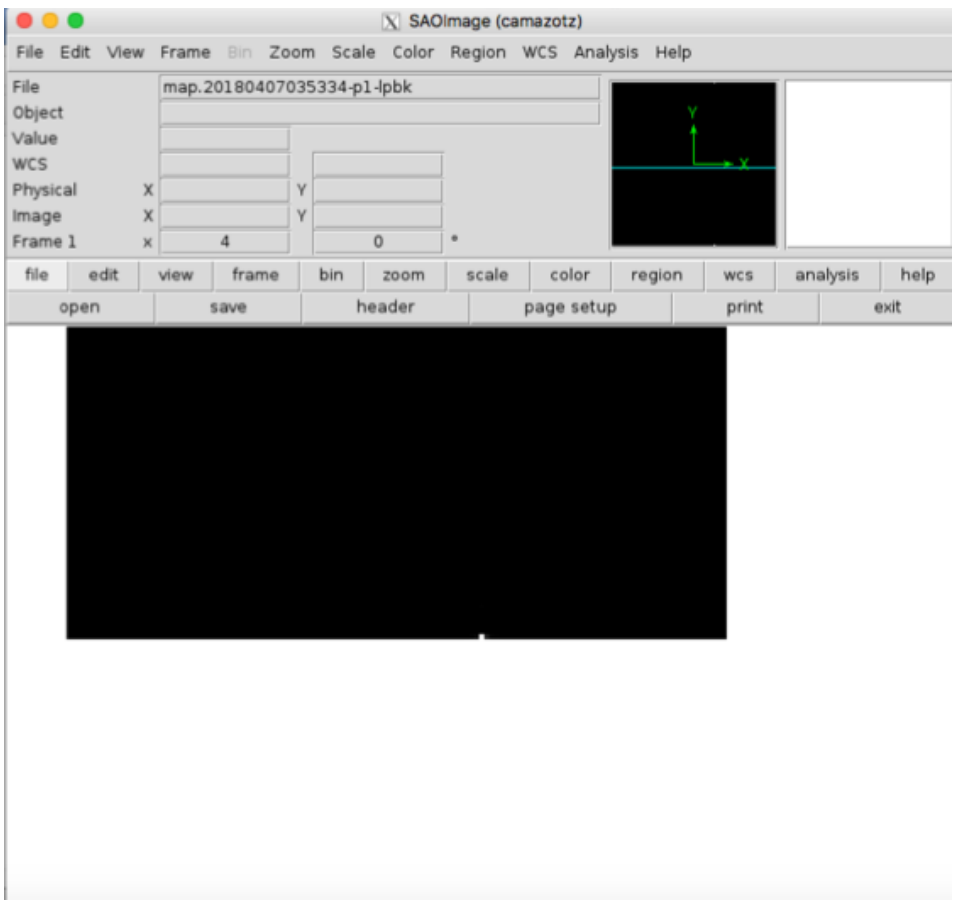

Figure 58. BPC 10 us loopback file for 2018EB97.

Part 2. BPC data

Now, process the rest of the BPC data, remember to modify the ephemerides file in the configuration file when indicated and also remember to update sampling rates and baud times for the different ranging configurations.

```
035555 – 035923
 4 runs 10us s12
040407 – 041547
11 runs 1us s12
042054 – 043934
17 runs 0.25us s14
044353 – 052441
36 runs 0.125us s14
```

RESULT FOR 10 us

```
autorng.pl ../../HD/2018EB_97/dss14/data20180407035555.000
../../HD/2018EB_97/dss14/data20180407035923.000 -e bpc_empty.10us

mapssum.pl ./map.20180407035555-p1 ./map.20180407035923-p1 -v 128:127

mk_mpeg.pl 128 127 -v sum.map-p1-035555-035923-4-SD -c 1 -z 4

      mappeak 128 127 sum.map-p1-035555-035923-4-SD
      Signal Strength:
            0  @ frq    81, range bin   115 =        12.74
            1  @ frq    82, range bin   115 =         4.46
            2  @ frq    43, range bin    27 =         4.23
```

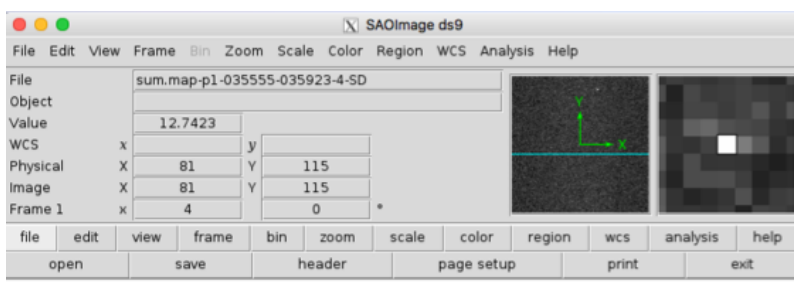

Figure 59. BPC 10 us processed for 2018EB97.
Note that echo was expected in bin 82 according to the planning email.

RESULT FOR 1 us

Remember to modify accordingly to the recorder configuration and the and the planning email information.

- ⇒ Fs = 8MHz, 1 channel, quantization bits 2 (mode=3)
- ⇒ Baud 1 usec
- ⇒ Code length 255
- ⇒ Number of coherent sums 10
- ⇒ Bandwidth 392.2 Hz
- ⇒ FFT length 256
- ⇒ Frequency resolution 1.5 Hz
- ⇒ TXOFF +50 Hz (echo is column 161)

```
rng_p.pl -f ../../HD/2018EB_97/dss14/data20180407040407.000
 -e bpc_empty.1us -r -d
autorng.pl ../../HD/2018EB_97/dss14/data20180407040407.000
../../HD/2018EB_97/dss14/data20180407041547.000 -e bpc_empty.1us
mapssum.pl ./map.20180407040407-p1 ./map.20180407041547-p1 -v 256:255
mk_mpeg.pl 256 255 -v sum.map-p1-040407-041547-4-SD -c 1 -z 4

mappeak 256 255 sum.map-p1-040407-041547-11-SD
Signal Strength:
      0  @ frq   162, range bin   135 =        12.18
      1  @ frq   161, range bin   135 =         8.21
      2  @ frq   164, range bin   136 =         6.76
```

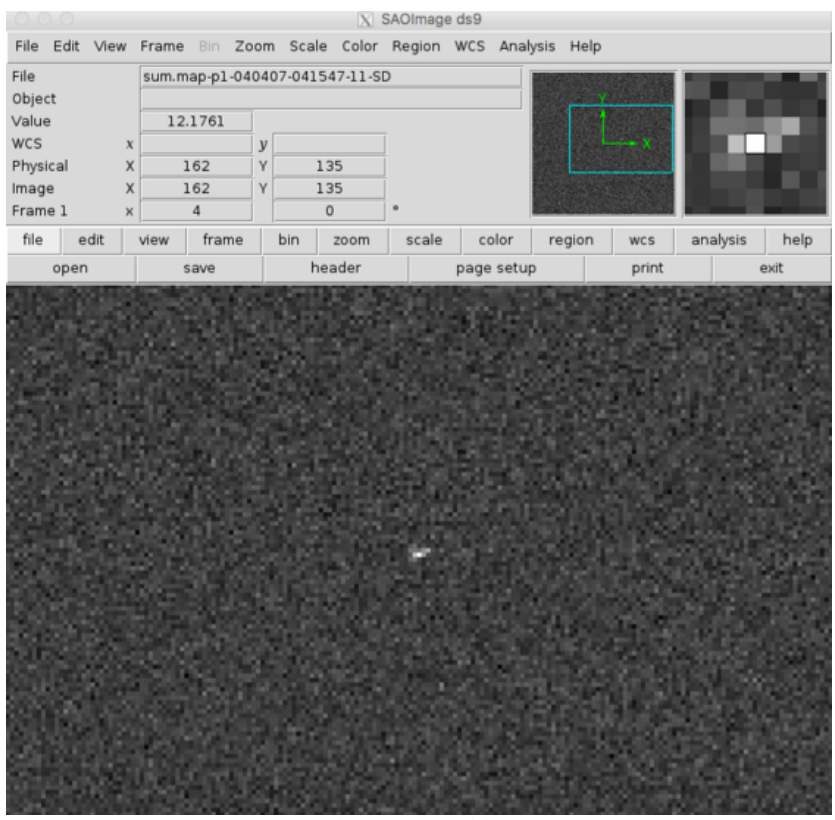

Figure 60. BPC 1 us data processed for 2018EB97.

RESULT FOR 0.25 us

Remember to modify accordingly to the recorder configuration. Note that the ephemerides file is updated to solution s.14. Note that the planning email did not include specific instructions for 0.25 us, instead it said decide what to do next based on the SNRs.

The instructions where given online, while tracking the object, since the SNR where good enough.

- ⇒ Fs = 20MHz, 1 channel, quantization bits 2 (mode=3)
- ⇒ Baud 0.25 usec
- ⇒ Code length 127
- ⇒ Number of coherent sums 240
- ⇒ Bandwidth 131 Hz
- ⇒ FFT length 128
- ⇒ Frequency resolution 1.025 Hz
- ⇒ TXOFF +20 Hz (echo is column 84)

```
rng_p.pl -f ../../HD/2018EB_97/dss14/data20180407042054.000
 -e bpc_empty.0.25us -r -d

autorng.pl ../../HD/2018EB_97/dss14/data20180407042054.000
../../HD/2018EB_97/dss14/data20180407043934.000 -e bpc_empty.1us

mapssum.pl ./map.20180407042054-p1 ./map.20180407043934-p1 -v 128:127

mk_mpeg.pl 128 127 -v sum.map-p1-042054-043934-17-SD -c 1 -z 4

        mappeak 128 127 sum.map-p1-042054-043934-17-SD
        Signal Strength:
              0  @ frq    84, range bin    10 =        11.59
              1  @ frq    83, range bin    10 =         8.93
              2  @ frq    85, range bin    11 =         8.45
```

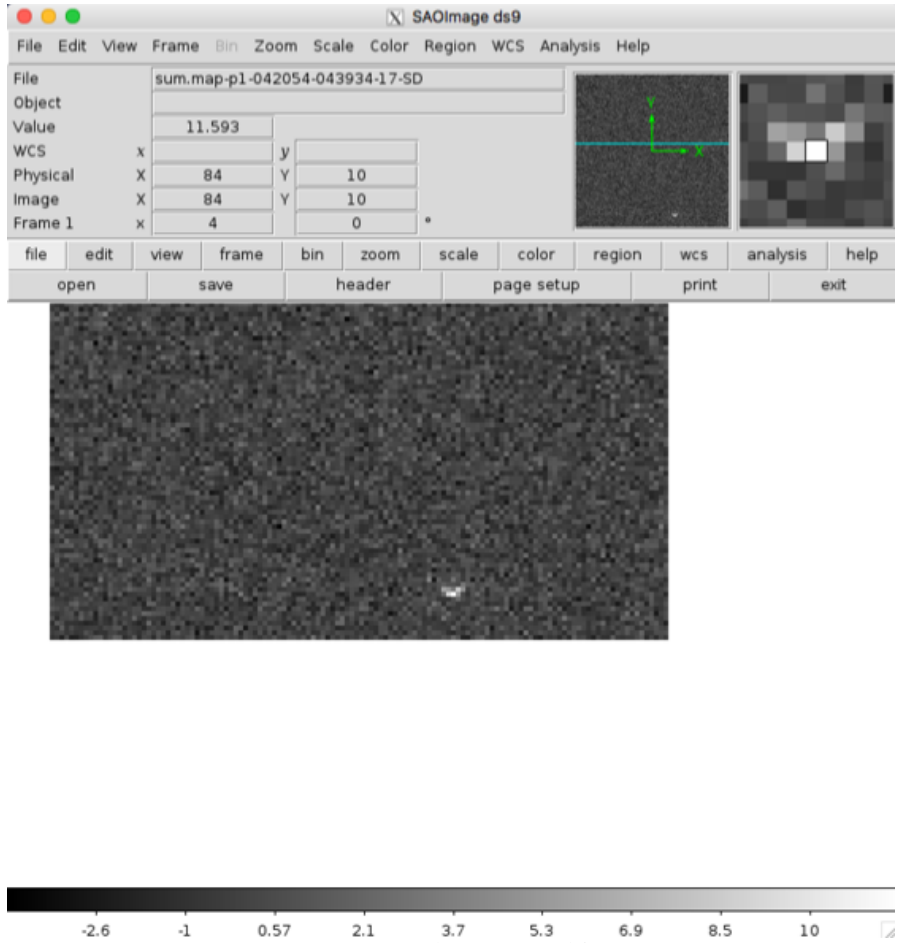

Figure 61. BPC 0.25 us data processed for 2018EB97

RESULT FOR 0.125 us

Remember to modify accordingly to the recorder configuration. Note that the planning email did not include specific instructions for 0.125 us, instead it said decide what to do next based on the SNRs. The instructions where given online, while tracking the object, since the SNR where good enough.

Remember to modify accordingly to the recorder configuration and the and the planning email information.

- ⇒ Fs = 32MHz, 1 channel, quantization bits 2 (mode=3)
- ⇒ Baud 0.125 usec
- ⇒ Code length 127
- ⇒ Number of coherent sums 460
- ⇒ Bandwidth 131 Hz
- ⇒ FFT length 128

⇒ Frequency resolution 1.07 Hz

⇒ TXOFF +20 Hz (echo is column 83)

```
rng_p.pl -f ../../HD/2018EB_97/dss14/data20180407044353.000
 -e bpc_empty.1us -r -d

autorng.pl ../../HD/2018EB_97/dss14/data20180407044353.000
../../HD/2018EB_97/dss14/data20180407052441.000 -e bpc_empty.1us

mapssum.pl ./map.20180407044353-p1 ./map.20180407052441-p1 -v 128:127

mk_mpeg.pl 128 127 -v sum.map-p1-044353-052441-36-SD -c 1 -z 4

       mappeak 128 127 sum.map-p1-044353-052441-36-SD
       Signal Strength:

             0  @ frq    83, range bin    21 =        13.09
             1  @ frq    84, range bin    21 =        11.69
             2  @ frq    82, range bin    22 =         7.98
```

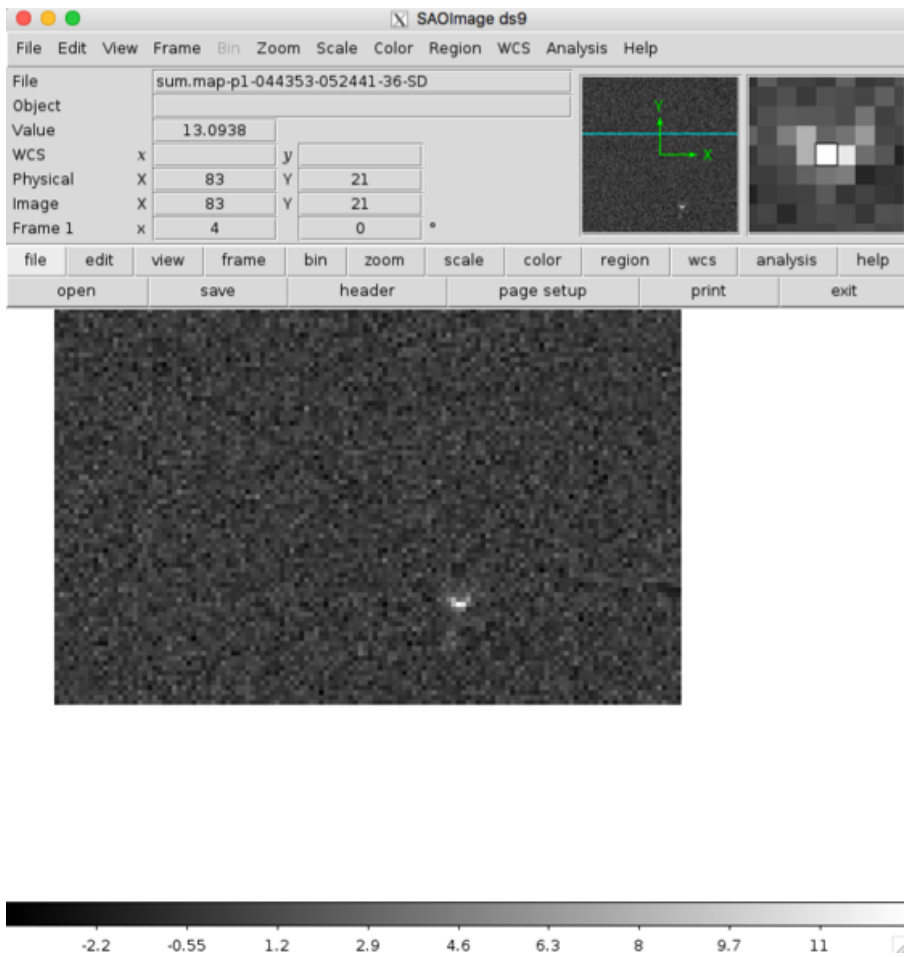

Figure 62. BPC 0.125 us data processed for 2018EB97

Appendix

A. Evolution of the GSSR Transmitter

The evolution of the GSSR transmitter is linked to the evolution of the planetary radar astronomy at Goldstone. This information has been extracted mainly from [47] and [48].

S-band transmissions at a 2388 MHz

Planetary radar was not initially recognized as a science activity within JPL programs. Consequently, the activity had no budget assigned, and JPL used planetary radar as a mean to test DSN performance, as part of some other programs. On the contrary, radio astronomy, in a more privileged position, managed to use the antennas at Goldstone at no cost whenever the proposed experiments had no conflict with spacecraft communications and data acquisition, the antenna's primary goal. During the 1960s, planetary radar survived on budget from some space missions and, mostly, NASA paid the Goldstone radar instrument operation and maintenance costs as part of the DSN and the DSN Advanced Systems Development (ADS) budget paid for hardware design and construction. JPL had an important role, when Richard Goldstein, as manager of section 331, pushed for the design and built of a hardware piece to be added to GSSR. To obtain time on the GSSR, Goldstein contacted many of the missions advocating on why the proposed radar experiment support was key. Once he got one mission to accept, he requested antenna time from DSN antenna time scheduling managers. With a selling history based on improving communications for spacecrafts, radar observations were supported by Mariner missions and both, Viking and Voyager, supported planetary experiments as Mars, Saturn's rings, and the Galilean satellites of Jupiter, [48].

The planetary radar at JPL had the dual functionality of 1) testing and validating DSN capabilities to support interplanetary missions, and 2) providing a platform to develop new hardware for the DSN. This dual functionality became the ideal justification for having ADS focus on radar astronomy hardware, [48]. In 1961, after the Venus radar experiment, Eb Rechtin, the DSN chief architect, decided to assign GSSR the specific task to develop and test new DSN hardware. Short after that, Goldstein and Carpenter conducted 1962 and 1964 Venus radar observations, [4]. Little by little, the planetary radar research resulted in an increase of the CW radar's average power, i.e. an improvement of the GSSR capabilities. From 10-13 kW in 1962, the CW radar's power went up to 100 kW in 1964. As Goldstein continued his radar experiments, we needed bigger antenna dishes. For example, for the 1967 Venus experiment, Goldstein used a 64-m diameter S-band antenna located at the Mars station (DSS-14). The need to improve communications to handle mission going further and further away, made JPL to push for bigger antenna dishes. Space missions, therefore, pushed the final design of DSS-14. The co-existence of new missions, designed to use S-band capabilities, and previous missions created the need of a hybrid technology capable of

handling missions operating at either the higher or lower frequency bands. The equipment was design by a JPL team, allowing DSS-14 to support Mariner 4, Pioneer 7, Surveyor flights, Apollo Moon's pictures and planetary radar and topographical maps, [7].

Later on, in the 1970's, JPL research allowed the detection of Saturn' rings, [49]. The results indicated a number of conclusions that surprised radar astronomers. For example, as the received echoes were stronger that those of Mercury and Venus, the particles needed to be large (as compared to the wavelength), irregular and rough particles. Those results were evaluated by astronomers as Gordon Pettengill and Tor Hagfors, who based on their experience, thought that the radar cross section observed by [49] was too high and made the ring particle density or composition unreasonable. The contradicting results between the finding on Saturn's rings by [49] and the radio astronomers general Galilean moons studies resulted in the radar astronomy community contributing to planetary science.

X-band transmissions at 8495 MHz

In the 1970s, in order to accommodate Viking and Voyager spacecraft missions, DSS-14 underwent a major upgrade. Both missions required X-band frequencies: Viking was a dual-frequency craft (S- and X-bands); and Voyager data were coded and transmitted at X-band. This need triggered the construction of the 400 kW, X-band (8495 MHz; 3.5 cm) transmitter for DSS-14, that was completed by ADS and became operational in 1975. During some time both S-band and X-band radars operated at the same time. According to [50] three S-band transmitters were arranged to operate through one of the feeds: one for routine spacecraft, one for special communication situations, and one 400-kW CW transmitter operated at S-band (2388 GHz) for planetary radar. In addition to this there was an extra feed dedicated to the 400 kW X-band radar system at 8495 GHz. The X-band radar operated since 1975 to the early 1999's.

As the years passed, with the increase on spacecraft missions, DSN antenna time availability became more and more difficult to obtain. A total of 19 spacecrafts were using the DSN by 1978. With such saturation of antenna time, the DSN stop funding planetary radar experiments. The capability was maintained at JPL, but it went through hard funding times. It was then when JPL management took the decision to stop pushing planetary radar science through proposals to improve the DSN hardware, and support instead the competition of planetary radar science with other JPL science activities. The, nowadays, NASA Office of Space Science and Instruments was the instrument selected to get this funding. The initial focus of planetary radar, hurt the image of this science because, from DSN and NASA, it was understood as a tool to test and improve DSN hardware rather than a tool for experiments with high scientific return.

Planetary radar followed a long way until it had the current value and recognition. In particular, the study of planetary surfaces through radar delay-Doppler images resulted very valuable to the scientific community. It was a clear example of what such measurements could accomplish. Later events, as the landing of an American on the Moon, made clear the need to use radar to explore

planet surfaces from Earth. The idea, of course, had opposers as [51], who wrote: "It is inevitable that the importance of the exploration of the planetary system by radar will diminish as instruments and men are carried directly to the scene by space vehicles. However, that time is still to come. In the meantime, the information that radar provides will be vital in man's great effort to conquer space", or the Soviet radar astronomers B. I. Kuznetsov and I. V. Lishin, who expressed "Certainly, radar bombardment of the planets gives less information than a direct investigation of them with spaceships and interplanetary automatic stations". Even though their opinions pointed to the limited usefulness of planetary radar in time, they recognized the current value and saw that prior knowledge of the surface of a planet would help mission design to plan for better landings, [49]. NASA, slowly, funded more and more planetary radar experiments that help better designs of spacecraft missions.

X-band transmissions at 8560 MHz

By the early 1990's and motivated by the Voyager Neptune encounter [52], the GSSR was updated from a 64 m to a 70 m dish antenna and counted with: 1) a high-power transmitter, capable of radiating ~450 kW by low-loss power combining of the output from two 250-kW klystrons, 2) vacuum tube electron beam devices, that are the key amplifying elements of most radio frequency telecommunications, and 3) radar transmitter systems.

In 1991, two new klystrons, designed specifically for the GSSR by Varian Associates to achieve higher power and better reliability [53] were installed, upgrading the GSSR to 450 kW. All klystrons delivered based on the model VKX-7864A design showed matching and bandwidth insufficiencies and failed in their early lifetime stages. After this Communications & Power Industries (CPI) took over the DSN klystron design and developed the model VKX-7864B [54], with an output power of 250 kW, a bandwidth of 50 MHz, and a center frequency of 8510 MHz. This therefore led to the beginning of GSSR transmissions at 8510 MHz in September 1991, [55].

Between years 1999 and 2000, a total of four new klystrons were installed. During this time the center frequency changed again to 8560 MHz (March 1999), [55]. For a long time, those klystrons served the GSSR supporting an increasing number of planetary radar experiments. In the last 20 years, all of those klystrons have failed, causing expensive repairs impacting the availability of DSN radar services.

Evolution of GSSR Klystrons

As an evolution from the earlier design, with identical key requirements for center frequency, output power, and bandwidth, CPI assigned the model number VKX-7864C to the new klystron. CPI had recently collaborated with JPL [56] on the successful design of a new 100-kW klystron (VKX-7976A) to power an 80-kW transmitter system for DSN 34-m beam-waveguide (BWG) antennas, providing a telecommunications X-band uplink capability equivalent to the 20-kW X-band capability on the DSN 70-m antennas. Because of this experience, the technical specifications

document for the GSSR VKX-7864C klystron amplifier was influenced by lessons learned during the 100-kW klystron development as well as the earlier B-series design and the field history from more than a decade of GSSR operations.

A detailed statement of work (SOW) was incorporated into the CPI subcontract, guiding the new klystron development, defining its objectives and schedule, and establishing partial payment milestones. At a high level, the SOW consisted of:

1. reviewing the technical specifications document,
2. performing nonrecurring engineering (NRE), including reviewing the performance, field history, and build methodology of the VKX-7864B devices,
3. fabricating and testing the prototype, and
4. meeting JPL quality assurance standards and providing for witnessed acceptance testing prior to delivering the device to the DSN High-Power Transmitter Test Facility (HPTTF) at the Venus site at GDSCC.

The NRE was based on new simulation codes and techniques not available at the time of the B-series design, nearly 20 years ago. To validate the VKX-7864C design, CPI focused on a number of key elements:

- Electron beam optics. A well-focused electron beam and better beam confinement as electrons traverse multiple RF cavities to achieve high gain would be required to improve performance and reliability. One of the failure modes of the GSSR klystrons has been singed cavity drift tube tips, indicating loss of control and confinement of the electron beam.
- RF body multicavity design. Employ progressively higher-fidelity large signal codes to establish the electrical design parameters and the number of cavities, and validate performance of a wideband output circuit to achieve 250-kW output power over a 50-MHz bandwidth centered at 8560 MHz with less than 1 dB variation across the band. Synthesize the geometry of the cavities and output circuit and fabricate and cold-test the cavities to verify the design.
- Solenoid magnet. Use high-fidelity signal codes to determine the magnetic field required to optimize beam focusing at full RF performance.
- Output waveguide. Review the electrical and mechanical design to ensure a low-voltage standing-wave ratio (VSWR) between the output circuit and output window and sufficient cooling to maintain RF stability.
- Isolated collector. Review the existing collector electrical, thermal, and mechanical design and propose changes to improve reliability, thermal performance, and mechanical stability, and eliminate shorting to ground. The collector was the least reliable component of the VKX-7864B design, resulting in multiple tube failures.
- Electron gun. Review the existing VKX-7864B electron gun assembly, which was also used in the VKX-7976A 100-kW klystron, to validate the electron beam diameter used in all large-signal simulations. The electron gun was a reliable element in the GSSR klystrons and planned to be used in the new device.

- Output window. Review the existing design to ensure it can support the 250-kW output power and 50-MHz bandwidth requirements, and modify if necessary.
- GSSR operational modes. Review current GSSR operational modes and new ranging modulations to ensure design revisions introduced in the VKX-7864C will support them with improved lifetime and reliability.

It is also relevant to understand the history of the Klystrons performance and how this affects to the DSN capabilities. As defined in this manual, Klystrons are specialized linear-beam vacuum tubes used as amplifier for high radio frequencies, from UHF up into the microwave range. When a Klystron fails, the transmitter power is limited. Next image shows a temporal diagram of the different Klystrons operating at the DSN.

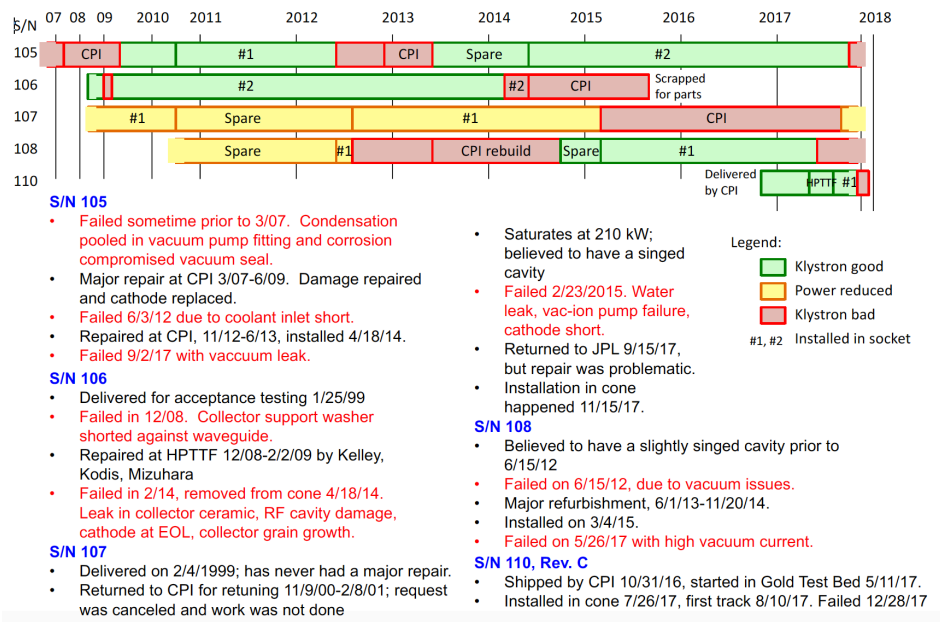

Figure 63. Recent Klystron failures. Source from Jet Propulsion Laboratory.

During the DSS-14 down time last summer, S/N 110 klystron was installed in the XKR Cone in the #1 socket, along with S/N 105 in the #2 socket. GSSR had full power (~470 kW) from August 2017 to September 2, when S/N 105 failed. With no other choice, GSSR operated at ~50% power using S/N 110 at 240 kW. CPI had returned S/N 107 as a nominal spare, but it spent from mid-Sept 2017 through November being "conditioned" at the GDSCC High Power Test Bed. It was returned to the XKR Cone, but not connected on 11/15/17. Then on Dec. 28, 2017, S/N 110 failed and S/N 107 was connected. At this moment the DSS-14 is operating with a single Klystron (S/N 107) and there are several power constraints in order to preserve it. The last operating advisory notice from Ronglin R. Liou said:

For the sake of preserving the availability of the remaining klystron and GSSR, the Operating Advisory needs to be updated.

1. *While SN 107 can produce RF output power exceeding 180 kW (out of the horn), being the only remaining GSSR klystron, it is strongly recommended to limit the output power to be 180 kW maximum.*
2. *SN 107 will experience vacuum current trips during tracks. When this occurs, it can be slowly brought back to operation while keeping the vacuum current at sufficiently safe level. This process can take on the order of 10 minutes. The recovery will take longer with larger gas bursts. Under the worst case scenario, the remainder of the scheduled track may need to be used to bring back the klystron.*
3. *SN 107 functions nominally with CW, chirp, and modula2on but will trip off much more frequently when the RF drive is on/off cycled. It is strongly recommended to plan the GSSR operation in the bistatic mode. If a track must be operated in the monostatic mode, the output power shall be limited to 100 kW maximum.*

These advisories are expected to remain effective till the end of 2018 when the next klystron is to become available and will be reevaluated quarterly or when determined necessary.

This operating advisory and the effect of having klystrons failing give a clear idea of how critical these elements are and how important is to preserve them. In order to preserve the last Klystron, the transmitted power is limited. Particularly, in the case of monostatic measurements of NEO, the power is limited then to 100 kW.

New klystrons are being currently developed. Expected delivery dates are February 2019 for S/N 110, July 2019 for S/N 111, and September 2019 for 112. With the installation of S/N 111, and due to the lack of compatibility with the current S/N 107 (to be substituted) the power will be raised to an operational 250 kW. It won't be until S/N 112 becomes available that the GSSR will re-gain full power.

B. Description of a PUNCH file

The following describes the contents of a DSN planetary radar punch file.

INTRODUCTION:

"Punch file" refers to formatted information used as input at the DSN planetary radar site to control transmitter/receiver oscillators. Formerly provided on actual punch cards, the data is currently transmitted as an 80-column electronic (ASCII) file. An example is provided at the end.

GENERAL FILE OUTLINE:

An outline of the punch file provided to the DSN is as follows. Transmitter and receiver sections are distinguished by the column 80 code only:

```
Transmitter section:
--------------------
  rise/set interval header
    8 data records [each 6 lines long; 1 header, 5 coefficient lines]
      (8 Chebychev parameter records for 8 quantities; fit based on integration/computations
       from rise to set at 10 minute intervals)
  rise/set interval header
    8 data records [each 6 lines long; 1 header, 5 coefficient lines]
      (8 Chebychev parameter records for 8 quantities; fit based on integration/computations
       from rise to set at 10 minute intervals)
  ...
Receiver section:
-----------------
  rise/set interval header
    8 data records [each 6 lines long; 1 header line, 5 coefficient lines]
      (8 Chebychev parameter records for 8 quantities; fit based on integration/computations
       from rise to set at 10 minute intervals)
  rise/set interval header
    8 data records [each 6 lines long; 1 header line, 5 coefficient lines]
      (8 Chebychev parameter records for 8 quantities; fit based on integration/computations
       from rise to set at 10 minute intervals)
   ...
END-OF-FILE (no marker)
```

The 10-minute interval for the Chebychev fit is user-selectable in our software, but 10 minutes is standard. A polynomial of 15th degree (maximum) is fit.

POLYNOMIAL FIT METHODOLOGY

If you use the MATH77 routine "dpfit" (recommended), set SEEKN, COMTRN, CHBBAS = .true. in the FORTRAN call. This requests automatic determination, of optimum degree for polynomial fit (NDEG <= 15), transformation parameters (below) and Chebyshev basis.

In this case, the Chebyshev polynomial is defined as:

$$P_n(x) = \sum_{i=0}^{n} P(i+3)T_i(u)$$

Where:

$$T_0(u) = 1;\ T_1(u) = u;\ T_2(u) = 2u^2 - 1;$$

$$T_i(u) = 2uT_{i-1}(u) - T_{i-2}(u); for\ i = 3, 4, \ldots$$

and the transformation formula is:

$$u = \frac{x - P(1)}{P(2)}$$

$P(1)$ and $P(2)$should be computed by:

$$P(1) = (xmax + xmin)/2$$

$$P(2) = (xmax - \ xmin)/2$$

where xmax and xmin are maximum and minimum values of x in the data array to be fit. This causes the transformed variable u to range from -1 to +1 as x goes from xmin -> xmax.

DATA RECORD STRUCTURE AND DEFINITION:

If we begin at the start of an example file and show output for a complete rise/set fit cycle, the first line identifies a new interval as follows:

Line 1 (rise/set interval header)
==========

example:
A#1620 RISE 1994 AUG 27 06 20 SET 1994 AUG 27 08 00 4494 827999 T

col 1-6 : Arbitrary label. In this case, asteroid #1620 (Geographos)
col 7-12 : ' RISE '
col 13-29: YYYY MMM DD HH MM
(U.T. rise time, where MMM is capitalized 3-letter month abbrev.)
col 30-34: ' SET '
col 35-51: YYYY MMM DD HH MM
(U.T. set time, where MMM is capitalized 3-letter month abbrev.)

Common (lines 1-6)
==========

Columns 67-80 are common to all lines in the file. Quantity definitions are taken from JPL IOM 314.10-009 Standish/Yeomans 12/07/92. Normally, uplink frequency is constant, with the receiving station(s) tuned to receive the Doppler-shifted signal frequency. It is also possible for the uplink frequency to be ramped so a constant frequency is received at one of the receiver stations denoted as the primary receiver.

col 67 : last digit of transmitter stn. code (4=DSS 14, 1=Arecibo)
col 68 : last digit of receiver stn. code (4=DSS 14, 3=DSS 13, 1=Arecibo)
col 69-70: last two digits of year of predict record (rise time)
col 71-72: month number of prediction record (1-12) (rise time)
col 73-74: day of month number of prediction record (1-31) (rise time)
col 75-77: object type code (NAIF_ID): 999 = comet/asteroid (also Pluto)

col 78-79: Predicted quantity represented by Chebyshev fit as follows:

If

Fr = received frequency
Ft = transmitted frequency
Fb = Base frequency (i.e. 8510 MHz for X-band)
Tx = Transmission time (UTC) of given signal at xmitter
Tr = Reception time (UTC) of signal at a receiver
Tr'= Reception time (UTC) of signal at primary receiver

then we have

' ' (blank) = interval header line,

Output for transmitter (referenced to transmit time Tx):

```
RG = Tr' - Tx        in seconds (range)
DP = Fr(Tr') - Ft(Tx) in Hz      (Doppler shift)
HA = Local Hour Angle in deg
DC = Declination      in deg
AZ = Azimuth          in deg     (meas. east from north)
EL = Elevation        in deg     (above local horizon)
FQ = Xmit frequency   in Hz
DR = Differential range (0 for xmit station)

(Angular data (HA, DC, AZ, EL) are pointing angles
 appropriate for aiming at the target body so that the
 radar signal will hit the target one light time from the
 transmit time)
```

Output for receiver (referenced to receive time Tr)

```
RG = Tr - Tx         in seconds (range)
DP = Fr(Tr) - Ft(Tx)  in Hz      (Doppler shift)
HA = Local Hour Angle in deg
DC = Declination      in deg
AZ = Azimuth          in deg     (meas. east from north)
EL = Elevation        in deg     (above local horizon)
DD = Fr(Tr) - Fb      in Hz      (Differential Doppler)
DR = Tr - Tr'         in sec     (Differential range)

(Angular data  (HA, DC, AZ, EL) are apparent pointing
 angles appropriate for receiving the radar signal from
 the target body)
```

```
 col 80   :  Predict Chebyshev record is for ...
            T = transmitter
            R = receiver
```

Line 2 (record header)
==========

example:
A#1620 1994 AUG 27.0 = JD2449591.5 22800. TO 28800. SECS. 4494 827999RGT

```
 col 1-6  :  Arbitrary label. In this case, asteroid #1620
 col 7    :  blank
```

col 8-18 : YYYY MMM DD
col 19-25: '.0 = JD'
col 26-34: xxxxxxx.x (Julian Day Number for YYY MMM DD.0)
col 35-41: Integer seconds past YYYY MM DDD.0 for rise time (F7.0)
col 42-45: ' TO '
col 46-52: Integer seconds past YYYY MM DDD.0 for set time (F7.0)
col 53-66: ' SECS. '

Line 3-7 (Chebyshev parameters)
==========
DPFIT output P(3)-P(17) array with FORTRAN output scaling/formatting 1p3d22.15

Recommended MATH77/DPFIT Subroutine

```
C>> 19871209 DPFIT  Lawson  Initial code.
      SUBROUTINE DPFIT (M,X,Y,SIG,NMAX,SEEKN,COMTRN,CHBBAS,P,NFIT,
     1 SIGFAC, W)
C       LEAST SQUARES POLYNOMIAL FIT TO DISCRETE DATA.
C     USES EITHER THE MONOMIAL OR THE CHEBYSHEV BASIS.
C     ----------------------------------------------------------------
C     M            NO. OF DATA POINTS
C     (X(I),I=1,M)  ABCISSAS OF DATA
C     (Y(I),I=1,M)  ORDINATES OF DATA
C     (SIG(I),I=1,M)  STANDARD DEVIATIONS OF DATA Y()
C                 IF SIG(1) .LT. 0., THE SUBR WILL FUNCTION AS
C                 THOUGH ALL SIG(I) ARE EQUAL TO ABS(SIG(1)).
C                 In this latter case SIG() can be dimensioned
c                 1 rather than M.
C
C     NMAX          NMAX      SPECIFIES HIGHEST DEGREE POLYNOMIAL TO
C                 BE CONSIDERED.
C
C     SEEKN         IF .TRUE.      THE SUBR WILL DETERMINE OPTIMUM
C                 NFIT NOT EXCEEDING NMAX.
C                 IF .FALSE.      THE SUBR WILL SET NFIT = NMAX
C                 UNLESS THIS PRODUCES A NEAR-SINGULAR PROBLEM, IN
```

Example of PUNCH file (Geographos)

```
A#1620 RISE 1994 AUG 27 06 20 SET 1994 AUG 27 08 00            4494 827999  T
A#1620 1994 AUG 27.0 = JD2449591.5 22800. TO  28800. SECS.       4494 827999RGT
 3.576960713858465D+01 9.091355753638951D-02 6.449026171455213D-044494 827999RGT
```

```
-3.394087343788476D-07-2.839281914680723D-07-4.637600661035625D-104494 827999RGT
 1.284248365200909D-09 6.637693026261035D-11 1.987546064894382D-094494 827999RGT
 5.062800047357350D-11 1.468354568036870D-09 0.000000000000000D+004494 827999RGT
 0.000000000000000D+00 0.000000000000000D+00 0.000000000000000D+004494 827999RGT
A#1620 1994 AUG 27.0 = JD2449591.5 22800. TO  28800. SECS.       4494 827999DPT
-2.578885577516154D+05-7.311102167591072D+03 5.788323390014625D+004494 827999DPT
 6.425894149786183D+00 1.245576221819390D-02-3.917046851651782D-034494 827999DPT
 5.994491549034885D-05-7.743188479301301D-06 1.489111808059300D-044494 827999DPT
-6.316869582297373D-06 7.167463800703016D-05 0.000000000000000D+004494 827999DPT
 0.000000000000000D+00 0.000000000000000D+00 0.000000000000000D+004494 827999DPT
A#1620 1994 AUG 27.0 = JD2449591.5 22800. TO  28800. SECS.       4494 827999HAT
 3.647981365656414D+02 1.254224463596186D+01-1.245287010858535D-044494 827999HAT
-3.527256153113285D-05 4.254066864007554D-07 2.664190874102353D-084494 827999HAT
-1.186135716835834D-07-2.861035907916804D-08-3.313282125538301D-074494 827999HAT
 1.507681348897297D-08-1.623320884437562D-07 0.000000000000000D+004494 827999HAT
 0.000000000000000D+00 0.000000000000000D+00 0.000000000000000D+004494 827999HAT
A#1620 1994 AUG 27.0 = JD2449591.5 22800. TO  28800. SECS.       4494 827999DCT
-4.766368777605415D+01 3.660175979427515D-01 2.935049600694953D-054494 827999DCT
-4.232263606945468D-06-4.781172909804081D-07 1.149891220567028D-094494 827999DCT
-3.990530559319011D-09 9.962794785597935D-10-6.664389989446430D-094494 827999DCT
 4.070678458304338D-11-3.327651087811041D-09 0.000000000000000D+004494 827999DCT
 0.000000000000000D+00 0.000000000000000D+00 0.000000000000000D+004494 827999DCT
A#1620 1994 AUG 27.0 = JD2449591.5 22800. TO  28800. SECS.       4494 827999AZT
 1.832566088957998D+02 8.474569412213842D+00 4.270429943683087D-034494 827999AZT
-1.245701892531188D-02 3.075977663691785D-05 3.168723696947818D-054494 827999AZT
-1.683763689253054D-07-1.270547291295520D-07-2.232953715211919D-074494 827999AZT
 1.070566172874354D-08-1.096915686321581D-07 0.000000000000000D+004494 827999AZT
 0.000000000000000D+00 0.000000000000000D+00 0.000000000000000D+004494 827999AZT
A#1620 1994 AUG 27.0 = JD2449591.5 22800. TO  28800. SECS.       4494 827999ELT
 6.420653628928096D+00-2.149073537302517D-01-3.782498074257176D-014494 827999ELT
-7.884573115483345D-05 4.532956718006244D-04-6.306662868588778D-074494 827999ELT
-1.010546875047465D-06 1.231599610866784D-08 1.238318763302162D-084494 827999ELT
 7.578810089837617D-09 3.256913367030733D-09 0.000000000000000D+004494 827999ELT
 0.000000000000000D+00 0.000000000000000D+00 0.000000000000000D+004494 827999ELT
A#1620 1994 AUG 27.0 = JD2449591.5 22800. TO  28800. SECS.       4494 827999FQT
 8.510257888557751D+09 7.311102167611226D+03-5.788322986659082D+004494 827999FQT
-6.425894304317952D+00-1.245554309558344D-02 3.917095359884429D-034494 827999FQT
-6.023202494793798D-05 7.788590331644151D-06-1.492396504153606D-044494 827999FQT
 6.766433689143130D-06-7.179297481915768D-05 0.000000000000000D+004494 827999FQT
 0.000000000000000D+00 0.000000000000000D+00 0.000000000000000D+004494 827999FQT
A#1620 1994 AUG 27.0 = JD2449591.5 22800. TO  28800. SECS.       4494 827999DRT
 0.000000000000000D+00 0.000000000000000D+00 0.000000000000000D+004494 827999DRT
 0.000000000000000D+00 0.000000000000000D+00 0.000000000000000D+004494 827999DRT
 0.000000000000000D+00 0.000000000000000D+00 0.000000000000000D+004494 827999DRT
 0.000000000000000D+00 0.000000000000000D+00 0.000000000000000D+004494 827999DRT
 0.000000000000000D+00 0.000000000000000D+00 0.000000000000000D+004494 827999DRT
```

…